

Marianne Helno Jahren

# On Reduced Order Drivetrain Model Integrated With Wind Turbine and Wind Farm Simulation Tools

Master's thesis in Marine Technology

Supervisor: Amir R. Nejad

July 2022

NTNU  
Norwegian University of Science and Technology  
Faculty of Engineering  
Department of Marine Technology



Norwegian University of  
Science and Technology



Marianne Helno Jahren

# **On Reduced Order Drivetrain Model Integrated With Wind Turbine and Wind Farm Simulation Tools**

Master's thesis in Marine Technology  
Supervisor: Amir R. Nejad  
July 2022

Norwegian University of Science and Technology  
Faculty of Engineering  
Department of Marine Technology





---

## Preface

This Master's thesis is written as the final delivery in Master of Science in Marine Technology at Department of Marine Technology at the Norwegian University of Science and Technology (NTNU).

There are three main motivations for me choosing this topic for my Master's thesis. Firstly, one of my interest through my studies has been machine dynamics, making drivetrains of wind turbines relevant for my background. Secondly, wind energy combines many disciplines and different physical domains, making it a complex field that I therefore deem interesting. Lastly, I wanted to perform my work within a field relevant for the transition to greener power.

There are many people that have helped me in my work during my Master's Thesis. First and foremost, I would like to thank my supervisor Amir R. Nejad for the opportunity to write my thesis within a field that I find very interesting and for all the helpful guidance and good discussions. Secondly, I would like to thank Diederik van Binsbergen, who have helped me throughout the work, contributed to good discussions and who has been vital in getting my model to work. I would also like to thank Irene Rivera Arriba that have helped me with getting OpenFAST and FAST.farm to work and Shuaishuai Wang for assisting me in debugging the drivetrain model. Lastly, I would like to thank my brother, Marius Helno Jahren, who assisted with the spell checking and formulations in the thesis.

I want to thank my good friends that I have shared an office with during the last year. They have helped keeping the spirit up and having good times every day, even during the most stressfull times.

Lastly, I would like to thank my family and my fellow students at Marine Technology.

*Marianne H. Jahren*  
*July 2022*

---

## Abstract

Existing wind turbine and wind farm simulation tools tend to have a simplified drivetrain model integrated within the global model. This makes simulation of the drivetrain fast, but does not capture the internal dynamics of the wind turbine, nor can it provide information regarding the damage of the drivetrain components. Because drivetrain failures stands for a significant portion of the wind turbine failures and these result in long downtime, it is beneficial to capture this as well. However, there is a trade off between the drivetrain fidelity and the computational cost, which should be considered.

This Master's Thesis have been looking into the possibility of integrating a reduced order model of the drivetrain with wind energy simulation tools to capture the internal dynamics of the drivetrain, which may be used for estimation of fatigue on drivetrain components. As part of this work, a reduced order model have been developed and simulations run with a global model.

Several wind energy tools have been reviewed and OpenFAST and FAST.farm was deemed the most promising to do simulations with the reduced order drivetrain model. This was both due to the similarity of these programs, making it easy to use both, and because FAST.farm was the best alternative of the wind farm tools investigated.

A reduced order model for the 10 MW reference wind turbine model from DTU was developed in Simpack and includes two DOF for the main shaft; axial and torsional. Additionally, a script for calculating the fatigue on the main bearings due to thrust force was written. It was attempted to include the gear dynamics, but due to validation challenges, this was abandoned.

The result will show that it has been difficult to achieve a co-simulation with OpenFAST, FAST.farm and a third drivetrain tool. Nevertheless, an integrated simulation with OpenFAST and Simpack was developed using Simulink<sup>®</sup>, where the outputs was be used to estimate the damage of the main bearings from the thrust forces. This was done using the Nautilus model of a floating 10 MW wind turbine model developed in the LIFE50+ project [21] [54] [74].

It will be shown that different sea states does not affect the main bearing damage from thrust significantly. However, the simulation showed that the damage of main bearing INP-B due to thrust forces is almost twice that of INP-A due to the parameters of this bearing.

The damage of the main bearings due to thrust follows the thrust curve and show that the fatigue damage below the rated wind speed is lower than for the wind speeds above the rated wind speed. Still, the power production is higher above, hence the damage per MW may not be lower.

A time analysis shows that using Simulink<sup>®</sup> for the integrated simulation makes the simulation slower, not faster. This indicates that Simulink<sup>®</sup> is not the best solution for simulating the reduced order drivetrain model with the global model.

---

## Sammendrag

Eksisterende vindturbin- og vindparksimuleringsverktøy tenderer til å ha forenklete modeller av drivverket integrert i modellen. Dette gjør simuleringene av drivverket raske, men fanger ikke opp den interne dynamikken i vindturbinen. Den kan heller ikke gi informasjon om delskaden på komponenter i drivverket. Fordi svikt i drivverk står for en stor del av svikt av vind turbiner og disse resulterer i lange nedetider, er det fordelaktig å inkludere denne dynamikken. På en annen side er det en balanse mellom detaljnivå på modellen og tiden simuleringen tar.

Denne masteren har sett på mulighetene for å integrere en forenklet modell av drivverket med vindkraftsimuleringsverktøy. Dette er gjort for å fange den interne dynamikken i drivverket, som kan brukes for å estimere utmattingen på komponentene i drivverket. En forenklet modell er utviklet som en del av dette og simuleringer har blitt kjørt ved bruk av denne.

Flere simuleringsverktøy for vindkraft er utforsket og OpenFAST og FAST.farm ble utvalgt som de mest lovende verktøyene for simuleringer med den forenklete drivverkmодellen. Dette er både fordi disse programmene er ganske like, som gjør det lettere å bruke begge, men også fordi FAST.farm var det beste alternativet av simuleringsverktøy for vindparker.

En forenklet modell basert på referanseturbinen for 10MW vindturbin utviklet av DTU ble laget i Simpack. Denne inkluderer frihetsgrader i både aksiell- og torsjonsretning for hovedakslingen. I tillegg er det laget et skript for estimering av utmatting på hovedlagrene på grunn av trustkrefer. Girdynamikken var forsøkt inkludert, men på grunn av problemer under valideringen ble dette gitt opp.

Resultatene vil vise at det har vært vanskelig å få til en co-simulering med OpenFAST, FAST.farm og et verktøy for drivverkmодellen. Allikevel har en integrert modell med OpenFAST og Simpack blitt laget ved bruk av Simulink<sup>®</sup>. Resultatene fra dette er brukt til å estimere delskade på hovedlagrene fra trustkraften. Dette er gjort ved bruk av Nautilusmodellen for 10 MW flytende vindturbin som ble utviklet i LIFE50+prosjektet [21] [54] [74].

Det vil vise seg at forskjellige sjøtilstander ikke vil påvirke delskaden fra trust i hovedlagrene særlig. Simuleringen viste dog at delskaden på hovedlager INP-B fra trustkraften er nesten det dobbelte av INP-A på grunn av parameterne til dette lageret.

Delskaden på hovedlagrene følger trustkurven og viser at utmatting under nominell vindhastighet er lavere enn for vindhastigheter over. Allikevel er effekten høyere over og utmatting per MW trenger ikke å være lavere under nominell vindhastighet.

En tidsanalyse viser at å bruke Simulink<sup>®</sup> for den integrerte simuleringen gjør den mindre effektiv. Det tyder på at Simulink<sup>®</sup> ikke er den beste løsningen for simulering av en forenklet drivverkmодell og en global modell.

---

# Table of Contents

<b>List of Figures</b>	<b>viii</b>
<b>List of Tables</b>	<b>ix</b>
<b>Abbreviations &amp; Nomenclature</b>	<b>xi</b>
<b>1 Introduction</b>	<b>1</b>
1.1 Motivation and Objective . . . . .	1
1.2 Limitations . . . . .	2
1.3 Presentation of thesis: Structure . . . . .	2
<b>2 Background theory</b>	<b>5</b>
2.1 Aerodynamics of wind turbines . . . . .	5
2.1.1 Simple momentum theory . . . . .	5
2.1.2 Momentum theory with wake rotation . . . . .	9
2.1.3 Airfoil theory . . . . .	11
2.1.4 Blade Element Momentum (BEM) theory . . . . .	12
2.1.5 Prandtl correction . . . . .	14
2.1.6 Dynamic wake model / Dynamic inflow . . . . .	15
2.1.7 Tower shadow . . . . .	15
2.1.8 Dynamic stall . . . . .	15
2.1.9 Wind turbine wake interactions . . . . .	16
2.2 Turbulence . . . . .	16
2.2.1 Kaimal spectrum model . . . . .	17
2.3 Hydrodynamics for wind turbines . . . . .	18
2.4 Wave modelling and wave spectrum . . . . .	19
2.5 Wind turbines . . . . .	19
2.5.1 Floating wind turbine concepts . . . . .	19
2.5.2 Floating wind turbines and negative damping . . . . .	20

---

2.6	Wind Turbine Simulation Tools . . . . .	20
2.6.1	HAWC2 . . . . .	20
2.6.2	SIMA . . . . .	21
2.6.3	FAST and OpenFAST . . . . .	21
2.7	State-of-the-Art Wind Farm Simulation Tools . . . . .	24
2.7.1	FLORIS . . . . .	24
2.7.2	SOWFA . . . . .	24
2.7.3	DWM . . . . .	25
2.7.4	FAST.farm . . . . .	25
2.8	Wind turbine drivetrain . . . . .	28
2.8.1	DTU 10 MW drivetrain . . . . .	30
2.8.2	Gear general . . . . .	30
2.8.3	Bearing general . . . . .	33
2.9	Existing drivetrain models . . . . .	33
2.9.1	Simple two mass drivetrain model . . . . .	33
2.9.2	Torsional 5 mass model . . . . .	35
2.9.3	High fidelity drivetrain model . . . . .	36
2.9.4	Mathematical drivetrain model . . . . .	37
2.9.5	Fidelity requirements . . . . .	38
2.10	Drivetrain modelling tools . . . . .	39
2.10.1	Simpscape . . . . .	39
2.10.2	Simpack . . . . .	40
2.10.3	Multibody system (MBS) simulation . . . . .	40
2.11	Fatigue of drivetrain components . . . . .	41
2.11.1	Palmgren-Miner hypothesis . . . . .	41
2.11.2	Cycle counting method . . . . .	42
2.11.3	Bearing Fatigue . . . . .	43
2.11.4	Gear fatigue . . . . .	44
2.12	De-coupled analysis . . . . .	44

---

---

2.13	Possibility of co-simulation and integrated simulation . . . . .	45
2.13.1	Inputs and outputs . . . . .	45
2.13.2	Dynamic Drivetrain Model . . . . .	46
2.13.3	S-Functions in Simulink® . . . . .	47
2.13.4	FMI/FMU . . . . .	48
2.13.5	Dynamic-Link Library - .dll . . . . .	48
<b>3</b>	<b>Methodology</b>	<b>49</b>
3.1	Reference models . . . . .	49
3.2	FAST.farm . . . . .	49
3.3	OpenFAST . . . . .	50
3.4	Simscape Driveline . . . . .	51
3.5	Development of reduced order model . . . . .	52
3.5.1	Drivetrain model with gears . . . . .	52
3.5.2	Drivetrain model . . . . .	55
3.6	Fatigue calculation of bearings . . . . .	56
3.6.1	Script for real time fatigue . . . . .	57
3.6.2	Script for fatigue . . . . .	57
3.7	Simulink® and S-Functions . . . . .	58
3.7.1	OpenFAST S-function - Global model . . . . .	58
3.7.2	Simpack S-function - Drivetrain model . . . . .	60
3.8	TurbSim . . . . .	61
3.9	Full model in Simulink® . . . . .	61
3.10	Validation . . . . .	63
3.10.1	OpenFAST . . . . .	63
3.10.2	Drivetrain . . . . .	64
3.11	Simulation cases . . . . .	64
3.11.1	Fatigue from sea state . . . . .	64
3.11.2	Fatigue based on wind speed . . . . .	64

---

3.11.3	Simulation time . . . . .	65
<b>4</b>	<b>Result and Discussion</b>	<b>66</b>
4.1	Global model . . . . .	66
4.2	Drivetrain . . . . .	66
4.3	Fatigue . . . . .	68
4.4	Co-simulation vs de-coupled simulation . . . . .	69
4.5	Validation . . . . .	69
4.5.1	Global Model in OpenFAST . . . . .	69
4.5.2	Drivetrain model with gears . . . . .	72
4.5.3	Drivetrain model with one gear . . . . .	73
4.6	Tuning of PI parameters . . . . .	74
4.7	Fatigue based on sea state . . . . .	74
4.8	Fatigue . . . . .	77
4.9	Simulation time . . . . .	80
4.10	Simulation of full model . . . . .	80
<b>5</b>	<b>Challenges and further work</b>	<b>82</b>
5.1	Challenges . . . . .	82
5.2	Further work . . . . .	82
<b>6</b>	<b>Conclusion</b>	<b>84</b>
6.1	Contribution . . . . .	85
	<b>Bibliography</b>	<b>86</b>
	<b>Appendix</b>	<b>91</b>
<b>A</b>	<b>Simpack Driveline model</b>	<b>91</b>
<b>B</b>	<b>2D figure of model</b>	<b>92</b>
<b>C</b>	<b>Full model in Simulink<sup>®</sup></b>	<b>93</b>

---

---

## List of Figures

1.1	Levels of Wind Energy Modelling . . . . .	3
2.1	Overview of Actuator Disk Model with Control Volume Used in Momentum Theory	6
2.2	The Lift and Drag Forces and Pitching Moment on an Airfoil . . . . .	11
2.3	Forces and relative inflow velocity of a foil . . . . .	12
2.4	Overview of FAST.farm Modules . . . . .	26
2.5	Overview of 5MW Baseline Drivetrain . . . . .	29
2.6	Example of helical gear pair modelled in Simpack . . . . .	31
2.7	Example of planetary gear modelled in Simpack . . . . .	31
2.8	Common Parameters for Gears . . . . .	32
2.9	Drivetrain Two Mass Model with Gear . . . . .	34
2.10	Drivetrain Two Mass Model without Gear . . . . .	34
2.11	Final Drivetrain Two Mass Model . . . . .	35
2.12	Drivetrain Model with Stiffness and Damping . . . . .	35
2.13	3D Model of 10 MW Drivetrain . . . . .	36
2.14	2D Model of 10 MW Drivetrain . . . . .	37
2.15	Figure Showing How the LDD Method is Used . . . . .	43
3.1	Error message in OpenFAST for DTU controller and AeroDyn . . . . .	51
3.2	Simscape Driveline Two Mass Model . . . . .	51
3.3	3D Figure of Drivetrain Model with Gears in Simpack . . . . .	52
3.4	2D Figure of Drivetrain Model with Gears in Simpack, Part 1 . . . . .	53
3.5	2D Figure of Drivetrain Model with Gears in Simpack, Part 2 . . . . .	53
3.6	3D Figure of Drivetrain Model in Simpack . . . . .	55
3.7	2D Figure of Drivetrain Model in Simpack . . . . .	56
3.8	Screenshot of OpenLoop Example Model From OpenFAST . . . . .	58
3.9	Screenshot of Test01_SIG example model from OpenFAST . . . . .	59
3.10	Screenshot of Simple Induction Generator from Test01_SIG example model from OpenFAST . . . . .	59
3.11	Block Parameters for Simpack S-function [12] . . . . .	61



---

3.12 Full Model in Simulink <sup>®</sup> . . . . .	62
3.13 Function f(u) to Pick Output . . . . .	63
4.1 Angular velocity and Torque at Rotor side . . . . .	70
4.2 Average blade pitch degree per wind speed . . . . .	70
4.3 Angular velocity and Torque at Rotor side . . . . .	71
4.4 Angular velocity and Torque at Generator side . . . . .	71
4.5 Platform Pitch Motion and Rotor Rotational Speed with Standard Deviations . . . . .	72
4.6 Animation of Natural Frequency mode of Drivetrain . . . . .	73
4.7 Damage of INP-A for Different Sea States . . . . .	75
4.8 Damage of INP-B for Different Sea States . . . . .	75
4.9 Damage of INP-B to INP-A for Different Sea States . . . . .	76
4.10 Forces in INP-A and INP-B for Base Case . . . . .	76
4.11 Damage of INP-A Per Simulation Case . . . . .	77
4.12 Damage of INP-B Per Simulation Case . . . . .	78
4.13 Thrust with Standard Deviations . . . . .	79
4.14 Forces in INP-B . . . . .	79
4.15 Error message in OpenFAST for wind speed above 20 m/s . . . . .	80
A.1 Simscape Driveline Two Mass Model . . . . .	91
B.1 2D Figure of Drivetrain Model in Simpack . . . . .	92
C.1 Full Model in Simulink <sup>®</sup> . . . . .	93

## List of Tables

2.1 Wind Turbine Class Parameters . . . . .	16
2.2 Some of the Modules of FAST in Version 8 . . . . .	22
2.3 Main Parameters for the DTU 10 MW Drivetrain . . . . .	30
2.4 Recommendation of Minimum Fidelity . . . . .	39
2.5 Recommendation of Minimum Fidelity . . . . .	39
2.6 Coefficients for Gear Root Bending Stress Calculation . . . . .	44

---

2.7	Possible Outputs for Hub and Rotor Loads from ElastoDyn . . . . .	46
2.8	Relevant Input to S-function of OpenFAST . . . . .	47
3.1	Bearing Details for SIMPACK Model . . . . .	54
3.2	Mass and Inertia of the Drivetrain Components . . . . .	54
3.3	Gear Parameters . . . . .	55
3.4	Stiffness and damping of the main bearings [46] [73] . . . . .	56
3.5	Bearing details used in this study . . . . .	57
3.6	Inputs and Outputs Defined for Simpack Model S-function . . . . .	60
3.7	Validation Cases for OpenFAST . . . . .	63
3.8	Simulation cases for sea state . . . . .	64
3.9	Simulation cases . . . . .	65
3.10	Computer Details for Simulation Time Test . . . . .	65
4.1	Normalised Simulation Times for the Models . . . . .	80
4.2	Thrust Force and Forces on the Bearings for Base Case . . . . .	80

---

## Abbreviations & Nomenclature

### Abbreviations

<b>ABLSolver</b>	Ambient Boundary Layer Solver
<b>API</b>	Application Programmin Interface
<b>AWAE</b>	Ambient Wind and Array Effects
<b>BEM</b>	Blade Element Momentum
<b>DLL</b>	Dynamic-Link Library
<b>DOF</b>	Degree of Freedom
<b>DTU</b>	Technical University of Denmark
<b>DWM</b>	Dynamic Wake Meandering
<b>FEM</b>	Finite Element Method
<b>FLORIS</b>	FLOw Redirection and Induction in Steady state
<b>FMI</b>	Functional Mock-up Interface
<b>FMU</b>	Functional Mock-up Unit
<b>GCH</b>	Gauss-Curb-Hybrid
<b>GEBT</b>	Geometrically ExactBeam Theory
<b>HAWC2</b>	Horizontal Axis Wind turbine simulation Code 2nd generation
<b>HAWT</b>	Horizontal Axis Wind Turbines
<b>HSS</b>	High Speed Shaft
<b>INP-A</b>	Main shaft bearing A
<b>INP-B</b>	Main shaft bearing B
<b>ISS</b>	Intermediate Speed Shaft
<b>LCOE</b>	Levelized Cost of Energy
<b>LDD</b>	Load Duration Distribution
<b>LES</b>	Large Eddy Simulation
<b>LSS</b>	Low Speed Shaft
<b>MBS</b>	Multibody system
<b>NREL</b>	National Renewable Energy Laboratory

---

**ODE** Ordinary Differential Equation  
**rpm** Rounds per minute  
**SBR** Simpack Binary Result  
**SC** Super Controller  
**SOWFA** Simulator fOr Wind Farm Applications  
**WD** Wake Dynamics

## Nomenclature

$\alpha$  Angle of attack [rad] or [°]  
 $\alpha_{rot}$  Rotor acceleration  
 $\beta$  Twist of the blade [rad] or [°]  
 $\Delta\omega$  Wave frequency interval  
 $\Delta\theta$  Wave direction interval  
 $\Delta p$  Pressure difference [Pa]  
 $\dot{m}$  Mass flow [kg s<sup>-1</sup>]  
 $\epsilon_{ij}$  Phase angle for wave modelling  
 $\eta_{Gen}$  Generator efficiency  
 $\Gamma$  Circulation  
 $\hat{\eta}$  Fourier coefficient for wave elevation  
 $\hat{\mathbf{X}}$  Wave diffraction forces  
 $\hat{\xi}$  Fourier coefficient for motion structure  
 $\lambda$  Tip speed ratio [-]  
 $\lambda_r$  Local tip speed ratio [-]  
 $\Omega$  Angular velocity of the wind turbine rotor [rad s<sup>-1</sup>]  
 $\omega$  Angular velocity [rad s<sup>-1</sup>]  
 $\omega$  Induced angular velocity on the free stream [rad s<sup>-1</sup>]  
 $\omega_i$  Wave frequency  
 $\omega_{ref}$  Reference value of rotational velocity [rad s<sup>-1</sup>]  
 $\omega_{rpm}$  Rotational speed [rpm]

---

$\phi$	Angle between inflow velocity and plane of rotation for foil [rad] or [°]
$\phi_p$	Pitch angle [rad] or [°]
$\rho$	Density [kg m <sup>-3</sup> ]
$\sigma$	Standard deviation
$\sigma_k$	Standard deviation of velocity component of Kaimal spectrum
$\tau_1$	Time constant for dynamic inflow
$\tau_2$	Time constant for dynamic inflow
<b>A</b>	Added mass matrix
<b>B</b>	Damping matrix
<b>C</b>	Stiffness Matrix
<b>J</b>	Inertia matrix
<b>M</b>	Mass matrix
$dP$	Power per radial segment
$dQ$	Torque per radial segment
$dT$	Thrust per radial segment
$\theta_j$	Wave direction angle
$\tilde{u}$	Fluctuating component of turbulent wind [m s <sup>-1</sup> ]
$\zeta$	Wave elevation
$a'$	Angular induction factor
$A$	Area [m <sup>2</sup> ]
$a$	Axial induction factor
$a$	Parameter for bearing type
$A_0$	Area at inlet of momentum theory actuator disk control volume [m <sup>2</sup> ]
$A_1$	Area at outlet of momentum theory actuator disk control volume [m <sup>2</sup> ]
$B$	Number of rotor blades [-]
$C$	Basic load rating
$c$	Chord length
$C_D$	Drag coefficient
$C_d$	Drag coefficient from unit drag force [-]

---

---

$C_L$	Lift coefficient
$C_l$	Lift coefficient from unit lift force [-]
$C_n$	Normal coefficient [-]
$C_P$	Power coefficient [-]
$C_T$	Thrust coefficient [-]
$C_t$	Tangential coefficient [-]
$D$	Damage
$D$	Drag force [N]
$F$	Prandtl's correction
$f$	Exponent in Prandtl's correction
$f$	Frequency [Hz]
$F_a$	Axial forces on bearing [N]
$f_n$	Natural frequency [Hz]
$F_r$	Radial forces on bearing [N]
$H_s$	Significant wave height
$i$	Gear ratio [-]
$i$	Wave frequency index
$j$	Wave direction index
$J_G^*$	Inertia of generator when gear is removed
$J_R$	Rotor inertia
$J_G$	Generator inertia
$J_{rot}$	Rotor inertia
$K$	SN-curve parameter
$k$	Index for direction of velocity component
$k_{TG}^*$	Stiffness of generator shaft when gear is removed
$k_i$	PI-controller integral gain
$k_i$	Wave number
$k_p$	PI-controller proportional gain
$k_{TEQ}$	Equivalent shaft stiffness

---

---

$k_{TG}$	Generator shaft stiffness
$k_{TR}$	Rotor shaft stiffness
$L$	Lagrangian equation
$L$	Life of bearing
$L$	Lift force [N]
$l_i$	Actual million revolutions at load case $i$
$L_k$	Integral scale parameter of velocity component of Kaimal spectrum
$m$	SN-curve parameter
$n$	Inverse of gear ratio [-]
$N_i$	Number of stress cycles to failure [-]
$n_i$	Number of stress cycles [-]
$n_p$	Number of poles
$P$	Dynamic equivalent load
$P$	Power [W]
$p$	Pressure [Pa]
$p_0$	Pressure far in front of rotor [Pa]
$p_1$	Pressure far behind the rotor [Pa]
$p_A$	Pressure before the rotor disk [Pa]
$p_B$	Pressure after the rotor disk [Pa]
$p_N$	Force angular to the rotor plane [N]
$p_T$	Force tangential to the rotor plane [N]
$Q$	External forces
$q_i$	DOF
$R$	Rotor radius [m]
$r$	Radius of interest [m]
$S(\omega)/S(\omega_i, \theta_j)$	Wave spectrum
$s$	Second
$S_i$	Stress cycles
$S_k$	Single-sided velocity component of Kaimal spectrum

---

---

$T$	Torque [Nm]
$T_p$	Peak period
$T_{Aero}$	Aerodynamic torque
$T_{gen}$	Generator torque [Nm]
$T_{Opp}$	Opposing torque
$TI$	Turbulence intensity
$U$	Mean wind speed [ $\text{m s}^{-1}$ ]
$u$	Turbulent wind speed [ $\text{m s}^{-1}$ ]
$U_\infty$	Inflow velocity [ $\text{m s}^{-1}$ ]
$v_0$	Velocity far in front of rotor [ $\text{m s}^{-1}$ ]
$v_1$	Velocity far in behind rotor [ $\text{m s}^{-1}$ ]
$v_A$	Inflow velocity on rotor [ $\text{m s}^{-1}$ ]
$V_{rel}$	Relative velocity [m/s]
$W$	Final induced velocity
$W_{int}$	Intermediate induced velocity
$W_{qs}$	Quasi-static value of induced velocity
$X$	Radial bearing factor [-]
$Y$	Radial bearing factor [-]



---

# 1 Introduction

One of the sustainability goals of the United Nations (UN) is to achieve both affordable and sustainable energy sources for all [70]. In order to achieve a transition to cleaner energy sources, DNV claims that floating offshore wind energy will be an important contributor [15].

The cost of offshore wind energy have been significantly reduced over the last decade.

According to Ørsted [53], the offshore wind power cost was reduced by 63 % from 2011 to 2017, from 177 EUR/MWh to 65 EUR/MWh, compared to 54 EUR/MWh for onshore wind.

The main contributions to the reduction have been upscaling of the wind turbines when installed offshore, innovations within the field and the impact of economy of scale [53]. DNV estimates that the Levelized Cost of Energy (LCOE) will reach 40 EUR/MWh in 2050 [15]. However, to reduce the cost of wind turbines, decent simulation tools are required to reduce failures, expenses and increase wind farm performance [30].

The conventional wind turbines today are the Horizontal Axis Wind Turbines (HAWT) with upwind rotors, meaning that the hub and blades are installed upwind of the nacelle [40]. These wind turbines consist of a foundation, a tower, the rotor and the nacelle. The rotor is made up of the hub and blades to create the rotational energy from the wind, and the nacelle contains the drivetrain that convey this energy to the generator, which in turn produce the electric power to the grid.

The main wind turbine model, with tower, nacelle and blades, are referred to as the global model [49]. This is used to perform a global analysis to find the motions and loads to estimate the behaviour of the global system. Global models often only implement simple models of the wind turbine drivetrain and does not account for the internal loads and dynamics, as will be seen in this thesis.

## 1.1 Motivation and Objective

There exist several wind turbine simulation tools and some wind farm simulation tools for the global model, and some of these will be presented later. However, as mentioned, the drivetrain in these tools tend to be simplified and does not include the complex internal dynamics within the turbine, even though the gearbox, generator and drivetrain stands for about 11 % of the total failure rate of wind turbines [18]. They are also among the components with the longest downtime per failure. If the aim is to extend the lifetime and avoid downtime, these components should also be included in investigation for reducing downtime.

Although the global models tends to have simple drivetrain models, there does exist high fidelity drivetrains that may be used in de-coupled simulations with the global model, as done by Binsbergen [5]. However, these simulations takes time and the simulation will not yield fast answers.

One of the applications for a drivetrain model could be for the use in digital twins. Digital twins is a digital model of a system that represent the physical system in a virtual environment [26]. It takes in the real-time data and may be used for decision making of the

---

physical system. However, since it shall be used for real-time data, these tools must be fast and yield the results within short time to be of use.

It is with this in mind that this work is performed, where the objective is to look into the possibility of a reduced order model of a drivetrain integrated with wind energy simulation tools. This is done to capture the responses in the wind turbine drivetrain from the external loads on the wind turbine. Additionally, for these simulations to be of use, the computational demand and simulation time should be limited. Therefore, the aim is also to develop a reduced order drivetrain model including both axial and torsional degree of freedom (DOF) to use with a global model of the wind turbine. The ambition is to use the output of the integrated simulation of the wind energy tool and drivetrain model to estimate the fatigue on drivetrain components due to the axial forces.

## 1.2 Limitations

Although offshore wind turbines consist of both bottom-fast and floating structures, the focus in this Master's Thesis will be on floating wind turbines. This is because floating wind turbines may provide more and new possibilities for installation of the wind turbines [15]. Additionally, only cylindrical tower shapes will be considered.

The models that have been evaluated for the floating wind concepts are the two developed in the LIFE50+ project, available at Gitlab<sup>1</sup>, with details in [54] and [74]. These are the Nautilus model [21] and the OO-star model [55] which both use the 10 MW reference model from DTU. No further models or sizes will be reviewed.

For the drivetrain model, only axial and torsional DOF will be included for the main shaft and only the torsional DOF is included for the components within the gearbox and the generator.

The simulation cases uses mainly normal weather conditions, and have only some extreme conditions for reference. It is assumed that for the more extreme conditions it would be better to use a model of higher fidelity.

## 1.3 Presentation of thesis: Structure

This Master's Thesis will present some of the topics required for wind energy and for achieving the above-mentioned goal. It consist of background theory, methodology, results and discussions of these. Some challenges and further work will be discussed before the thesis is concluded.

The background theory relevant for floating wind energy is presented in Section 2 and introduce the relevant external forces. These are covered the aerodynamics, turbulence and hydrodynamics including how these are modelled in Section 2.1, 2.2, 2.3 and 2.4. The topics related to the wind energy extraction follows and these are divided in to three levels as visualised in Figure 1.1. At the top level is the wind farm, that includes the whole farm with

---

<sup>1</sup><https://rwt.windenergy.dtu.dk/dtu10mw/dtu-10mw-rwt/-/tree/master/>

---

turbine interaction included in the analysis. Level II is the wind turbine itself where only the one turbine is viewed. The lowest level reviews the internal dynamics of the wind turbine, with drivetrain gear meshing and bearings. Topics related to level I is given in 2.6, topics related to level II is in Section 2.5 and Section 2.6 while level III is covered in Section 2.8, 2.9, 2.10 and 2.11.

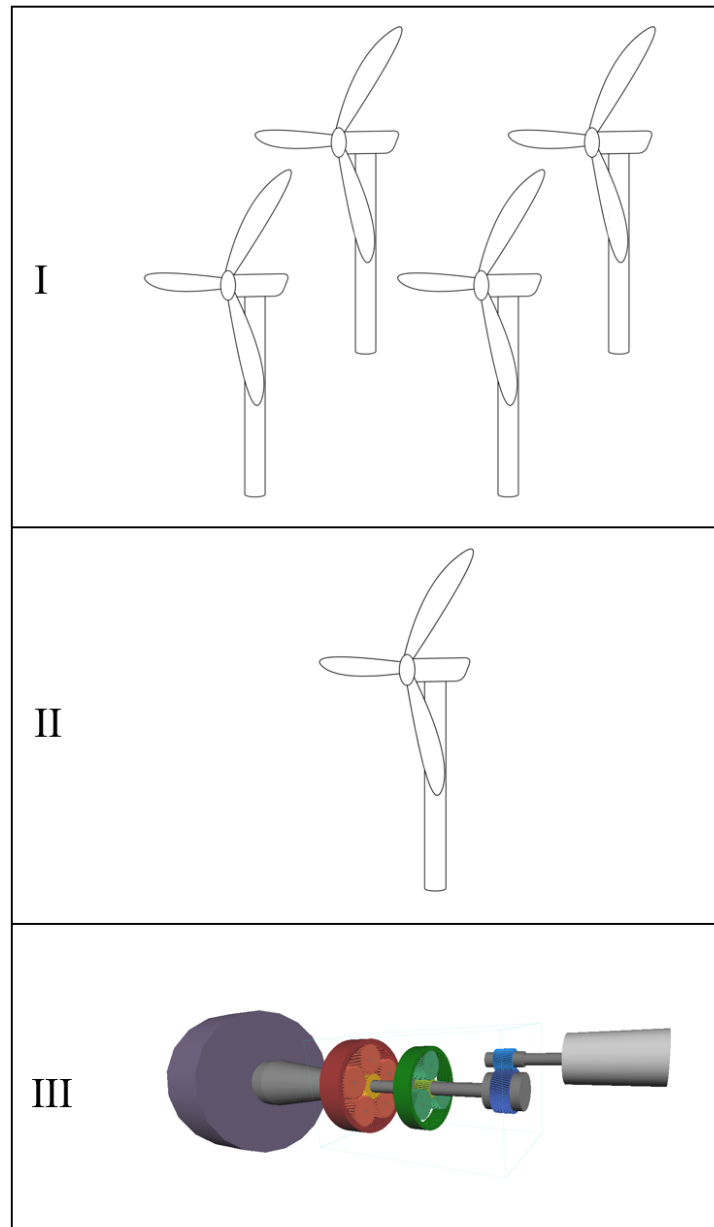


Figure 1.1: Levels of wind energy modelling, level I farm level, level II turbine level, level III internal dynamics

At the end of the background theory section, a brief background for the possibility of simulations between the global model and the drivetrain model is included.

Section 3 covers the methodology including the steps performed in the Master's Thesis regarding modelling and simulation. The reference models are presented before the attempts of using wind farm simulation tool related to level III in Figure 1.1 is described in Section 3.2.

---

The wind turbine simulation tool of level II is presented in Section 3.3 and the methodology related to the drivetrain in level III follows in Section 3.4, 3.5 and 3.6. Lastly, before the full model is presented, the turbulence model from TurbSim is covered Section 3.8. The rest of the methodology section will present the full model that have been developed in Section 3.9, validation of the sub models in Section 3.10 and the simulation cases in Section 3.11.

In Section 4, the results and discussion is included.

Section 5 of the thesis presents challenges and further work related to what has been presented before the thesis is concluded in Section 6.

---

## 2 Background theory

The following section will present some of the relevant background theory for this Master's Thesis. This includes environmental loads on the global model, the wind farm- and wind turbine simulation tools and some wind turbine models. Drivetrain models with its component and the fatigue calculation of these are also covered. Additionally, some information regarding de-coupled analysis and the possibility of co-simulations and integrated simulation is presented.

### 2.1 Aerodynamics of wind turbines

The main function of a wind turbine is to produce electric power by extracting kinetic energy from the wind [24]. This is done by utilising the kinetic energy in the wind to induce rotational speed and torque on the rotor, which is further transformed to electrical power in the generator. The power from the rotor and shaft of a wind turbine is shown in Equation (1) where  $T$  is the torque in  $Nm$  and  $\omega$  is the rotational power in  $rad/s$ .

$$P = T \cdot \omega \tag{1}$$

For wind turbine aerodynamics, the Blade Element Momentum (BEM) theory is used. It combines momentum theory and airfoil theory, and these relations will be presented in the following sections.

#### 2.1.1 Simple momentum theory

Simple momentum theory is a basic aerodynamic theory for wind turbines and is based on theory that was developed for prediction of ship propellers performance [40]. Within this method, the rotor is considered an actuator disk, also called a rotor disk, with a pressure drop over this disk [24] [40].

In order to apply the momentum theory, some assumptions must be made. The flow must be incompressible, homogeneous and a steady state flow [24] [40]. Additionally, the following assumptions are made [24] [40]:

- No frictional drag
- No external force acts on the fluid
- Infinite number of blades
- The wake is non-rotating
- The thrust is uniform over the rotor disk
- Pressure far upstream and downstream of rotor is equal to ambient pressure

Figure 2.1 shows how the air flows from the inlet, over the actuator disk and to the outlet, and the actuator disk drawn vertically in the middle. The solid black lines is the control volume boundary with the assumption that no air will flow across these lines [8]. The development of the velocity and the pressure in the control volume is shown as blue and red lines respectively.

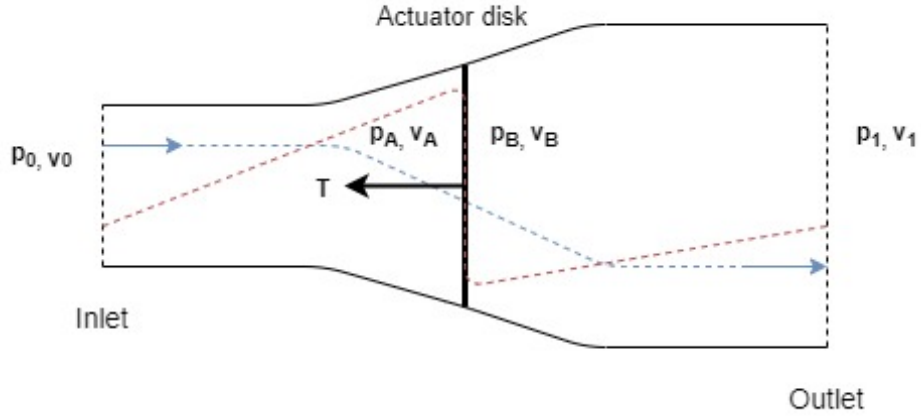


Figure 2.1: Overview of actuator disk model with control volume used in momentum theory, adopted from [1] and [8]. The blue and red lines are development of the velocity and pressure respectively.

where

- $T$  is thrust
- $v_0$  is the flow velocity far in front of rotor
- $v_A$  is the flow velocity before rotor disk
- $v_B$  is the flow velocity after rotor disk
- $v_1$  is the flow velocity far behind the rotor
- $p_0$  is the pressure far in front of rotor
- $p_A$  is the pressure before rotor disk
- $p_B$  is the pressure after rotor disk
- $p_1$  is the pressure far behind the rotor

The wind flows from the inlet far upstream of the rotor and will slow down as it approaches the rotor disk and up to the outlet, which is why the boundary stream lines diverges [24]. At the same time, the pressure will increase from ambient pressure, experience a pressure drop over the disk and then increase up to ambient pressure far behind the disk. Hence, the velocity is the largest at the inlet and smallest at the outlet, while the pressure is highest right in front of the rotor disk and lowest right after.

Since there is no flow exchange across the lines in Figure 2.1 and the flow is incompressible, the conservation of mass between the inlet and outlet will follow Equation (2), meaning that the mass flow over the inlet of the control volume must be equal to the mass flow over the outlet [8].

$$\rho A_0 v_0 = \rho A_1 v_1 = \dot{m} \quad (2)$$

where

- $A_0$  is the inlet area
- $A_1$  is the outlet area

---

$\rho$  is the air density  
 $\dot{m}$  is the mass flow

By using conservation of momentum between the inlet and the outlet of the flow, the rate of change of momentum across the rotor disk must be equal to the thrust force [1] [8]. The thrust may therefore be expressed according to Equation (3) [1].

$$T = v_0 (\rho A_0 v_0) - v_1 (\rho A_1 v_1) \quad (3)$$

This may now be used to find an expression for the inflow velocity on the disk,  $v_A$ , but first, another expression for the thrust must be derived.

Thrust is a force and thus a function of an area and pressure, meaning that the thrust may be expressed as the rotor disk area and the pressure difference across this disk. This pressure difference may not be calculated directly, but by using Bernoulli's equation on the control volume in front and behind the rotor disk separately, the pressure difference may be derived [8]. Equation (4) shows Bernoulli's equation for each of the mentioned control volumes, with the difference from the inlet to the rotor disk and from the rotor disk, to the outlet.

$$\begin{aligned} p_0 + \frac{1}{2}\rho v_0^2 &= p_A + \frac{1}{2}\rho v_A^2 \\ p_B + \frac{1}{2}\rho v_B^2 &= p_1 + \frac{1}{2}\rho v_1^2 \end{aligned} \quad (4)$$

By adding the two equations and rearranging, the equation for the pressure difference may be expressed according to Equation (5).

$$\Delta p = (p_A - p_B) = \frac{1}{2}\rho v_0^2 - \frac{1}{2}\rho v_1^2 \quad (5)$$

The thrust in Equation (6) is developed by combining the rotor disk area with Equation (5) [40].

$$T = (p_A - p_B)A = \frac{1}{2}\rho A (v_0^2 - v_1^2) \quad (6)$$

By demanding that the conservation of mass also applies across the rotor in combination with the two expressions for thrust given by Equation (3) and (6), the inflow velocity  $v_A$  may be expressed according to Equation (7) [40].

$$\rho A v_A (v_0 - v_1) = \frac{1}{2}\rho A (v_0^2 - v_A^2) \implies v_A = \frac{1}{2}(v_0 + v_1) \quad (7)$$

The axial induction factor,  $a$  is defined according to Equation (8) and is the ratio between the change in velocity between inflow and rotor, and the inflow velocity [24]. This may be used to

---

find a relation between the inlet velocity and inflow velocity on the rotor disk, but also between the inlet velocity the outlet velocity as shown in Equation (9)..

$$a = \frac{v_0 - v_A}{v_0} \quad (8)$$

By combining the solution for  $v_A$  in Equation (7) and Equation (8),  $v_A$  and  $v_0$  may be expressed as shown in Equation (9) [40].

$$\begin{aligned} v_A &= v_0 (1 - a) \\ v_1 &= v_0 (1 - 2a) \end{aligned} \quad (9)$$

It follows from the expression for  $v_1$  in Equation (9) that the axial induction factor can never be 0.5 or higher in this theory, as that would demand that the wind flow velocity for  $v_1$  must be zero or negative, meaning that the flow velocity at the outlet in Figure 2.1 is either zero or flowing backwards [40].

By using the fact that the wind turbine is slowing down the air by extracting energy, the power available in the wind may be calculated by the change in kinetic energy over time from the inlet to the outlet in Figure 2.1 as given by Equation (10) [1].

$$P = \frac{1}{2} \dot{m} (v_0^2 - v_1^2) = \frac{1}{2} \rho A v_A (v_0^2 - v_1^2) \quad (10)$$

Equation (9) and (10) may be combined and rearranged to formulate the power according to Equation (11) [40].

$$P = \frac{1}{2} \rho A 4 v_0^3 a (1 - a)^2 \quad (11)$$

Both the thrust and the power of a wind turbine are often given as dimensionless coefficients which are shown in Equation (12) and (13) respectively [40].

$$C_T = \frac{\text{Thrust force}}{\text{Dynamic force}} = \frac{T}{\frac{1}{2} \rho v_0^2 A} \quad (12)$$

$$C_P = \frac{\text{Rotor power}}{\text{Power in the wind}} = \frac{P}{\frac{1}{2} \rho v_0^3 A} \quad (13)$$

The power coefficient can be further developed by expressing the power in the numerator of Equation (13) according to Equation (11) to express the power as shown in Equation (14) [40].

$$C_P = 4 a (1 - a)^2 \quad (14)$$


---



---

It may further be shown that the maximum value for  $C_P$  is 16/27 or 0.5926 given for  $a = 1/3$  [40].

### 2.1.2 Momentum theory with wake rotation

One of the assumptions of the simple momentum theory is that there is no rotation of the wake. Nevertheless, the torque working on the flow from the rotor will cause the flow to rotate in the opposite direction from the rotor [40]. The kinetic energy required for inducing this rotation will reduce the power extraction by the wind turbine and should be accounted for.

Taking into account that the angular velocity of the air relative to the blade increases from  $\Omega$  to  $\Omega + \omega$ , but that the axial velocity is unaffected by the rotation, the pressure difference across the wind turbine rotor may be expressed by Equation (15) [40]. Note that  $\Omega$  is the angular velocity of the rotor and  $\omega$  is the induced angular velocity on the free stream [1].

$$\Delta p = (p_A - p_B) = \rho \left( \Omega + \frac{1}{2} \omega \right) \omega r^2 \quad (15)$$

In order to account for the changes over the disk, the thrust and torque is calculated over segments of the disk area and integrated to get the total value.

The angular induction factor is introduced and is defined according to Equation (16) [40].

$$a' = \frac{\omega}{2\Omega} \quad (16)$$

Since the thrust is given by Equation (6) and the pressure difference is redefined, the thrust per radial segment of the rotor disk may be expressed according to Equation (17) [40].

$$dT = \left[ \rho \left( \Omega + \frac{1}{2} \omega \right) \omega r^2 \right] 2\pi r dr \quad (17)$$

Equation (16) and (17) may be combined and rewritten to express the thrust according to Equation (18) [40].

$$dT = \frac{1}{2} \rho \Omega^2 4a'(1+a') r^2 2\pi r dr \quad (18)$$

However, the thrust may also be expressed according to the axial induction factor according to Equation (19) [40].

$$dT = 4a(1-a) \frac{1}{2} \rho v_0^2 2\pi r dr \quad (19)$$

Additionally, the induction factors may be related to the local tip speed ratio,  $\lambda_r$ . The tip speed ratio  $\lambda$  and the local tip speed ratio  $\lambda_r$  are given in Equation (20) and (21) [40].

---


$$\lambda = \frac{\Omega R}{v_0} \quad (20)$$

$$\lambda_r = \frac{r \lambda}{R} = \frac{r \Omega}{v_0} \quad (21)$$

where

$R$  is the radius of the rotor  
 $r$  is the local radius  
 $\Omega$  is the rotor angular velocity  
 $v_0$  is the free stream velocity

From combining Equation (18), (19), (20) and (21), the relation of the induction factors and the local tip speed ratio is expressed according to Equation (22) [40].

$$\frac{a(1-a)}{a'(1+a')} = \lambda_r^2 \quad (22)$$

The torque is also influenced by the rotational flow of the wake and may now be updated. Since the change in momentum of the wake must be equal to the torque on the rotor, the torque may be formulated as shown in Equation (23) [40].

$$dQ = d\dot{m}(\omega r)r = (\rho v_A 2\pi dr) (\omega r) r \quad (23)$$

By including the relation of Equation (9) and (16), the torque may further be developed as given in Equation (24) [40].

$$dQ = 4a'(1-a)\frac{1}{2}\rho v_0 \Omega r^2 2\pi r dr \quad (24)$$

Equation (1) show that the power is given by the torque and rotational speed, hence the incremental power may be given as the incremental torque multiplied with rotational velocity [40]. Using this relation in addition to Equation (20) and (21) the power per radial section may be expressed according to Equation (25).

$$dP = \frac{1}{2}\rho A v_0^3 (8a'(1-a))\frac{\lambda_r^3}{\lambda^2} d\lambda_r \quad (25)$$

This result combined with the expression for the power coefficient  $C_P$  given in Equation (13), gives the expression for the power coefficient given in Equation (26) [40].

$$C_P = \frac{8}{\lambda^2} \int_0^\lambda a'(1-a)\lambda_r^3 d\lambda_r \quad (26)$$

---

By solving this and re-writing, the angular induction factor may be given by the axial induction factor and the local tip speed ratio as shown in Equation (27) [40].

$$a' = -\frac{1}{2} + \frac{1}{2} \sqrt{1 + \frac{4}{\lambda_r} a(1-a)} \quad (27)$$

The maximum power production will occur when  $a'(1-a)$  reaches its maximum value, and with this, it may be shown that Equation (27) can be developed into Equation (28) to give a relation between the two induction factors [40].

$$a' = \frac{1-3a}{4a-1} \quad (28)$$

### 2.1.3 Airfoil theory

The blades of the wind turbine are shaped like airfoils that span the length of the blade and use the wind to generate the force which make the rotor spin with an angular velocity and a torque, i.e. mechanical power [40]. Due to the shape of this airfoil there is a pressure decrease on the suction side of the foil and a pressure increase on the pressure side, which will generate a force. This force combined with the frictional forces are the origins of the lift and drag forces and a pitching moment. As may be seen in Figure 2.2, the lift force  $L$  works perpendicular to the inflow wind, while the drag force  $D$  works parallel. The pitching moment  $M$  works a quarter of a length from the front of the foil, which is called the leading edge. Note that in this figure, the suction side is on the top side of the foil, and the pressure side is on the bottom side.

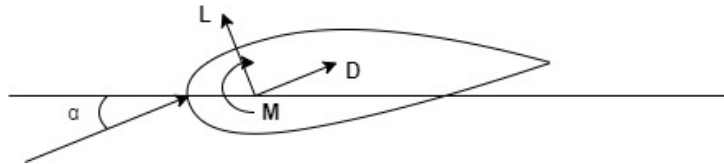


Figure 2.2: The lift and drag forces and pitching moment on an airfoil, adopted from [1]

In Figure 2.2, the inflow angle of attack,  $\alpha$ , is shown. This angle is important for the lift force and is one of the parameters that is usually controlled in a wind turbine by pitch control. For a thin and symmetric foil, the lift coefficient is given by Equation (29) [1]. Note that the lift coefficient depends on the camber, i.e. the shape of the foil as well, and may not be zero at zero angle of attack for cambered foils. However, the slope of  $2\pi$  is the same as for thin and symmetric foils.

$$C_L = 2\pi\alpha \quad (29)$$

As mentioned above, the pressure difference on each side of the foil is the cause of the lift. The lift force may be expressed according to the Kutta-Joukowski equation per radial section of the blade as given in Equation (30), where  $\rho$  is the fluid density,  $U_\infty$  is the inflow velocity and  $\Gamma$  is

the circulation [8].

$$L = \rho U_\infty \times \Gamma \quad (30)$$

Circulation is the vorticity integrated over the area of interest where the vorticity comes from the flow over the foil [40]. The foil causes the flow to rotate and the angular velocity of the particles is characterised by the vorticity. This means that there must be a circulation around the foil, and the lift may be understood based on this circulation.

#### 2.1.4 Blade Element Momentum (BEM) theory

The Blade Element Momentum (BEM) method developed by Glauert in 1935 allows calculation of steady loads of the rotor that may be used to find the aerodynamic forces and velocities [24]. This combines the theories already presented above, including the induction factors and the airfoil theory.

From the induction factors, the thrust and torque at each radial segment may be calculated. However, these may also be calculated from the lift and drag from the foil theory, as will be presented in the following section [40]. Hence, by combining these values, it is possible to do iterations to find the correct angle of the foil and the induction factors, allowing for calculation of the thrust and torque used in simulations. In order to reach the desired results, a few things must be defined first.

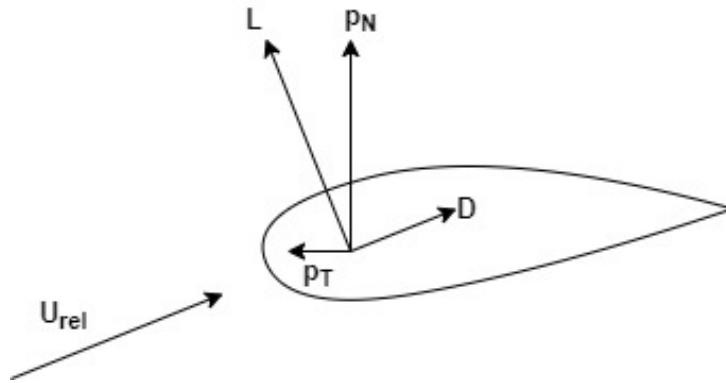


Figure 2.3: Forces and relative inflow velocity of a foil, adopted from [1]

Figure 2.3 shows the lift and drag forces on the foil, which may be translated to a force normal and tangential to the rotor plane, denoted  $p_N$  and  $p_T$  respectively [24]. The angle  $\phi$  is defined as the angle between the relative velocity  $U_{rel}$  and the plane of rotation, or the angle between the lift and drag and the rotor plane coordinates. The angle  $\phi$  consist of the angle of attack  $\alpha$ , pitch angle  $\theta_p$  and the twist of the blade  $\beta$  as shown in Equation (31). The relations between these forces and the angle  $\phi$  are given in Equation (32) and (33).

$$\phi = \alpha + (\theta_p + \beta) = \alpha + \theta \quad (31)$$

---


$$p_N = L \cos(\phi) + D \sin(\phi) \quad (32)$$

$$p_T = L \sin(\phi) - D \cos(\phi) \quad (33)$$

The torque and thrust may be expressed by using these relations as shown in Equation (34) and (35) where  $B$  is the number of rotor blades [24].

$$dT = B p_N dr = B L \cos(\phi) + D \sin(\phi) dr \quad (34)$$

$$dQ = B p_T dr = B L \sin(\phi) - D \cos(\phi) dr \quad (35)$$

These equations are set equal to the thrust and torque equations given in Equation (18) and (24) respectively [1]. Additionally, the lift and drag coefficients are required, and these are defined in Equation (36) and (37) where  $L/l$  is the unit lift force and  $D/l$  is the unit drag force.  $\rho$  is the fluid density,  $c$  is the chord length and  $U_{rel}$  is the relative wind velocity [40].

$$C_l = \frac{L/l}{\frac{1}{2}\rho U_{rel}^2 c} \quad (36)$$

$$C_d = \frac{D/l}{\frac{1}{2}\rho U_{rel}^2 c} \quad (37)$$

The normal and tangential coefficients,  $C_n$  and  $C_t$ , are used in the upcoming calculations and are given by Equation (38) and (39) respectively [24].

$$C_n = C_l \cos(\phi) + C_d \sin(\phi) \quad (38)$$

$$C_t = C_l \sin(\phi) - C_d \cos(\phi) \quad (39)$$

Setting Equation (18) equal to Equation (34) and using Equation (38), the axial induction factor may be expressed according to Equation (40) [24]. Here the solidity  $\sigma$  is defined as given by Equation (41), where  $c(r)$  is the chord length at a given radial segment  $r$  [24].

$$a = \left[ \frac{4 \sin^2(\phi)}{\sigma C_n} + 1 \right]^{-1} \quad (40)$$

$$\sigma(r) = \frac{c(r) B}{2\pi r} \quad (41)$$

---

Similarly, the angular induction factor may be expressed by Equation (24) and (35) combined with Equation (39) [24]. The result is shown in Equation (42).

$$a' = \left[ \frac{4 \sin(\phi) \cos(\phi)}{\sigma C_t} - 1 \right]^{-1} \quad (42)$$

The angle  $\phi$  is dependent on the induction factors because it is being calculated using Equation (43) [24].

$$\tan(\phi) = \frac{(1 - a) v_0}{(1 + a') \omega r} \quad (43)$$

These equations must therefore be solved by iteration [1]. The induction factors are chosen, then  $\phi$ ,  $C_l$  and  $C_d$  are calculated. The results from these are then used to calculate the induction factors again by the use of Equation (38), (39), (40) and (42). This is repeated until the value of the induction factors converges within a chosen tolerance.

### 2.1.5 Prandtl correction

In the BEM theory, infinite number of blades are assumed as described in Section 2.1.1 although the actual rotor will have finite number of blades. The pressure difference over each blade will cause the airflow to flow around the tip of the foil, which leads to reduced lift near the tip of the blade [40]. The effect of this is more significant when there are fewer and wider blades. This may be corrected using Prandtl's correction, which is given in Equation (44) and (45) [24].

$$F = \frac{2}{\pi} \cos^{-1}(e^{-f}) \quad (44)$$

$$f = \frac{B(R - r)}{2r \sin(\phi)} \quad (45)$$

The Prandtl correction  $F$  is added to the induced velocities as shown in Equation (46) and (47) [24].

$$a = \left[ \frac{4 F \sin^2(\phi)}{\sigma C_n} + 1 \right]^{-1} \quad (46)$$

$$a' = \left[ \frac{4 F \sin(\phi) \cos(\phi)}{\sigma C_t} - 1 \right]^{-1} \quad (47)$$

---

### 2.1.6 Dynamic wake model / Dynamic inflow

The above mentioned aerodynamic model assumes steady state aerodynamics where a change in the wind speed will lead to the axial induction factor being updated instantaneously with the change of power production [40]. However, when the wind flow and operation of the rotor changes rapidly, for example due to turbulence or wind turbine control, there may be delays in the flow field response to these changes.

These changes due to the dynamic inflow may be included in the BEM code by S. Øye's model, which is applied as a filter to the induced velocities as given in Equation (48) and (49) [24].

$$W_{int} + \tau_1 \frac{dW_{int}}{dt} = W_{qs} + k \tau_1 \frac{dW_{qs}}{dt} \quad (48)$$

$$W + \tau_2 \frac{dW}{dt} = W_{int} \quad (49)$$

where

$W_{qs}$  is the quasi-static value of the resulting induced velocity by using both induction factor

$W_{int}$  is the intermediate induced velocity

$W$  is the final induced velocity

$\tau_1$  and  $\tau_2$  are time constants

### 2.1.7 Tower shadow

Tower shadow occurs when the tower is blocking the wind flow and causes a wind speed reduction both in front and behind the tower [8]. It will be most significant with tubular towers, and because of the separation behind a cylindrical shape, the tower shadow effects will be larger behind the tower, while still present in front. The blades will feel the effect of the tower shadow when it passes in front of the tower, once per revolution. It will cause rapid power drop and a dynamic change in the bending moments for the blades [8] [40].

### 2.1.8 Dynamic stall

The wind is dynamic and the flow on the blades may change rapidly, meaning that the angle of the foil may not fit the air inflow, which again may either delay or induce stalling [40]. The inflow may change due to the turbulence in the wind or because of the tower shadow effects when the blades pass in front of the tower. Because of the dynamic changes, it may cause the blades not to stall during increasing wind speeds, resulting in large transient loads. There exist several models for this phenomenon; Beddoes-Leishman model, used in AeroDyn or the Stig Øye model used in HAWC2 [1]. AeroDyn and HAWC2 will be presented later.

---

### 2.1.9 Wind turbine wake interactions

As already seen in Section 2.1, the extraction of energy by one wind turbine will influence the wind flow in the wake, which may affect the downstream wind turbines operating in this wake. The main disadvantages of a wind turbine operating the wake are reduced power production, added turbulence causing unsteady loads and increased emissions of noise of the downstream turbine, although the latter is most important onshore [9]. The added loads may contribute to a reduced lifetime of the wind turbine.

## 2.2 Turbulence

Turbulence is the fluctuation of the wind that may vary quite a lot within short time, but that over time, typically 10 min, have an average of zero [8] [40]. As shown in Equation (50), turbulent wind in the main direction  $u$  will therefore have a mean velocity component  $\bar{U}$  and a fluctuating component  $\tilde{u}$ .

$$u = \bar{U} + \tilde{u} \quad (50)$$

The turbulence is mainly from the friction from the surface of the earth with the wind and from thermal effects [8]. The latter is due to warm air having a lower density than cold air and will therefore raise. The turbulence is often represented by the turbulence intensity,  $TI$ , which is defined according to Equation (51) where  $\sigma$  is the standard deviation of the wind speed.

$$TI = \frac{\sigma}{\bar{U}} \quad (51)$$

When using Equation (51) in design, the parameters must often be estimated. This may be done by choosing a wind speed class and turbulence class according to [10] as shown in Table 2.1. These classes are defined to cover the external conditions in different areas without having to define a specific site [10].

Table 2.1: Wind turbine class parameters from IEC 61400-1 [10]

Wind turbine class		I	II	III
$U_{avg}$	[m/s]	10	8.5	7.5
$U_{ref}$	[m/s]	50	42.5	17.5
A+	$I_{ref}$	0.18		
A	$I_{ref}$	0.16		
B	$I_{ref}$	0.14		
C	$I_{ref}$	0.12		

where

$U_{avg}$  is average wind speed per year

$U_{ref}$  is the 10 min average reference wind speed



---

$I_{ref}$  is the reference turbulence intensity for 15 m/s

A+, A, B, C are the category for the turbulence characteristics from very high to lower

The turbulence intensity with another velocity at the hub height may be found using the normal turbulence model shown in Equation (52) where  $U_{hub}$  is the wind speed at the hub [5].

$$\sigma_1 = I_{ref}(0.75 U_{hub} + 5.6) \quad (52)$$

The equation requires the wind speed at the hub and the average wind speed must be known, which will change based on the wind profile. These wind profiles have commonly been modelled using the logarithmic law or the power law which are shown in Equation (53) and Equation (54) respectively [10] [40]. These are both used for homogeneous and flat terrain, which is applicable for offshore conditions.

$$U(z) = U(z_r) \frac{\ln(z/z_0)}{\ln(z_r/z_0)} \quad (53)$$

$$U(z) = U(z_r) \left(\frac{z}{z_r}\right)^\alpha \quad (54)$$

where

$U(z)$  is the wind speed at  $z$

$z$  is the height

$z_r$  is the reference height

$z_0$  is the roughness length

$\alpha$  is the wind shear exponent

$U(z_r)$  is the wind speed at reference height

There are several different models for the turbulence in terms of power spectral density [40]. One of them is the von Karman spectrum that was developed for wind tunnels, meaning it is less applicable for the offshore estimation of the wind turbulence. According to IEC61400-1 either the the Kaimal model with coherence model or the Mann model must be applied [10]. In this thesis, TurbSim with the Kaimal spectral model and exponential coherence will be used, which is in accordance with the above mentioned standard.

### 2.2.1 Kaimal spectrum model

When selecting the IEC Kaimal model in Turbsim, the default input is to use the IEC Spatial Coherence model for the u-component [27]. The Kaimal spectrum is governed by Equation (55) [10].

$$\frac{f S_k(f)}{\sigma_k^2} = \frac{4 f L_k / U_{hub}}{(1 + 6 f L_k / U_{hub})^{5/3}} \quad (55)$$

---

where

$$\sigma_k^2 = \int_0^\infty S_k(f) df \quad (56)$$

and the parameters are:

- $f$  Frequency [Hz]
- $k$  Index for the direction of velocity component
- $S_k$  Single-sided velocity component spectrum
- $\sigma_k$  Standard deviation of velocity component
- $L_k$  Integral scale parameter of velocity component

A coherence model is a way of accounting for the fact that the wind and turbulence in each point are not completely independent within the same time [24]. The coherence model used in TurbSim is shown in Equation (57), but will not further be explained [10] [27].

$$\text{Coh}(r, f) = \exp\left[-12\left(\left(\frac{f r}{U_{hub}}\right)^2 + \left(0.12 \frac{r}{L_c}\right)^2\right)^{0.5}\right] \quad (57)$$

Note that IEC 61400-1 [10] does not specify any coherence for the wind speed components  $v$  or  $w$  [27].

For further information on the Kaimal spectrum or the coherence model and how all of the components are calculated, see [10] or [27].

The user's guide for TurbSim v2.00.00, [27], used in this thesis is a draft version. Nevertheless, since it is written by Bonnie Jonkman who have developed TurbSim, is from 2016 and is posted on NREL's webpage, it is considered a trustworthy source for information about the software.

### 2.3 Hydrodynamics for wind turbines

For a floating wind turbine, the hydrodynamic forces are also external excitation forces that may affect the wind turbine response. The hydrodynamic forces acting on a floating body may be found by summation of the diffraction and radiation problem if assuming linear response [56].

Equation (58) shows the equation of motion in frequency domain where  $\mathbf{M}$  is the mass matrix,  $\mathbf{A}(\omega)$  is the added mass matrix,  $\mathbf{B}(\omega)$  is the damping matrix,  $\mathbf{C}$  is the stiffness matrix,  $\hat{\mathbf{X}}(\omega)$  is the diffraction forces vector from the waves and  $\hat{\xi}$  and  $\hat{\eta}(\omega)$  are both Fourier coefficients, the first from the motions of the structure and the latter from elevation of the waves [55].

$$[-\omega^2(\mathbf{M} + \mathbf{A}(\omega)) + i\omega\mathbf{B}(\omega) + \mathbf{C}]\hat{\xi}(\omega) = \hat{\mathbf{X}}(\omega)\hat{\eta}(\omega) \quad (58)$$

---

## 2.4 Wave modelling and wave spectrum

For a sea of irregular waves it is common to assume it is stationary, the wave elevation is normally distributed and that the wave process is ergodic, meaning that each time series of waves may represent another time series of waves [2] [56]. The wave surface elevation,  $\zeta$ , may then be represented by Equation (59) in the  $x$ - and  $y$ -direction at time  $t$ .

$$\zeta(x, y, t) = \sum_{i=1}^I \sum_{j=1}^J \sqrt{2 S(\omega_i, \theta_j) \Delta\omega \Delta\theta} \cos(\omega_i t - k_i x \cos(\theta_j) - k_i y \sin(\theta_j) + \epsilon_{ij}) \quad (59)$$

where

$i$  is the frequency index

$j$  is the direction index

$\omega_i$  is the frequency

$\theta_j$  is the direction angle

$\Delta\omega$  is the frequency interval

$\Delta\theta$  is the direction interval

$k_i$  is the wave number

$S(\omega_i, \theta_j)$  is the wave spectrum that will be further presented below

$\epsilon_{ij}$  is the phase angle that is a stochastic variable uniformly distributed between 0 and  $2\pi$

To model the wave elevation, a wave spectrum is required. There are different spectrums used for this, where Pierson-Moskowitz, ITTC and JONSWAP are examples [2]. These spectrums are specified by the significant wave height  $H_s$ , which is the average of the one third highest waves, and peak period  $T_p$  of the desired site. When the wave spectrum is known, Equation (59) may be used to model the wave surface elevation.

## 2.5 Wind turbines

This section will cover some of the topics that is related to the wind turbines.

### 2.5.1 Floating wind turbine concepts

In the LIFE50+ project, two models for floating wind turbines were developed, and these are openly available at Gitlab [16]. Details regarding the models may be found in [54] and [74]. These are both concept for substructures of the 10 MW reference drivetrain that DTU have developed.

Both of the models are developed at a water depth of 130 m and hub height of 119 m [54] [74].

---

## OO-Star

OO-Star is a semi-submersible design of a floating wind turbine with a 10 MW turbine by Olav Olsen [74]. It is made in the shape of a submersed star that connects three outer column pontoons to a central column where the tower is attached. The structure is moored using three chains with  $120^\circ$  where each have a clump weight attached. Further details regarding the model may be found in [55].

## Nautilus

The Nautilus semi-submersible design of a 10 MW wind turbine is designed with a submersed square structure that connects to a structure in the shape of an X, where the tower for the wind turbine is located in the middle [74]. This is also a part of the LIFE50+ project. Further information regarding this model may be found in [21].

### 2.5.2 Floating wind turbines and negative damping

The negative damping problem is caused by the controller for floating wind turbines when trying to achieve maximum power output while stabilising the structure [38]. The problem is that when the structure pitches forward, the relative velocity on the blades increases. The blades are then pitched to reduce the generator speed, which in turn causes a reduction in the thrust. With less thrust, the forward pitching motion of the structure is further accelerated. When the structure pitches backwards, the inverse will happen. This must be accounted for in the controller for the floating wind turbine [69].

## 2.6 Wind Turbine Simulation Tools

Before presenting the wind farm tools, a few common wind turbine tools will be presented, some of them only briefly. Simulating one wind turbine instead of a whole farm demands less computational power, but the influence the wind turbines have on each other is not directly included in the simulation.

### 2.6.1 HAWC2

HAWC2 is a tool for aero-elastic simulation of wind turbines in the time domain and was developed at DTU Wind Energy [32]. The name stands for Horizontal Axis Wind turbine simulation Code 2nd generation and it can simulate onshore wind turbines as well as some bottom fast and floating offshore wind turbines.

The aerodynamics used in HAWC2 is the BEM model presented in Section 2.1 with correction for dynamic stall, dynamic inflow in addition to some effects for skew inflow, shear effects and near wakes [32]. A turbulence generator is included in the software based on the Mann model, but external turbulence models may also be used as input instead.

---

Hydrodynamic loads are included using common models like Morrison's equation etc, while the kinematics of the water includes waves and currents [32].

### 2.6.2 SIMA

SIMA is another program that may be used for wind turbine modelling. It was developed for simulation and analysis of floating structures and marine operations, and may be used for simulation of offshore wind turbines for both fixed and floating substructures [64] [65]. The SIMA model can combine important physics within a model and perform an integrated analysis in time domain [64]. This analysis includes hydrodynamic loads, aerodynamics, the wind and structural loads on the tower and the control system for both torque and blade pitch.

The aerodynamics in SIMA is solved using BEM theory including the dynamic inflow and dynamic stall as presented in Section 2.1 [64]. The wind input may be either 2D wind, uniform wind or 3D wind, that may be included by importing wind field files from either TurbSim or IECWind.

SIMA calculates the hydrodynamic loads, the drag forces on the wind turbine body and can perform integrated analysis of wind and wave effects [64]. It also allows for including control of blade pitch or generator torque to achieve the desired performance or rotational speed of the wind turbine rotor.

### 2.6.3 FAST and OpenFAST

FAST is a simulation tool written in Fortran that was developed for coupled analysis of the dynamic response of wind turbines [37]. It solves the aero-hydro-servo-elastic non-linear dynamics in time domain, meaning that the simulation tool consist of the following models [30].

- Aerodynamic model
- Hydrodynamic model
- Control and electrical system (servo) dynamic model
- Structural (elastic) model

Version 8 is the latest version of FAST and is what has been the basis for transition to OpenFAST to facilitate the open-source development of the tool [37]. This include establishing a GitHub file and online documentation as referenced here. Some of the modules of FAST/OpenFAST are shown in Table 2.2, and each of the modules corresponds to different domains of the coupled solution to the aero-hydro-servo-elastic dynamics [30] [37]. A module interface and coupler ensures coupling between all the sub modules [37].

---

Table 2.2: Some of the modules of FAST in version 8, from [35]

Module	Description
ElastoDyn	Structural Dynamics
BeamDyn	Finite element blade structure dynamics
AeroDyn	Aerodynamics
InflowWind	Inflow Wind
ServoDyn	Dynamics of control and electrical drive
HydroDyn	Hydrodynamics
SubDyn	Substructure dynamics
MAP++	Mooring statics
MoorDyn	Mooring dynamics
IceFloe	Ice Dynamics, DNV
IceDyn	Ice Dynamics, UMich

The program allows for several different wind turbine configurations, and the user may choose between the following options, among others [35].

- Two- or three-blade horizontal axis rotor
- Stall or pitch regulation
- Teetering or rigid hub
- Rotor upwind or downwind
- Tubular or lattice tower
- Onshore or offshore installation, the latter including floating or bottom-fixed structure

Some of the most significant parts of FAST/OpenFAST for this report will be presented. Since the model will not look at the ice loads on a wind turbine, these will be omitted. Additionally, the SubDyn will not be discussed as it is used for calculation of fixed-bottom substructures like monopiles, tripods, jackets etc [13].

### **AeroDyn - Aerodynamic module**

AeroDyn is the aerodynamic module of OpenFAST and may be used on its own or interfaced with other programs like FAST and SIMPACK for aero-elastic simulation of wind turbines [33] [37]. The aerodynamic loads on tower and blades are calculated using the inflow data, and consider both dynamic stall and wake effects of the rotor [37].

AeroDyn consist of four models; one for the rotor wake and induction, one for the aerodynamics of the airfoil, one for the influence of the tower on the blades and one for the tower drag model [37].

The aerodynamic module use the BEM theory that was presented in Section 2.1 and under Section 2.1.4 and uses the induction factors to account for the wake influence [37].

---

## **HydroDyn - Hydrodynamic model**

HydroDyn is a hydrodynamic model that simulates the currents and waves in time-domain with either regular or irregular-, and short crested or long crested waves [34] [37]. As with AeroDyn, it may be used either alone or in combination with FAST [34]. The hydrodynamic loads may be calculated both for bottom fast and floating wind turbines and are solved either by use of strip-theory or potential theory, or with a combination of these [34] [35].

## **ServoDyn - Control and electrical system model**

The ServoDyn module focus on the control and the electrical system of the simulation [37]. This simulate the sensors and all the control devices like blade pitch actuators, generator torque, electrical power converters and controller logic among others.

## **ElastoDyn - Structural dynamics**

The ElastoDyn module simulates the drivetrain, support structure and the rotor elasticity based on the aerodynamic, hydrodynamic and gravitational loads in addition to the reactions from ServoDyn [37]. Note that the blades are only included in ElastoDyn if BeamDyn is not used.

The input file for the drivetrain requires the gearbox efficiency and gear ratio in addition to the drivetrain torsional spring and damper values [37].

## **BeamDyn - Finite Element Blade Structural Dynamics**

This module may be used to simulate the structural dynamics for slender structures, and in FAST this is used to model the structural dynamics of the blades [71]. This uses the Geometrically Exact Beam Theory (GEBT) model that support both large deflection and geometric non-linearity.

## **InflowWind**

The InflowWind module is used for processing the data for the wind inflow and supports wind files from TurbSim, Bladed and HAWC, while also including an internal wind model [57]. The internal model of InflowWind includes the following wind types to choose between [29]:

- Simple ambient wind
- Uniform wind
- Discrete wind events

Turbulent wind may be added by making wind files and using these as input to this module.

---

## Input files and running

The program is run using Windows command with input from the main input file, which is a .fst file [37]. Typical parameters here is the step size and the length of the simulation. Additionally, it includes the location of the files for the sub modules.

The sub module inputs are provided in .dat files with a file for each of AeroDyn, ServoDyn, HydroDyn, MoorDyn etc. This allows for a vast number of parameters that may be adjusted to suit the desired model.

## 2.7 State-of-the-Art Wind Farm Simulation Tools

As shown, there are several tools for simulation of wind turbines used today. However, the wake interaction between the turbines is not captured in the simulation of single turbines. By running simulations with the wind farm as a whole, this interaction may be captured.

In the following, some wind farm tools will be presented. Note however, that the tools that were quickly deemed not fit for co-simulation with a drivetrain is not extensively covered.

### 2.7.1 FLORIS

The FLOW Redirection and Induction in Steady state (FLORIS) model is a low fidelity wind farm modelling tool with low computational demand [30] [51]. FLORIS is used for estimating the performance of wind farms and for designing wind farm control [30].

There are several models included in FLORIS to model the wake. The Jensen model and Multi zone model are included for velocity deficit, the Jimenez model for wake deflection while the Gaussian model and the Curl model include both of these phenomenon [51]. Additionally, the TurbOPark model is added for wake velocity deficit and the Gauss-Curb-Hybrid (GCH) model includes the second-order wake steering effects.

FLORIS is a steady state model, meaning that it will not include the dynamics of a wind farm, hence it cannot predict the dynamic loads on the wind turbine [30].

### 2.7.2 SOWFA

Simulator fOr Wind Farm Applications (SOWFA) is developed by National Renewable Energy Laboratory (NREL) and is a Large Eddy Simulation (LES) model that is coupled with OpenFAST [28]. It is the FAST module, presented in Section 2.6.3, that is used for prediction of the wind farm performance and the wind turbine loads [30].

Large Eddy Simulation (LES) is a way of simulating turbulence by splitting the turbulent flow into large scale motions and small scale motions [75]. Then only the large scale motions are solved directly, significantly reducing the computational demand required compared to other turbulence models.



---

SOWFA is a high fidelity tool and includes computations of the turbulence and wake dynamics that requires days or weeks of computing time per 10-minute simulation [28] [30].

### 2.7.3 DWM

The Dynamic Wake Meandering (DWM) model is a mid-fidelity model consisting of three parts for predicting the performance and load dynamics of the wind farm [30]. These parts are the wake deficit model, the wake transport model and the wake turbulence model.

The wake deficit evolution is the reduction of the flow velocity in front of and over the rotor mentioned in Section 2.1.1 and the recovery of the flow to free stream downstream of the rotor. The evolution of the wake deficit is important for the performance, while wake meandering and added turbulence is important for the loads [29]. Wake meandering is the movement of the wake and in DWM this is considered as caused by the large turbulent eddies. In addition, the added turbulence due to the wake is usually added by an upscaling of the background turbulence [30].

Hence, the DWM model uses "splitting of the scales" to simulate the wake flow, where it considers that the wake deficit evolution are affected by small turbulent eddies, while the larger turbulent eddies influences the wake meandering [29]. Here, the small turbulence eddies are defined as less than two diameters while the large eddies are larger than two diameters.

The DWM model is coupled to the FAST module described in Section 2.6.3 for prediction of the loads on the wind turbines [30]. The way it is implemented allows simulation of a whole wind farm on a normal computer, which is an advantage. However, DWM does not account for two-way interaction of the wind turbines, making it less fit for control design and optimisation.

### 2.7.4 FAST.farm

FAST.farm is a mid-fidelity engineering tool developed by NREL for modelling of structural loads and power production of wind turbines in wind farms [28] [37]. It is an expansion of OpenFAST and is also coded in Fortran. FAST.farm aims to be a tool that provides accurate modelling and low computational cost to be used for engineering problems regarding wind farm performance and cost [30]. FAST.farm use FAST as presented in Section 2.6.3 to solve the aero-hydro-servo-elastic dynamics for each of the wind turbines within the wind farm, but is also based on some of the same principles as the DWM model presented in Section 2.7.3 [30] [37]. As for FAST, FAST.farm also allows for simulation of both bottom fast or floating wind turbines and include the loads from waves, wind and wake disturbances [30].

FAST.farm consist of four main computational modules and a driver that couples the calculations [30]. These four are the super controller (SC) that solves the dynamics of the controller, the FAST module that solves the aero-hydro-servo-elastic dynamics for each of the wind turbines individually, the wake dynamics module for each individual rotor and the module that calculates the ambient wind and wave effects across the wind farm. The driver combines these modules and ensure correct input to each module, in addition to driving the

time domain solution. A full overview of the modules is shown in Figure 2.4.

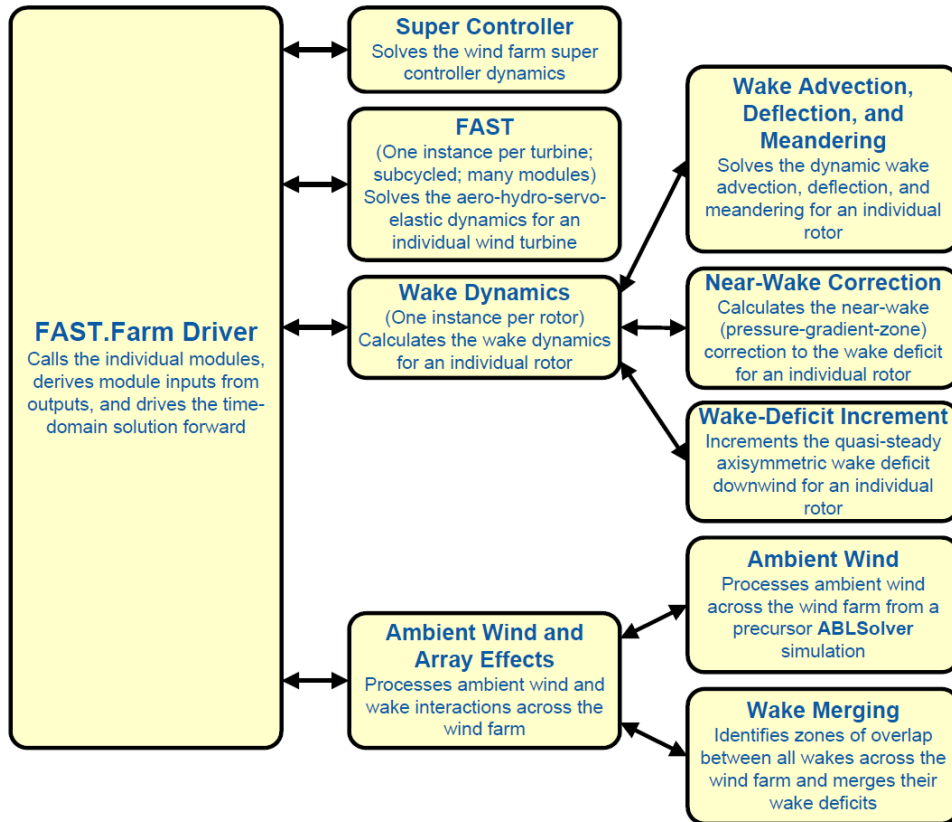


Figure 2.4: Overview of FAST.farm modules from [30]

The input file used is a .fstf file provided by the user, which also specifies the number of wind turbines and their location within the global coordinate system [30].

All states in FAST.Farm are given in discrete time both to simplify the coupling model and to ensure computational efficiency, and the time increment size is chosen by the user [30].

FAST.farm has been validated with the use of SOWFA presented in Section 2.7.2, and this showed that it performs reasonably well for predictions of generator power, torque, the rotor thrust and speed among other things [28]. The physics that were recommended to improve mostly concerns the wakes.

### Super controller (SC)

The super controller module may be used to control the wind farm so that the power performance is improved while the loads on the turbines are reduced [30]. The overall power production of the wind farm may be increased by either yawing the wind turbines to avoid wake interaction or by reducing the wake through induction control, meaning limiting the wind turbines by changing blade pitch or the generator torque.

The SC is more or less identical to the super controller used in SOWFA and the user may include the desired control for the whole wind farm in discrete time [30].

---

The inputs to the SC module are global measurements like the wind condition and input from individual turbines from either commands or measurements [30]. The outputs are the commands from the controller to the whole farm and to the individual turbine.

## **FAST and Module F**

This module is more or less FAST with the sub modules as described in Section 2.6.3, although it also includes a wrapper called module F that enables the coupling of FAST to FAST.farm [30]. Note that there is one module F per wind turbine and that this module both take inputs from and give inputs to several modules. The FAST module calculates the dynamics of each individual turbine, meaning the loads and motions from the environmental excitation and the coupled responses from the complete wind turbine model, including for example the nacelle, rotor etc.

The FAST module input file is a .fst file where the overall inputs for the wind turbine are chosen; for instance which parts to compute and which input files to use [37]. There will be one FAST input file per wind turbine, as specified in the .fstf file.

One of the modules is the inflow wind, that includes both ambient wind and wakes, and determines the local wind by using four-dimensional interpolation; three spatial in addition to the time-domain [30].

As mentioned above, the controller commands from the super controller for both the turbine and the global controller are used as input to module F [30]. The controller for each turbine may then account for the wind farm effects. The super controller is also provided with measurements and commands from each of the wind turbines through module F.

Many of the outputs from the FAST module are required as input to the wake dynamic (WD) module [30]. This includes the orientation of the turbine centreline, the position of the rotor in the global reference frame, the rotor diameter, the yaw error of the rotor etc.

Note that the submodules within FAST are of algebraic or continuous solutions, while some of them utilises time steps much smaller than what is used as the FAST.Farm time steps [30]. These differences are solved by calling the F module at the discrete time step of FAST.farm and delaying the output relative to input.

## **Wake Dynamics (WD)**

The Wake Dynamic (WD) module is used for the calculation of the wake dynamics for each rotor, meaning that there is one WD module per rotor [30]. As mentioned above, many of the inputs required for the WD module comes from the FAST module. The wake dynamic calculations includes the following [29]:

- Wake advection, deflection and meandering, solved for each rotor
- Near-wake correction
- Wake-deficit increment

---

Figure 2.4 shows an overview of the functions of each sub module [30].

The calculations requires many user-specific parameters that may be dependent on how the turbine is operated and what the atmospheric conditions are [30]. These parameters may be found by running high fidelity simulation as a preprocessor to the simulation by FAST.Farm, or by allowing the default values found from SOWFA simulations for each of the calibrated parameters.

### **Ambient Wind and Array Effects (AWAE) module**

The Ambient Wind and Array Effects (AWAE) module is added for processing the interactions between the ambient wind and the wakes in the wind farm [29]. It also includes two submodels as shown in Figure 2.4, one for the ambient wind and one for the wake merging [30].

For the modelling of the ambient wind, either precursor simulations or the InflowWind from OpenFAST/FAST may be used [29]. The precursor simulations may either come from high-fidelity Large-Eddy Simulations (LES) or from Ambient Boundary Layer solver (ABLSolver), and is then applied to the whole wind farm. The precursor simulations capture more physics, but are also more computational demanding, although they are only required to run once per condition.

## **2.8 Wind turbine drivetrain**

The drivetrain of a wind turbine is the part that converts the rotational power of the rotor to electrical power in the generator inside the nacelle of the wind turbine [49]. Drivetrains may be geared or gear-less and the choice between them will influence the required size of the generator [47] [49]. The types of gears are often divided in direct drive, medium speed and high speed drivetrains where the two latter are geared [47]. Only the geared types will be further discussed here.

The drivetrain of a wind turbine consist of several components and the design may differ from drivetrain to drivetrain. To go through of the typical layout of a drivetrain, the baseline drivetrain for a 5MW turbine designed by Nejad, A. R. et. al [48] [49] will be used.

In Figure 2.5, the above-mentioned drivetrain is shown, where the bearings are drawn as boxes with crosses. This drivetrain has a 4 point support layout, with two main bearings and two torque arms [49]. The main bearings are denoted INP-A and INP-B and are used to ensure that only torque loads are transferred to the gearbox.

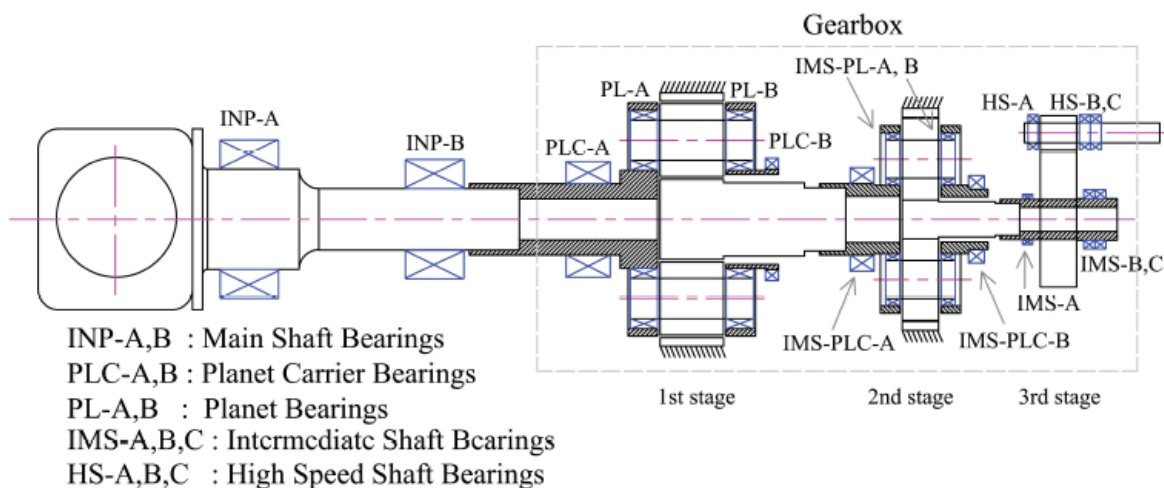


Figure 2.5: Overview of 5MW baseline drivetrain designed by A. R. Nejad [49]

This configuration of the drivetrain includes two planetary gear stages and a spur gear. The planetary gears are often used because of the high gear ratio within a compact design [49]. However, they are also more sensitive to manufacturing errors and elastic deformations in the other components. Note that only the gearbox including all the gears is outlined in Figure 2.5, hence the generator is not included in the figure.

The shafts are connected between each of the gear stages. The shaft between the rotor and the first gear stage is called the Low Speed Shaft (LSS) or main shaft, the shafts between the gears are called the Intermediate Speed Shafts (ISS) while the shaft between the spur gear and generator is called the High Speed Shaft (HSS).

As mentioned above, the drivetrain topology and the choice of gears will influence the size of the generator. There is a direct relationship between grid frequency, the rotational speed of the shaft and the number of poles in the generator, where the latter will influence the size of the generator [40]. This relationship is shown in Equation (60) where  $\omega_{rpm}$  is the rotational speed in rpm,  $f$  is the grid frequency and  $n_p$  is the number of poles in the generator.

$$\omega_{rpm} = \frac{120 f}{n_p} \quad (60)$$

Since the grid frequency is more or less constant, the number of poles must increase with lower shaft rotational speed [40]. This is the reason for including gears, because the increased rotational speed will decrease the number of poles and consequently the size of the generator.

The efficiency of a drivetrain and the gearbox, it depends on the configuration [49]. For planetary gears the efficiency is around 99% and helical gear stages around 98%.

---

### 2.8.1 DTU 10 MW drivetrain

The models referenced in Section 2.5 both use the DTU 10 MW wind turbine [74]. This is also used in the development of the high fidelity drivetrain developed by Wang. S, [73] that will be presented in Section 2.9.3. This model is developed at Technical University of Denmark (DTU) and the main parameters for the model is presented in Table 2.3.

Table 2.3: Main parameters for the DTU 10 MW drivetrain [73]

Parameter	Value	Unit
Rated power	10	MW
Cut-in wind speed	4	m/s
Rated wind speed	11.4	m/s
Cut-out wind speed	25	m/s
Rated rotational speed	9.6 / 1.0053	rpm / rad/s
Min rotational speed	6 / 0.6283	rpm / rad/s
Gearbox ratio	1:50	-
Rated generator speed	480 / 58.2655	rpm / rad/s
Torsional natural frequency (free-free)	4.003	Hz
Generator inertia	1500.5	kg m <sup>2</sup>
Equivalent drive-shaft torsional spring	2 317 025 352	Nm/rad
Equivalent drive-shaft torsional damping	9 240 560	Nm/(rad/s)

### 2.8.2 Gear general

Gears are used to transfer the power from one shaft to another with possibility of changing the direction of rotation and/or shaft, the rotational speed and the torque. This thesis will focus on gear pairs with parallel axis and planetary gears as these are the type of gears used in the drivetrain [49]. In drivetrains the gears are used to change the ratio between the rotational speed and the torque, from low speed and high torque at the hub to higher speed and lower torque in the generator.

There are several type of parallel axis gears, where one of the most simple is the spur gear with teeth perpendicular to the rotation of the gear [25]. A variation of this is the helical gear with teeth at an angle to make the gear meshing more gradual and thus softer. This will, however, create an axial force in the shaft that must be absorbed in the bearings. An example of a helical gear pair may be seen in Figure 2.6.

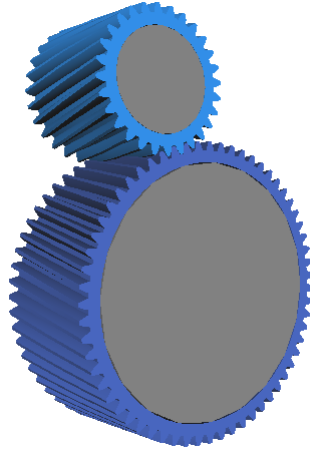


Figure 2.6: Example of helical gear pair modelled in Simpack

As mentioned, the planetary gears are used because they are compact while still being able to change the ratio of torque to rotational speed significantly [49]. Figure 2.7 shows the parts of these gears, with the sun gear in red, the planets in green and the ring gear in blue. In addition, the shaft may be seen in gray and the carrier that holds the planets are shown in orange. There will also be a shaft driving or being driven by the carrier.

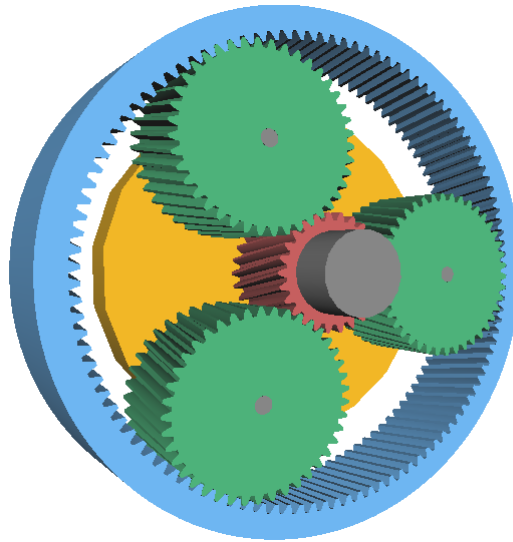


Figure 2.7: Example of planetary gear modelled in Simpack

The gear ratio is one of the parameters used for gears and explains the difference between the rotational driving gear and the driven gear [25]. Power equality between the gears means that the gear ratio will also equal the ratio of the radius of the driven gear to the driving gear. These relations are shown in Equation (61) for a basic gear pair with parallel axis.

$$i = \frac{\omega_{in}}{\omega_{out}} = \frac{r_{out}}{r_{in}} \quad (61)$$

For planetary gears, the relation between the rotational speed in and out will be different

because the ratio is dependent on several gears making up the total gear [25]. The relation will depend on if there is a speed reduction or increase. However, in the drivetrains reviewed in this thesis, the planet gears are used to increase the speed and the gear ratio will follow Equation (62).

$$i = \frac{\omega_{in}}{\omega_{out}} = \frac{1}{1 + Z_R/Z_S} \quad (62)$$

Another important parameter of gears is the module, that both explains the ratio of diameter to number of gear teeth, but also the diametrical pitch of the gear as shown in Equation (63) [25]. For two gears working together, the module must always be the same for each of the gears.

$$m = \frac{d}{z} = \frac{p}{\pi} \quad (63)$$

For a gear pair working together, the point of contact between two gears will follow a line, called line of action, as shown between A and B in Figure 2.8 [49]. The diameter at the point of contact for each gear is called the pitch circle, shown in blue in the same figure. The pressure angle is also marked in the figure, and the centre distance is the shortest distance between the centre of each of the gears [66].

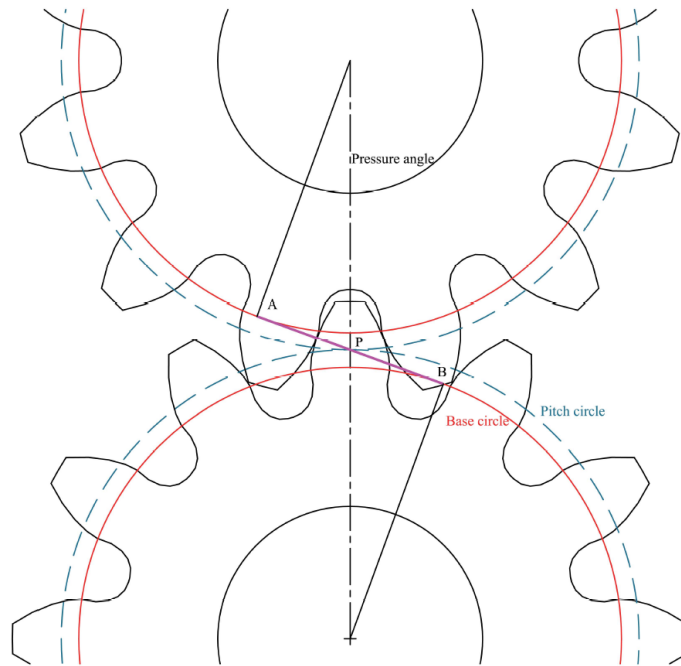


Figure 2.8: Common parameters for gears [49]

It should be noted that for a gear in a drivetrain, the mesh frequencies are the main contributor to the internal excitation [49]. The mesh frequencies,  $f_m$  is defined in Equation (64) where  $N_{gear}$  is the rotational speed for the gear in rounds per minute and  $Z$  is the number of teeth in the gear.



---

$$f_m = \frac{N_{gear} Z}{60} \quad (64)$$

### 2.8.3 Bearing general

Bearings are used to allow translation or rotation in one or more direction while restricting it in other directions. There are different types of bearings, but in this thesis the focus will be on the roller bearings as they are most common bearings used in wind turbines [49]. In roller bearings used for shafts, the relative motion between two elements is allowed using rolling parts like spheres or cylinders that are placed between two rings, where the outer and inner ring are connected to each of the machine elements [25].

The roller bearings are classified in two groups; radial bearings and thrust bearings [4]. The radial bearings are made to support the radial loads and either limited or no axial loads. Thrust bearings on the other hand, can take axial load and some radial loads or combined loads, but the rotational velocity cannot be as high as with radial bearings.

## 2.9 Existing drivetrain models

As mentioned, the drivetrain is the part of the wind turbine that transfer the power from the rotor to the generator and allows the wind power to be converted to electrical power [49]. The design of the drivetrain depends both on the generator chosen and on the power output as mentioned in Section 2.8. The current section will present some of the existing drivetrain models for a geared drivetrain.

### 2.9.1 Simple two mass drivetrain model

A simple way to model a drivetrain is the two mass model where the rotor and generator are modelled as single masses connected to shafts with a gear in between [49]. This model allows the user to add the first torsional mode of the drivetrain to the global analysis. Each of the masses have an inertia and each of the shafts have a stiffness which may be simplified by removing the gearbox entirely and introducing a rigid connection between the shafts. However, the gears introduce a change of rotational speed and torque that must then be accounted for as the loads on the two shafts will be different. How this is done will now be presented.

Firstly, the drivetrain is assumed to made up of the rotor mass, the generator mass and one gear only, and the model may be drawn as shown in Figure 2.9 [49].

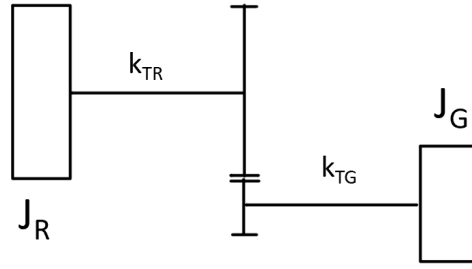


Figure 2.9: Drivetrain two mass model with gear, adopted from [49]

where

$J_R$  is the rotor inertia

$J_G$  is the generator inertia

$k_{TR}$  stiffness of the shaft connected to the rotor

$k_{TG}$  stiffness of the shaft connected to the generator

The model is further developed by removing the gear, but the gear must be taken into account in the representation of the stiffness and the inertia on the generator side [49]. These can be adjusted according to Equation (65) and (66) where  $n$  is the ratio between the rotational speed of the generator and the rotor, i.e. the inverse of the gear ratio. The resulting model is shown in Figure 2.10.

$$k_{TG}^* = n^2 k_{TG} \quad (65)$$

$$J_G^* = n^2 J_G \quad (66)$$

It should be noted that it is evident from Equation (65) and (66) that the gearbox will make the inertia and the stiffness on the generator side larger as compared to the rotor side [49]. This means that the drivetrain is not as sensitive to the variations in torque and this will reduce the component fatigue.

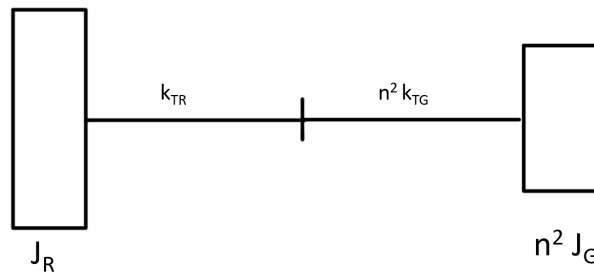


Figure 2.10: Drivetrain two mass model without gear, adopted from [49]

The two shafts are simplified into one shaft by combining the shaft stiffness. Since this means

that there are two stiffnesses in series, it may be shown that the equivalent stiffness will be as given in Equation (67) [25] [49]. The resulting model is shown in Figure 2.11.

$$k_{TEQ} = \left( \frac{1}{k_{TR}} + \frac{1}{n^2 k_{TG}} \right)^{-1} = \frac{k_{TR} n^2 k_{TG}}{k_{TR} + n^2 k_{TG}} \quad (67)$$

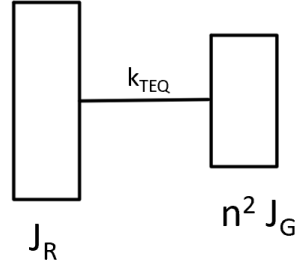


Figure 2.11: Final drivetrain two mass model, adopted from [49]

This model may now be utilised to find the equation of motion and hence the torsional natural frequency of the system [49]. The natural frequency in Hz is given by Equation (68).

$$f_n = \frac{1}{2\pi} \sqrt{\frac{k_{TEQ} (J_R + n^2 J_G)}{J_R n^2 J_G}} \quad (68)$$

Damping of the drivetrain may also be included in this model, which is what it used in OpenFAST and FAST.farm [45]. The model with damping and stiffness is given in Figure 2.12.

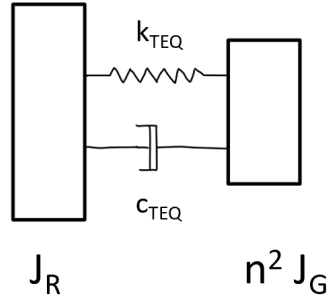


Figure 2.12: Drivetrain model with stiffness and damping, adopted from [45]

### 2.9.2 Torsional 5 mass model

A torsional 5 mass model have been created by Girsang, I.P. et. al. [22] [39]. This is using the Simscape/SimDriveline environment, now known as Simscape Driveline [42]. The drivetrain in this model consist of one planetary gear stage with three planets, two parallel gear sets and a fixed speed generator [39]. The five masses included is the rotor, the gear stages and the generator.

The five mass model may be used for co-simulation with FAST in Simulink [39]. For the gearbox, a purely torsional model is created of both the parallel gear stages and the planetary gear stage. This enables it to account for the gear dynamics related to the elastic deformation of the gear teeth, contributing to the gear stiffness.

For the co-simulation with FAST and Simscape, the internal drivetrain in FAST is reduced to a single mass drivetrain with only the main shaft [39]. This is achieved by setting the generator inertia to zero and the gear ratio to one. The model is implemented by changing some of the inputs in FAST so that the power and torque are given as input. See Section 3.7.1 for further information on how this is done. The equation of motion of the rotor may be expressed according to Equation (69).

$$J_{rot}\alpha_{rot} = T_{Aero} - T_{Opp} \quad (69)$$

where

- $J_{rot}$  is Rotor inertia
- $\alpha_{rot}$  Rotor acceleration
- $T_{Aero}$  Aerodynamic torque
- $T_{Opp}$  Opposing torque

The rotor inertia is assumed constant and the rotor acceleration is provided by the simple model in FAST [39]. The opposing torque is both provided to the FAST model and used to find the aerodynamic torque.

### 2.9.3 High fidelity drivetrain model

A high fidelity model of a medium speed drivetrain for the 10 MW reference turbine by Technical University of Denmark (DTU) was developed by Wang, S. [73]. The model is established using the multibody simulation modeling approach in Simpack, which is a multibody simulation tool that will be presented later in the thesis. The model of the drivetrain in 3D is shown in Figure 2.13 where the main components of the model are indicated.

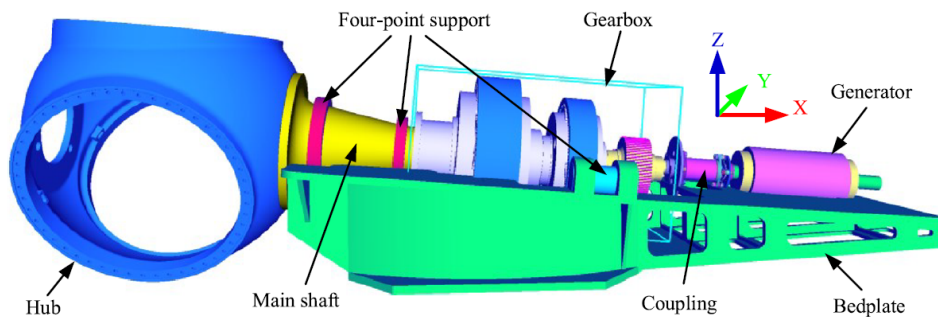


Figure 2.13: 3D model of 10 MW drivetrain from [73]

This drivetrain is designed as a four-point support drivetrain with three gear stages [73]. The model was validated by the use of the simplified drivetrain model that DTU uses and the design was also optimised with volume and weight in mind.

Figure 2.14 shows the design of the high fidelity drivetrain [73]. It includes two planetary gears and a helical gear. The planetary gears have five planets in the first gear stage and three planets in the second gear stage.

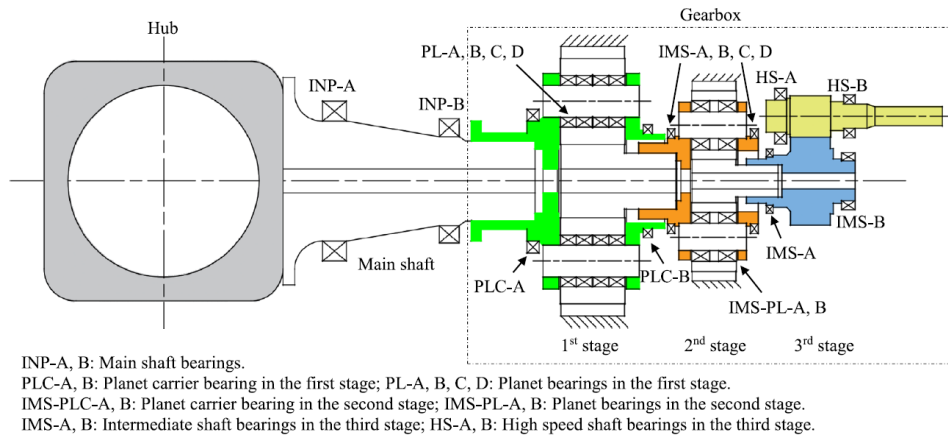


Figure 2.14: 2D model of 10 MW drivetrain from [73]

The model has capability of calculating the 20 year fatigue damage on the bearings and gears using the Palmgren-Miner hypothesis presented in Section 2.11 [73].

#### 2.9.4 Mathematical drivetrain model

Several of the existing models are analytical and solve the equations of motion (EOM) to find the load on the different components. Gallego-Calderon, J. et al. [20] obtained the equations of motions of the drivetrain from Lagrange's equation and used it in co-simulation with HAWC2. This was also the approach by Shi, W. et al. [62], which also used Fourier series to find the stiffness of each of the mesh stiffnesses. The EOM's are then solved using numerical methods [20] [62].

##### Dynamic Torsional model

The model by Shi, W. et al. [62] is a mathematical model of a drivetrain with one planetary gear stage with three planets and two stages of spur gears. It was developed for the torsional vibrations of the wind turbine and is a model with 10 DOF. Most of the shafts are modelled as flexible shafts and the gear mesh are modelled as springs with time varying stiffness expressed by Fourier series. The EOM was achieved using Lagrange, and is expressed according to Equation (70) with  $i = [rotor, c, cp1, cp2, cp3, s, g1, g2g3, g4, gen]$  for the wind turbine rotor, carrier, planet 1, 2 and 3, sun gear, gear 2, gear 2 to 3, gear 4 and generator respectively.  $L$  is the Lagrangian equation derived of the drivetrain,  $q_i$  is the DOF and  $Q$  is the external forces.

$$\frac{d}{dt} \left( \frac{\partial L}{\partial \dot{q}_i} \right) - \frac{\partial L}{\partial q_i} = Q \quad (70)$$

---

The EOM may then be summed up in matrix form and the response of the drivetrain may be solved using numerical techniques [62].

### 2.9.5 Fidelity requirements

For multibody models of drivetrains, there exist models with different fidelities that may be used for wind turbine drivetrain [59]. In this approach, each model is modelled with a number of DOFs where it may move as desired.

Torsional models only takes the torsional DOF into account and are among the simplest models for drivetrains [59]. They are achieved by fixing the five other DOFs than the torsional. These are generally connected with torsional stiffness or with the stiffness in gear contact, but may also include torsional damping.

Another approach to drivetrain modelling is to use rigid body models with several DOFs for each body and account for the flexibility of the components by using flexible connections [59]. This type of model is good for analyses of the internal dynamics of the drivetrain and bearing loads.

For even higher fidelity, the bodies may be modelled as flexible bodies that may deform due to the load and motions [59]. Here it is possible to use the Finite Element Method (FEM), which give each body DOF's in the range of 10,000-100,000.

NREL has given a recommendation for model fidelity for gearbox simulations from comparing multiple modelling tools and running sensitivity studies [23]. These recommendations are given to ensure accurate simulation of wind turbine gearboxes. Although it is done based on a three-point support of the drivetrain, it is assumed also to be relevant for the four-point support.

The conclusion of how to model each of the components of a drivetrain from the NREL study is included in Table 2.4 [23]. From a convergence study, the number of tooth slices should be 35, which was determined to be important for a gear designer for finding the tooth load distribution factor.

Table 2.4: Recommendation of minimum fidelity, from [23]

Component	Recommendation
Hub	Rigid body
Main shaft	Flexible body
Main Bearing	Stiffness matrix, 5 DOF
Gearbox housing	Flexible body
Panetary carrier	Flexible body
Gearbox shafts	Rigid body
Gearbox support	Stiffness matrix, 6 DOF
Gears	Rigid bodies, contact stiffness matrix of 6 DOF
Gearbox bearings	Stiffness matrix, 5 DOF
Spline	Stiffness matrix, 2 DOF
Bedplate	Rigid body
Generator coupling	Stiffness matrix, 5 DOF

Table 2.5 also include the parameters for the gearbox with corresponding importance for the gearbox motion [23].

Table 2.5: Recommendation of minimum fidelity, from [23]

Parameter	Importance
Manufacturing tolerance	Medium
Bearing clearance or preload	High
Gear tooth microgeometry	High
Bedplate tilting angle	Medium
Gravity	High
Nontorque loads	High
Gear mesh stiffness or transmission error	Medium

## 2.10 Drivetrain modelling tools

A few modelling tools have been evaluated for modelling of the drivetrain and these will be presented here.

### 2.10.1 Simscape

Simscape is an add-on to Simulink for modelling and simulation of physical systems and contains different modules for different disciplines; electrical, driveline, multibody and fluids [41]. Both Simscape Driveline and Simscape Multibody have been considered.

#### Simscape Driveline

Simscape Driveline contains libraries for creating models and running simulation of mechanical translational or rotational systems [42]. It includes models of important parts of a wind turbine drivetrain, like inertia, multiple type of gears in addition to springs and dampers. It is

---

also integrated with Simulink<sup>®</sup>, which may make MATLAB<sup>®</sup> and Simulink<sup>®</sup> a possible way to run co-simulations.

Although Simscape Driveline is a modeling tool for simulating rotational or translational mechanical system, it does not support having both rotational and translations movements [7]. That means that any model developed using Simscape Driveline cannot incorporate both torque and axial forces at the same time.

## **Simscape Multibody**

Simscape Multibody allows 3D modeling of mechanical systems for simulation, and as for Simscape Driveline, it is incorporated in Simulink<sup>®</sup> [43]. It is likely that this tool uses multibody system (MBS) simulation, however, finding background theory of the program was difficult hence it is difficult to ensure that it would be suitable for modelling of the drivetrain.

### **2.10.2 Simpack**

Simpack is a multibody system simulation (MBS) software that allows for simulation of non-linear motion of a system, and uses the theory presented in Section 2.10.3 [68]. The models may be made in 3D so that the dynamic motion and the coupling forces and stresses may be visualised, but may also be presented in 2D. It can be used for any mechanical or mechatronic systems, making it suitable for modelling of wind turbine drivetrains.

### **2.10.3 Multibody system (MBS) simulation**

Multibody system (MBS) dynamics or simulation are one of the most widely used numerical approaches for contact analysis, together with Finite Element Methods (FEM) [17]. Although FEM is a more powerful numerical method within this field, MBS demand less computational effort while still maintaining acceptable accuracy.

The MBS approach defines rigid bodies with mass that may move relative to each other [60]. These motions are restricted by joints that defines the constraints and the degrees of freedom (DOF) for each of the bodies. This means that a body may for example be restricted in rotational motions while allowing the body to translate in any direction. Further, force elements may be defined to rigid points on the bodies, called markers, and may represent forces, moments, dampers, contacts etc [49] [60]. These parts make up the main items within MSB simulation.

In addition to the types of items, there are two types of reference frames in MSB dynamics; global reference frame and body reference frame [61]. The global coordinate system is constant and does not change with time, making it a globally fixed frame of reference. The body reference system is the reference frame fixed to each body and will move with the body, hence it will change with time compared to the global reference frame.

By the use of markers and joints or forces, the influence one body or the global environment



---

have on another body may be modelled. These markers may be defined on any point on the body and the forces or joints are modelled from one marker to another [49].

## 2.11 Fatigue of drivetrain components

The drivetrain components, like the shafts, gears and bearing, may fail individually. Because of the rotation of the shafts of a wind turbine, the drivetrain is subject to many cycles, and the wind loads on the wind turbine also varies with time, which again affects the fatigue life [49]. It should be noted that the generator may also fail, but will not be considered in this part.

The Wöhler-curve, also called the SN-curve is the basis for the fatigue analysis of the components, especially for design [25]. This method is built on experimental fatigue results and depends both on the average stress and the amplitude of the stress cycle. Note that also corrections for size of material, the material surface, environmental effects, shape effects etc. may be accounted for in the stress. This also applies to different types of stress that can be combined to get the stress to use with the SN-curve. From the SN-curve, the ultimate number of cycles per stress case can be found.

The main parts of the drivetrain for fatigue analysis are the three mentioned above; the shaft, the gears and the bearing. How fatigue is estimated for these differ and will therefore be described separately in the following. But first the Palmgren-Miner hypothesis and the cycle counting method is presented.

### 2.11.1 Palmgren-Miner hypothesis

When the number of cycles are known, the damage may be estimated by the use of Palmgren-Miner linear damage hypothesis as shown in Equation (71) [25] [49]. Failure will happen when the damage  $D$  is equal to 1 [25].

$$D = \sum_{i=1} D_i = \sum_{i=1} \frac{n_i}{N_i} \quad (71)$$

where

$i$  count through each stress case

$n_i$  is the number of cycles for this stress

$N_i$  is the number of cycles the material can handle before failure under the same stress found from the SN-curve

$D$  is the damage

By using the values given in the SN-curve for each stress range, the total number of cycles may be re-written according to Equation (72), where  $K$  and  $m$  are given by the SN-curve and  $S_i$  is the stress level [50].

---


$$N_i = K S_i^{-m} \quad (72)$$

Consequently, the damage from Equation (71) may be rewritten to Equation (73).

$$D = \sum_{i=1} \frac{n_i}{K S_i^{-m}} = \frac{1}{K} \sum_{i=1} n_i S_i^m \quad (73)$$

This hypothesis is easy to use directly for shafts shaped like a cylinder. It may however, also be used for the gears, but then there are different ways of accounting for the geometry of the teeth and the gear to ensure that the root bending stress and surface pitting is taken into account [50]. This is done by adjusting both how the cycles are counted and how the bending stress is calculated.

### 2.11.2 Cycle counting method

The fatigue damage calculation of gears, shafts and bearings depends on the number of cycles that each of the components experience as shown in Equation (71) and (73). Therefore, it is important to find a way to count the cycles at each stress range.

Normally the method for cycle counting for gears and bearings in wind turbine design is the Load Duration Distribution (LDD) method [49]. This method bins the total time that the stress is within a certain range, and use that to find number of cycles [49]. With the LDD method, each measurement is registered with a time duration and the rpm. The number of cycles the load range last is then calculated using Equation (74) [50].

$$n_i = \frac{t_i}{60} \omega_{rpm} \quad (74)$$

where

where  $n_i$  is number of cycles

$t_i$  is the time in seconds

$\omega_{rpm}$  is the rotational speed in rounds per minute

The load bins are converted to stress ranges and the damage per stress range may be calculated according to Equation (71) or Equation (73) [50]. This method is visualised in Figure 2.15.

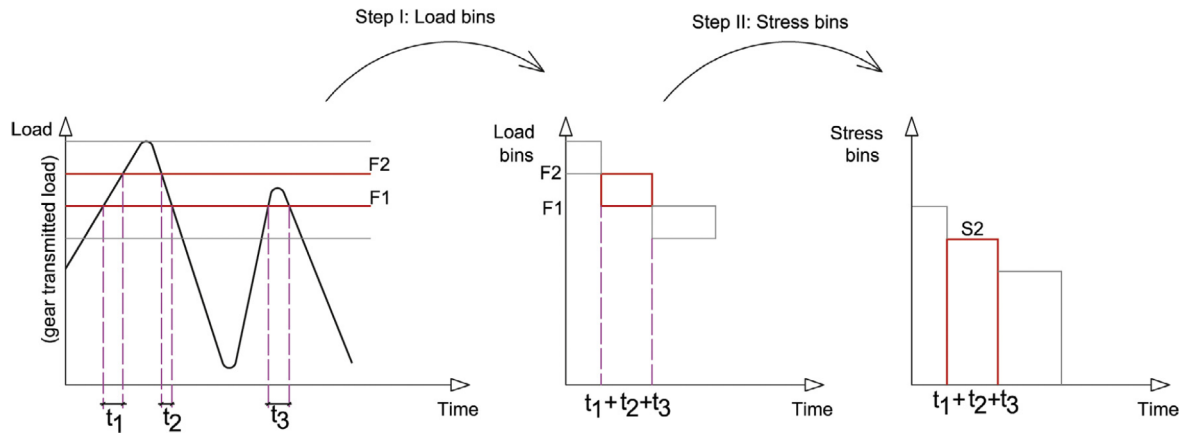


Figure 2.15: Figure showing how the LDD method is used, from [50]

There is another common cycle counting method called the Rainflow counting method, but because LDD is more common for gears and bearings it will not be discussed further here [49].

### 2.11.3 Bearing Fatigue

Fatigue for rolling contact bearings are calculated differently than for the shafts and gears. The way this is accounted for in roller bearings is based on testing performed by Lundberg and Plamgren in the 50's [49]. According to their hypothesis, the life of a roller bearing  $L$  may be calculated by the basic load rating  $C$  and the dynamic equivalent load  $P$  as shown in Equation (75). The life  $L$  refers to the number of million revolutions at the dynamic load  $P$  that 90% of bearings of the same type will tolerate before fatigue damage begin to occur [25] [49].

$$L = \left(\frac{C}{P}\right)^a \quad (75)$$

In Equation (75), the basic load rating  $C$  is constant and may be found from the manufacturer [49].  $a$  is a value that depends on the type of bearing where  $a = 3$  is used for ball bearings and  $a = 10/3$  is used for roller bearings.

The dynamic load  $P$  is calculated based on the radial and axial load on the bearing, and is given in Equation (76) [25].  $F_a$  and  $F_r$  are the axial and radial forces on the bearing respectively.  $X$  and  $Y$  are factors that are provided by the bearing manufacturer and are chosen based on the relation between  $F_a/F_r$  or  $F_a/C_0$  depending on the type of bearing [25] [49].

$$P = X F_r + Y F_a \quad (76)$$

Note that if the dynamic load  $P$  ends up being smaller than each of the forces  $F_a$  or  $F_r$ ,  $P$  is set equal to the largest of these [25].

The damage of the gear may then be estimated from Equation (77) where  $l_i$  is the million revolutions at the load case  $i$  [25] [49].

$$D = \sum_{i=1} \frac{l_i}{L_i} = \sum_{i=1} l_i \left( \frac{P_i}{C} \right)^a \quad (77)$$

#### 2.11.4 Gear fatigue

The gear fatigue is based both on tooth bending fatigue and surface pitting. How to calculate the first will be briefly presented here.

##### Tooth bending fatigue

The calculation of the tooth bending factor explained in ISO 3663-3 [67]. The gear root bending stress is calculated from Equation (78) and the coefficients that are used are included to account for the shape of the teeth in the gear [50].

$$S = \left[ \frac{F^t}{b m_n} Y_F Y_S Y_\beta Y_B Y_{DT} \right] K_A K_v K_{F\beta} K_{F\alpha} K_\gamma \quad (78)$$

The expression within the brackets are called the nominal tooth root stress [67]. The explanation of the coefficients is included in Table 2.6.

Table 2.6: Coefficients for gear root bending stress calculation [50] [67]

Coefficient	Meaning
$Y_F$	Form Factor
$Y_S$	Stress correction factor
$Y_\beta$	Helix angle factor. Account for lower bending moment intensity at the root than for spur gears
$Y_B$	Rim thickness factor. Applicable for thin rimmed gears
$Y_{DT}$	Deep tooth factor for contact ratios between 2 and 2,5
$K_A$	Application factor. Accounting for variation in load input and output
$K_\gamma$	Mesh load factor
$K_v$	Dynamic factor. Accounting for influence of the internal gear dynamics
$K_{F\beta}$	Face load factor
$K_{F\alpha}$	Transverse load factor

When the root bending stress is known, the stress is binned according to the LDD method, and ISO 6336-6 propose to use the maximum value of each bin to estimate the fatigue of the gear teeth [50].

#### 2.12 De-coupled analysis

The internal dynamic excitation of a wind turbine drivetrain tends to be in a much higher frequency range than the external excitation, as they are commonly within a frequency range of above 20 Hz and less than 2 Hz respectively [49]. This means that the frequencies of the

---

internal and external excitation does not overlap, and the required time step is much smaller for the drivetrain analysis than for external forces and dynamics of the wind turbine [49]. Therefore, a decoupled analysis may be performed, especially for a wind turbine drivetrain where the gearbox model may be very complex.

The decoupled analysis means that the analysis of different parts of the model is performed individually. For a wind turbine, the analysis may be performed according to the following steps, as explained by Nejad, A.R. [49]. First a global analysis is performed to find the forces and moments that is applied on the main shaft, which will be the input for the gearbox model in the second analysis. The second analysis may then be performed at a smaller time step to capture the important dynamics. However, this means that the outcome of the second analysis, i.e. vibrations and forces generated by the drivetrain, is not taken into account when the global analysis is run. Therefore, important dynamics that may cause fatigue or excitation of natural frequencies in the global system is not included.

## **2.13 Possibility of co-simulation and integrated simulation**

The aim of a co-simulation is to run simulations of the models and see how they interact with each other. This means that outputs are required from one model as input to the other model and vice versa. Integrated simulation is rather to run the simulations from one model with output to the next directly, but not necessarily with any values in return.

### **2.13.1 Inputs and outputs**

From the online documentation provided for OpenFAST and FAST.farm in [37], an excel file of all possible outputs is provided. Since ElastoDyn is the part that simulates the drivetrain, the values that would be of interest should come from this module. Additionally, the loads on the hub and the rotor would be of interest to simulate the loading on the drivetrain, main bearing and possibly gears. Because both FAST.farm and Dynamic Wake Meandering (DWM) model utilise FAST, the output required for the loads on the turbine will be the same for of these wind farm models as well. The possible outputs of ElastoDyn that are of interest are shown in Table 2.7.

---

Table 2.7: Possible outputs for hub and rotor loads from ElastoDyn [37]

Name	Description	Unit
LSShftFxa / RotThrust	Low-speed shaft thrust force, constant along the shaft and equivalent to the rotor thrust force	kN
LSShftFya	Rotating low-speed shaft shear force, constant along the shaft	kN
LSShftFza	Rotating low-speed shaft shear force, constant along the shaft	kN
LSShftFys	Nonrotating low-speed shaft shear force, constant along the shaft	kN
LSShftFzs	Nonrotating low-speed shaft shear force, constant along the shaft	kN
LSShftMxa / RotTorq	Low-speed shaft torque, constant along the shaft and equivalent to the rotor torque	kNm
LSSTipMya	Rotating low-speed shaft bending moment at the shaft tip, teeter pin for 2-blader, apex of rotation for 3-blader	kNm
LSSTipMza	Rotating low-speed shaft bending moment at the shaft tip, teeter pin for 2-blader, apex of rotation for 3-blader	kNm
LSSTipMys	Nonrotating low-speed shaft bending moment at the shaft tip, teeter pin for 2-blader, apex of rotation for 3-blader	kNm
LSSTipMzs	Nonrotating low-speed shaft bending moment at the shaft tip, teeter pin for 2-blader, apex of rotation for 3-blader	kNm
RotPwr	Rotor power, equivalent to the low-speed shaft power	kW

### 2.13.2 Dynamic Drivetrain Model

As mentioned in Section 2.10, one of the simulation tools that may be used for development of a dynamic drivetrain model is Simpack, which uses the Multibody System (MBS) simulation as described in Section 2.10.3. It is of interest for co-simulation and integrated simulation because of the advantages with lower computational demand than Finite Element Method (FEM), while still keeping acceptable accuracy [17]. However, this is dependent on the possibility of adding output from the wind farm tool as input to the drivetrain, as well as getting usable output from Simpack.

Excitations in Simpack is a force type that may be used to apply a force or torque from u-Vector Elements [12]. An Input Function may be defined using a database and .afs file. This way, the external input may be imported to Simpack as x and f(x) as tabled values with the possibility of interpolating between the points. The .afs file is the recommended file extension by Simulink<sup>®</sup> documentation and has some requirements for how the file is structured. The input is given to an Excitation element that is used in a u-Vector Element, which is further applied in Force Element 93: Force/Torque by u(t) Cmp. The torque and force from the external loads from the global model is added to the drivetrain model through this force element.

There is also a possibility of co-simulation of Simulink<sup>®</sup> and Simpack. However, this only supports OpenFAST and not FAST.farm [45]. This would be done using S-functions that allows for simulation of the models in Simulink<sup>®</sup> directly [44].

---

### 2.13.3 S-Functions in Simulink<sup>®</sup>

S-functions, or system-functions, is a functionality in Simulink<sup>®</sup> that allows for simulation of functions written in MATLAB<sup>®</sup>, C, C++ or Fortran in the Simulink<sup>®</sup> environment [44].

These functions are subroutines that are dynamically linked and that may be loaded and run by the MATLAB<sup>®</sup> execution engine. This is a functionality supported both by Simpack and by OpenFAST.

In order to use the Simpack S-function, u-Inputs and y-Outputs must be defined before the model is extracted [12]. These will be the inputs and outputs of the S-function in Simulink<sup>®</sup>. The u-Inputs uses u-Vector elements and the Simpack documentation [12] reveals that the combination of these are often used with external co-simulation signals. Additionally, Simpack allows for defining parameters in terms of *SubVars* that may be included as input to the S-function, making it possible for the user to specify these upon simulation.

The S-function is also available for FAST and OpenFAST and may be used for simulation in Simulink<sup>®</sup> [35]. This functionality was used when the five mass torsional model presented in Section 2.9.2 was simulated with FAST [39].

The S-function created for FAST requires an input array with 8 inputs in addition to NumAdditionalInputs, where the latter is set to zero according to recommendation according to normal practice [35]. These 8 inputs are given in Table 2.8 and are normally taken from ServoDyn. That means that to use these, some switches must be changed in the ServoDyn file in FAST in order to use the Simulink<sup>®</sup> inputs instead. Most of these are not applicable for the simulations in this thesis, and Table 2.8 shows which inputs that may be relevant. Using this functionality, a co-simulation may be performed.

Table 2.8: Relevant input to S-function of OpenFAST, directly from [35]

Parameter	Unit	Relevant input
Generator torque	Nm	Yes
Electrical power	W	Yes
Commanded yaw position	rad	No
Commanded yaw rate	rad/s	No
Commanded pitch for blade 1	rad	No
Commanded pitch for blade 2	rad	No
Commanded pitch for blade 3	rad	No
Fraction of maximum high-speed shaft braking torque	(0-1)	Yes

The input `VSContr1` in Servodyn is the Variable Speed Control where a value of 0 will give no control and set the turbine to fixed speed, value 4 will mean input from Simulink<sup>®</sup>, while value 5 will give input from the Bladed-style DLL [39]. The latter is what is originally part of the downloaded Nautilus model, while 4 is what should be used for co-simulation with the drivetrain from Simulink<sup>®</sup> and the global model in FAST.

---

#### 2.13.4 FMI/FMU

Functional Mock-up Interface (FMI) is a free standard made for the exchange of dynamic models [11]. It is created in the ITEA2 MODELISAR project and further work have been performed within the ITEA2 MODRIO project. The FMI define an Application Programming Interface (API). Each of the dynamic models are called a Functional Mock-up Unit (FMU) and the interface supports three different interface types:

- Co-simulation
- Model Exchange
- Scheduled Execution

The co-simulation contains both a scheduler and a solver and the interface connects this with the simulation environment [11]. The model exchange requires an external solver for the Ordinary Differential Equations (ODE), which may avoid any delays of the co-simulation. The scheduled execution is similar to the model exchange, but consist of several modules containing algorithms that are synchronised using a clock.

There are many programs today that supports FMI's, which may be viewed on the webpage of the project<sup>2</sup> [19]. Both MATLAB<sup>®</sup> and Simulink<sup>®</sup> support co-simulation, and the same does Simpack. However, neither of the wind turbine or wind farm tools presented in the thesis support it.

#### 2.13.5 Dynamic-Link Library - .dll

Dynamic-Link Library (DLL) is used in OpenFAST and FAST.farm for inputs to the program already, and both these programs may be downloaded with all the developer files as .dll-files [37] [52]. The DTU controller for the 10MW wind turbine is already included as a DLL, hence it is known that this is possible to use a DLL file with OpenFAST and FAST.farm. However, the challenge is to implement a library like this.

---

<sup>2</sup><https://fmi-standard.org/>



---

## 3 Methodology

From the presentation of the wind farm simulation tools, FAST.farm was deemed the most promising to run a dynamic analysis coupled with the drivetrain. For the wind turbine programs, OpenFAST was used.

This section covers the work done to achieve the objective of the Master's Thesis.

### 3.1 Reference models

The floating wind turbine used in this thesis is the Nautilus floating offshore wind turbine developed in the LIFE 50+ project presented in Section 2.5 [21] [54] [74]. The 10 MW drivetrain model developed by Wang, S., et al. [73] was for inspiration for the development of the reduced order drivetrain model, both because it fits the floating turbine and because some of the details are available.

### 3.2 FAST.farm

As previously mentioned, the two models for the 10 MW floating wind turbine OO-Star and Nautilus are available on Github [52]. To be able to run the models, the repository must first be downloaded to the computer. The same must be done with the OpenFAST and FAST.farm files, which are cloned to the computer using Windows command prompt. OpenFAST and FAST.farm executables are then built guided by the online documentation for these programs [35] [37]. Microsoft Visual Studio version 2022 was used for the builds.

The models in the LIFE 50+ project was developed for an older 32-bit version of OpenFAST, not FAST.farm. Because of this, the .dll file for the controller from DTU for 10 MW wind turbine did not work when compiling a 64-bit version of OpenFAST and FAST.farm. However, DTU have a controller open on Gitlab [3] that may be downloaded and compiled. To get the controller to work, the instruction was followed, however, the last step in the guide where the build is done did not work directly. Hence, it was attempted to do the build directly from Microsoft Visual Studio, but it did not work with the model either. These steps were attempted with both the Nautilus model and the OO-Star model.

However, a working version of the OpenFAST files for the Nautilus model with the DTU controller from Gitlab [16] was provided by PhD candidate Irene Rivera Arreba at NTNU. This model was first used with the OpenFAST executable files that was provided with the model, and was running well. It was advised to get OpenFAST to work before FAST.farm was tried, because debugging would be easier. Hence, the executables for version 3.0.0 of OpenFAST was run with the model that was provided by Arreba, I.R. To get this working, several of the model .dat files had to be updated, guided by both the error messages from OpenFAST and the online documentation [37].

It was also attempted to implemented the controller provided by Arreba, I.R. with the Nautilus model downloaded directly from the Gitlab [16] repository. This was done with

---

guidance from Arreba, I.R., but due to a combination of unclear documentation and various error messages in OpenFAST, this was abandoned.

With a working model in OpenFAST, the next step was to implement this in FAST.farm. When running the FAST.farm program, a new .fstf file must be made to give the input of all the files. A big challenge was that FAST.farm uses AeroDyn v15, while the model was using AeroDyn v14 [37]. The difference between these versions is quite significant and to help with update to the new AeroDyn version, Diederik van Binsbergen provided some files of the blades etc. However, FAST.farm continued to give errors and ultimately, the attempts of using FAST.farm was abandoned as agreed with supervisor Amir R. Nejad. This was done for two reasons. Firstly, FAST.farm includes FAST as one of the modules and is the only module required for the drivetrain. Secondly, it was desired to move on with the tasks more relevant to this thesis.

### 3.3 OpenFAST

OpenFAST allows the use of AeroDyn v14 and since FAST.farm utilise FAST for the calculation of the turbine loads, the hope when abandoning FAST.farm and using OpenFAST was that it may make it possible to integrate with FAST.farm later. The outputs from ElastoDyn that are used will be the same, although there will only be one output file as there is only one wind turbine.

As mentioned above, there was an unsuccessful effort to get the DTU controller to work, but through later investigation it was discovered that the DTU controller requires a very rigid and specific setup. This was eventually found and the program could be run with the Nautilus model.

OpenFAST version 3.0.0 was used and an update of the model parameters was performed according to the details provided in the online documentation [37] as well as by the error messages given by OpenFAST. This involved updating the files for HydroDyn, ServoDyn, ElastoDyn, AeroDyn and MoorDyn. Most of the updates involves new functionality of OpenFAST and were added without any value or specified to not include the additional functionality.

An advantage of using OpenFAST instead of FAST.farm is that there exist a possibility to add OpenFAST simulations to Simulink<sup>®</sup> by use of S-functions [35]. This functionality does not yet exist for FAST.farm.

#### Warning message in OpenFAST

When running the model in OpenFAST it gives the warning shown in Figure 3.1. According to Jonkman, J. [31], this is due to OpenFAST having an advanced algorithm that have an option for using corrective steps that are not supported by the DLL controller or by AeroDyn v14 when running ServoDyn.

```

FAST_Solution:FAST_AdvanceStates:SrvD_UpdateStates:DLL_controller_call:BladedInterface option was
designed for an explicit-loose coupling scheme. Using last calculated values from DLL on all
subsequent calls until time is advanced. Warning will not be displayed again.
FAST_Solution:CalcOutputs_And_SolveForInputs:SolveOption2:AD14_CalcOutput:AeroDyn was designed
for an explicit-loose coupling scheme. Using last calculated values from AeroDyn on all
subsequent calls until time is advanced. Warning will not be displayed again.

```

Figure 3.1: Error message in OpenFAST for DTU controller and AeroDyn

Nevertheless, Jonkman, J. mentioned that they found that adding the corrective steps made the convergence of some models better despite this warning [31]. Hence, this was ignored when running the model in this thesis.

### 3.4 Simscape Driveline

One of the drivetrain modelling tools that were investigated was Simscape Driveline, as presented in Section 2.10.1. The 10 MW drivetrain from DTU was used to make a two mass model and to get familiar with the modelling tool. The result is shown in Figure 3.2, and a larger figure may be seen in Appendix A.

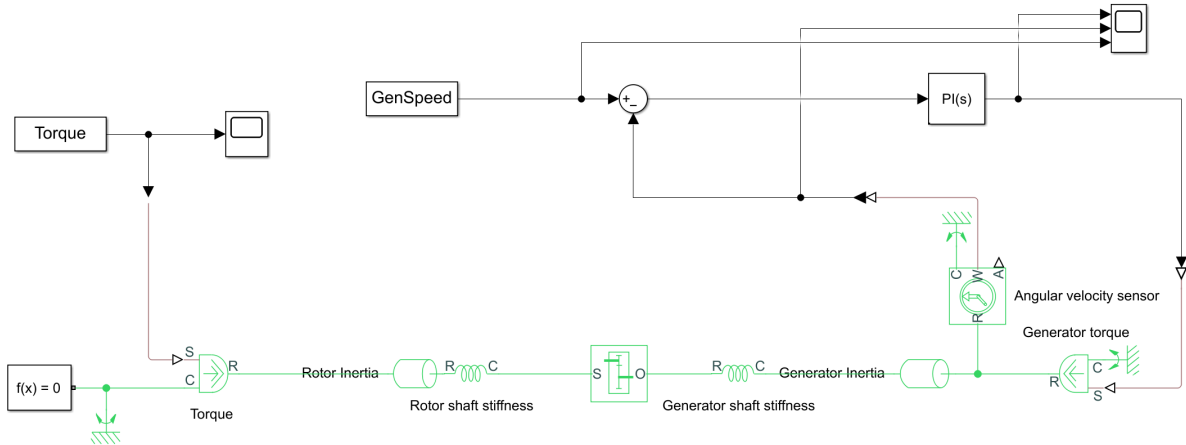


Figure 3.2: Simscape Driveline two mass model

However, including the thrust and torsional forces in the drivetrain have been one of the ambitions in this Master's Thesis. As presented in Section 2.10.1, Simscape Driveline only have the capability of either rotational or translational DOF. Based on this, Simscape Driveline was deemed not be suitable for the drivetrain model.

Nevertheless, the model was eventually used to find the values of the gains for the PI-controller that was included in the final drivetrain model. The generator in the developed drivetrain models is controlled using a PI-controller, governed by Equation (79) [73].

$$T_{gen} = k_p + k_i \int_0^t (\omega - \omega_{ref}) dt \quad (79)$$

where

---

$T_{gen}$  is the generator torque  
 $k_p$  is the proportional gain  
 $k_i$  is the integral gain  
 $\omega$  is the angular velocity  
 $\omega_{ref}$  is the reference value of the rotation velocity

The reference for the rotational velocity is taken from the global model using `GenSpeed` as input to the drivetrain model.

### 3.5 Development of reduced order model

Two different reduced order models of the drivetrain were made in Simpack as will be presented below. The first model have a higher fidelity than the second, but did not work as intended. This will be further discussed later.

#### 3.5.1 Drivetrain model with gears

The model shall be used to estimate the fatigue of the main bearings due to axial forces and rotational speed. Therefore, it must take in the torque and the axial load on the LSS from the global model. The LSS is allowed to rotate around its x-axis in addition to translation in the x-direction. However, to keep the model simple, the gears and high speed shaft are only allowed to rotate and take torque loads.

The reduced order model for drivetrain is also based on some of the model parameters of the drivetrain model developed by Wang, S. et al. [73]. The model of the drivetrain developed in Simpack is shown in Figure 3.3.

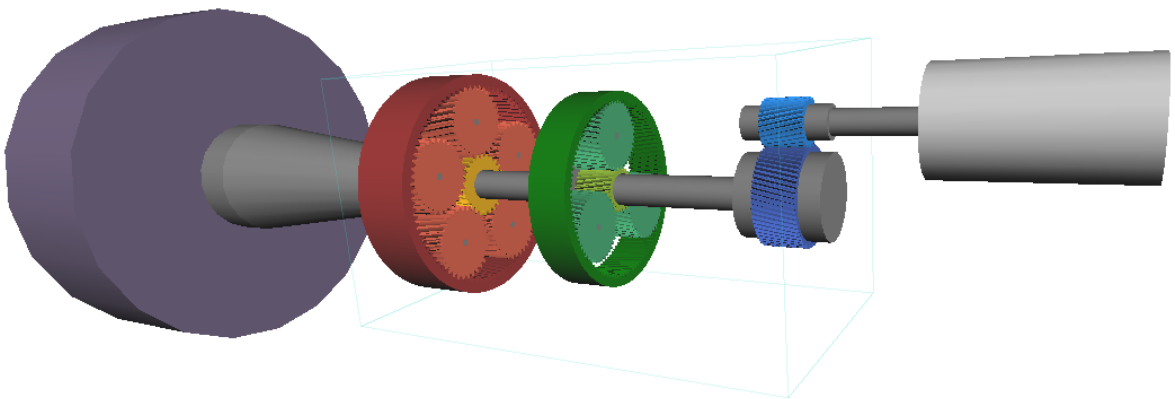


Figure 3.3: 3D figure of drivetrain model with gears in Simpack

Figure 3.4 and 3.5 shows the model in 2D with all the joints and forces added. The graphic is split in two, but a complete figure may be viewed in Figure B.1 in Appendix B. The 2D figures show all the bodies, joints and forces of the drivetrain model and are based on the information from Wang, S. et al. [73]. All joints with more than 0 DOF are marked with the DOF and the

force elements that represent the torque, thrust, bearing INP-A and INP-B as well as the force from the PI-controller. All force elements named 43 are the stiffnesses of the drivetrain, where 43 represent the force element number in Simpack. The force elements without numbers are those for the gears, where force element 225 is used.

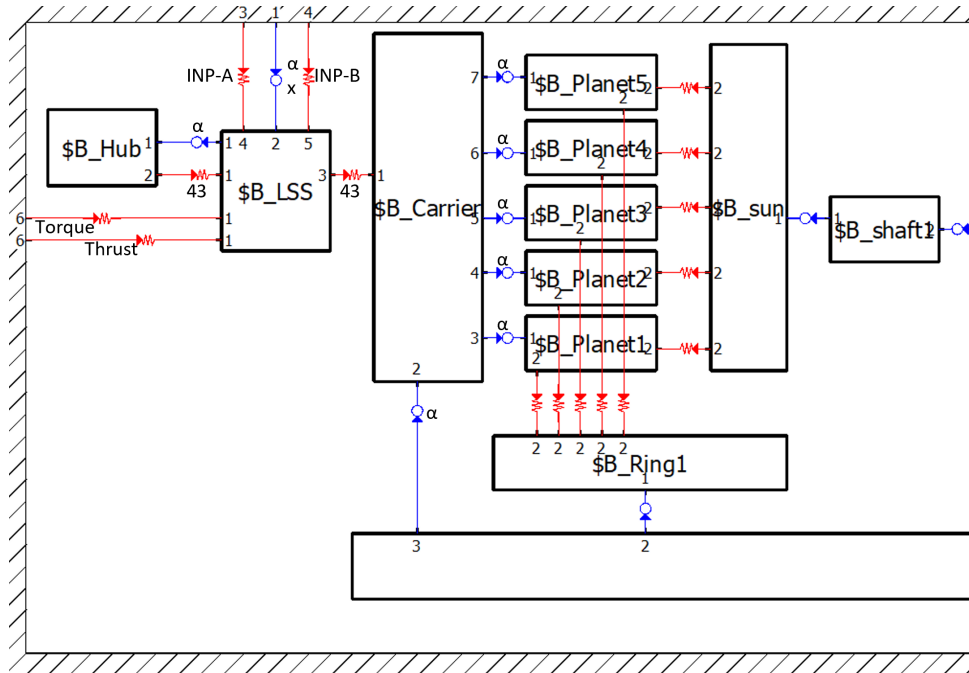


Figure 3.4: 2D figure of drivetrain model with gears in Simpack, part 1

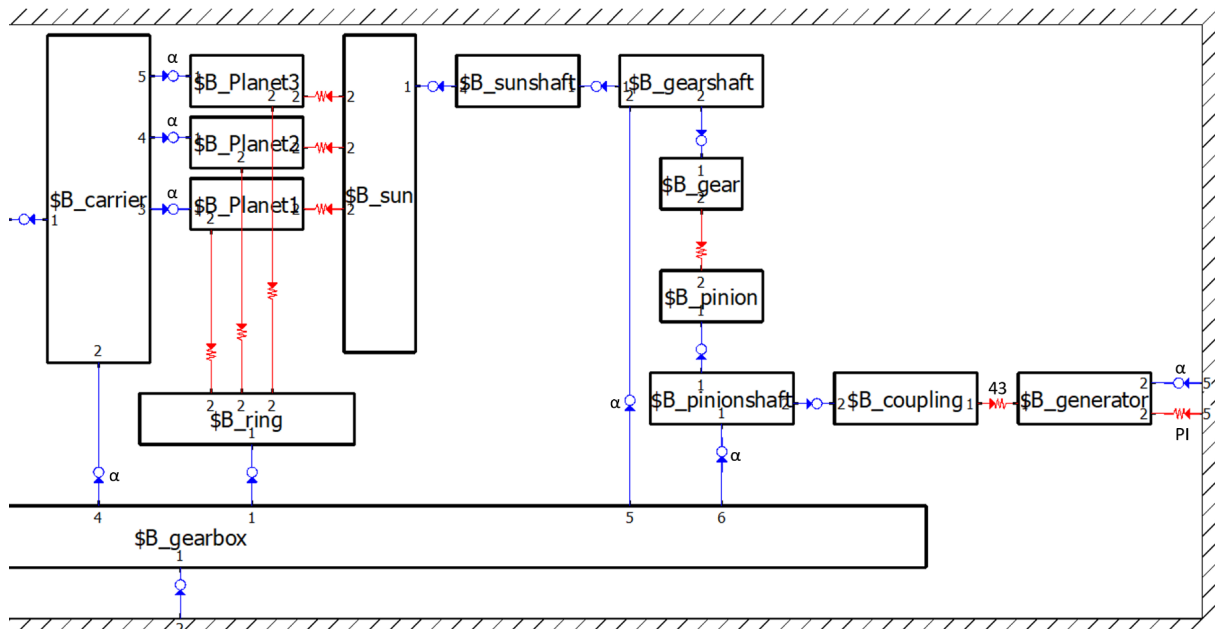


Figure 3.5: 2D figure of drivetrain model with gears in Simpack, part 2

The hub was added as a body to take the inertia into account for the natural frequency analysis only. The forces will be added directly to the LSS as the output from OpenFAST are the main shaft forces.

The main shaft was modelled as a cone with two cylinders on each side to accommodate the decreasing size, while still having the bearings acting on a flat surface on each side. This was purely for the graphic representation of the actual drivetrain, since the mass and inertia of the model was directly added to the bodies. The bearing sizes are presented in Table 3.1 and mass and inertia of the bodies are presented in Table 3.2. Note that although the inertia in all rotations as well as the mass used for translations are given, most are not required for the reduced order model because the degrees of freedom are limited in order to obtain a faster model.

Table 3.1: Bearing details for SIMPACK model [73]

Bearing	Outer Diameter	Inner Diameter	Bearing thickness
INP-A	1770 mm	1450 mm	145 mm
INP-B	1250 mm	950 mm	136 mm

Table 3.2: Mass and inertia of the drivetrain components [73]

Body	Gear stage	Mass [kg]	$I_{XX}$	$I_{YY}$	$I_{ZZ}$
Hub	-	227962.0	156699761.4	80000000	80000000
Main Shaft	-	58479.5	17878.6	157739.7	157739.7
Carrier	1	25360.2	19314.1	18029.5	18029.6
Planets gear	1	2353.7	393.0	554.3	554.3
Ring gear	1	10184.2	21272.4	11179.3	11179.4
Sun gear	1	2653.1	242.7	309.7	309.7
Sun shaft	1	1731.1	359.5	1002.0	1002.0
Carrier	2	10475.4	4873.7	3871.9	3871.8
Planets gear	2	989.6	133.9	148.7	148.7
Ring gear	2	4176.8	5744.5	2966.3	2966.4
Sun gear	2	776.3	31.8	39.1	39.1
Sun shaft	2	371.7	39.5	117.1	117.1
Wheel gear	3	3760.0	613.1	390.0	390.0
Wheel shaft	3	5849.2	679.0	727.6	765.4
Pinion gear	3	854.5	29.5	33.3	33.3
Pinion shaft	3	1797.9	40.9	568.7	568.7

To incorporate the gears in the model, they must be connected to the global coordinate system. For easier incorporation and to simulate the four-point support, a gear box was added to the model. This is also inspired by what was presented by Wang, S. et al. [73]. The gear parameters are shown in Table 3.3.

Table 3.3: Gear parameters, from [73]

Parameter	Gear stage 1	Gear stage 2	Gear stage 3
Helix angle	8 deg	8 deg	12 deg
Normal module	30 mm	20 mm	18 mm
Normal pressure angle	20 deg	20 deg	20 deg
Width	800 mm	520 mm	500 mm
Number of planets	5	3	-
Number of teeth			
Sun	26	26	-
Planet	31	41	-
Ring	89	109	-
Pinion	-	-	28
Gear	-	-	61
Profile shift coefficient			
Sun	0.2702	0.2787	-
Planet	0.2093	0.1213	-
Ring	-0.1591	-0.0024	-
Pinion	-	-	0.2976
Gear	-	-	0.1024

During validation of this model, some issues with the model and the natural frequency was discovered. This is further discussed in Section 4.5.2. Hence, a simpler model was created and the simulations was run using that model.

### 3.5.2 Drivetrain model

As mentioned, a simpler model of the drivetrain was made because of issues with the natural frequency of the model with gears. Because the analysis will be on the axial forces on the main bearings, the gear meshing will not be as important for the analysis [72]. Figures of the amended drivetrain model is shown in Figure 3.6 and 3.7.

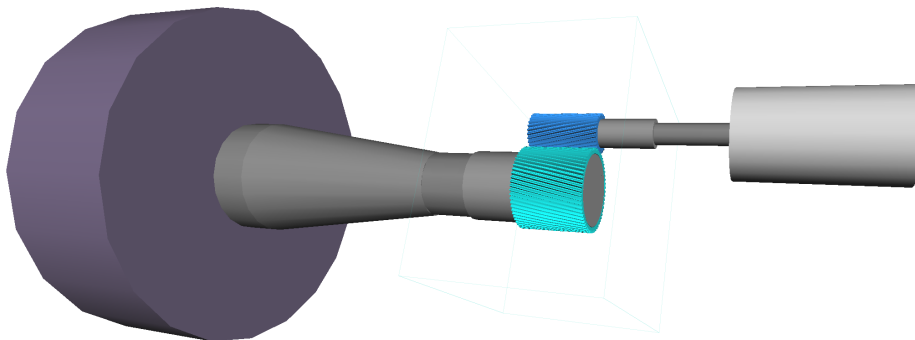


Figure 3.6: 3D figure of drivetrain model in Simpack

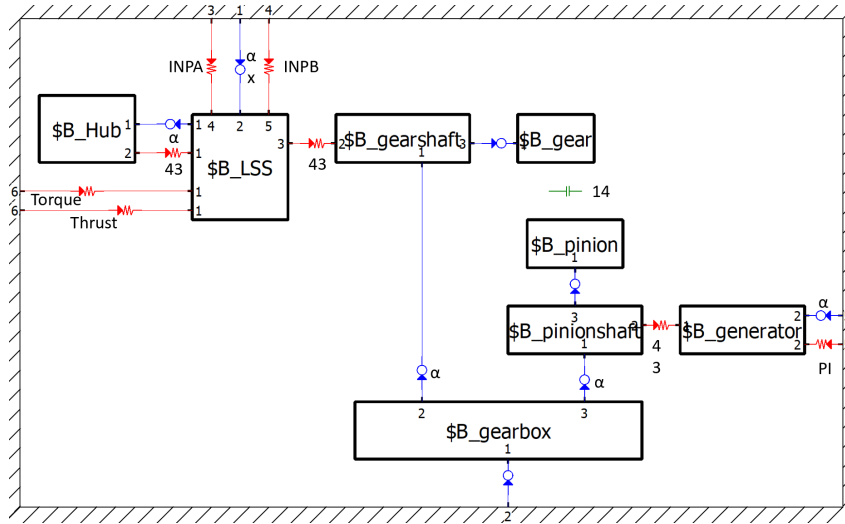


Figure 3.7: 2D figure of drivetrain model in Simpack

The bodies and force element details are the same as in the model with gears from Section 3.5.1, and the main difference is within the gearbox. Instead of force elements that accounts for stiffness and damping in the gears, the constraint element 14 is used. This is an element that is connected between two joints and gives a gear ratio. In this model, the constraint is added between the joint from the gearbox to gearshaft and the joint from the gearbox to the pinionshaft. The constraint only includes the gear ratio and does not simulate any of the gear dynamics. Additionally, the gear is added as one ratio instead of three gear stages.

It should be noted here that the gear bodies are kept for visual purposes; the teeth and geometry of the gears have no effect on the results.

The axial stiffness and damping in the bearings are given in Table 3.4. The stiffness is given by Wang, S. et al. [73] while the damping was more challenging. Through experimenting with various values to restrict the large oscillations the right damping was assumed to be 1 % of the stiffness [46].

Table 3.4: Stiffness and damping of the main bearings [46] [73]

Parameter	Stiffness Kx [N/m]	Damping Dx [N s/m]
INP-A	4.1442e+09	4.1442e+07
INP-B	4.0095e+09	4.0095e+07

### 3.6 Fatigue calculation of bearings

The fatigue calculation of the bearings was done using a script in MATLAB<sup>®</sup> based on the theory presented in Section 2.11.3. The fatigue script was run after the simulation of the full model so that it was easy to decide the bin size as the maximum value was already known. There was an ambition to add a script to the Simulink<sup>®</sup> model so the damage of the bearings could have been calculated as the model was running. A scope to show the damage during the



---

simulation could have been added. This script was made but never used, but as it is relevant for the purpose of the thesis, it will be presented here.

### 3.6.1 Script for real time fatigue

The script for real time fatigue takes in C, a, X and Y as shown in Equation (75) and (76). The damage from previous time step is also taken in as an input so the damage may be accumulated. Additionally, the rpm at current time step, the time step size, the bin size and a vector with the value of each bin are inputs. The details of X, Y and C for the bearings used are shown in Table 3.5.

Table 3.5: Bearing details used in this study

Bearing	Y	X	C
INP-A	1	0	5600 N
INP-B	1	0	4600 N

The dynamic loading is calculated according to Equation (76) before the appropriate bin for the load is found.

The life associated with the load at the current time step is then calculated using Equation (80) where  $l_i$  is the life in million revolutions,  $t_i$  is the time step in seconds and  $\omega_{rpm}$  is the angular velocity in rounds per minute. Note that it must be divided by one million as the life in Equation (75) is given in million revolutions.

$$l_i = \frac{t_i \omega_{rpm}}{60} / 10^6 \quad (80)$$

The damage for the current step is calculated using Equation (77). This is added to the accumulated damage.

### 3.6.2 Script for fatigue

The fatigue script that was used for fatigue calculation after simulation is a simplified script. First of all, it only takes in the axial force since X is 0 in Table 3.5. Although the radial force should be taken into account, the main focus here is the axial loads.

The script takes in the axial values, rpm, C and the number of bins. The dynamic loading is then calculated, and this is set equal to the axial loading as the radial forces are not included. From the number of bins, and the maximum and minimum values of the dynamic loading, the size of the bins are calculated according to Equation (81) where  $\Delta bin$  is the binsize,  $min$  and  $max$  are the minimum and maximum values of the dynamic loading and  $\#bins$  is the number of bins desired.

$$\Delta bin = \frac{max - min}{\#bins} \quad (81)$$

The force from the bearings have negative values, which became apparent when running the first simulation for 11.4 m/s. Therefore, the absolute value of the forces from the main bearings are used for the calculation, and the minimum value is set to 0.

The load is allocated to the correct bin and the number of cycles counted using Equation (80). First, the plan was to use the rpm from the global model that have a lot less values than the drivetrain model, and this had to be accounted for in the script. However, the model was later amended so that the rotational speed of the shaft was taken from the drivetrain model, for both a more accurate result and easier calculation.

Lastly, the damage is calculated according to Equation (77) using the middle value of each bin. The number of bins used is 64 according to Wang, S. et al. [73], which should be enough for the estimation of main bearing fatigue from the reduced order model. However, Nejad, A.R. et al. [50] recommends having at least 100 bins when evaluating gears.

### 3.7 Simulink<sup>®</sup> and S-Functions

Because both Simpack and OpenFAST support S-functions, this is chosen to perform the integrated simulation using the two programs. OpenFAST comes with two examples for S-functions in Simulink<sup>®</sup> and these are used as a basis for implementing both the global wind turbine model and the drivetrain model in the Simulink<sup>®</sup> environment.

#### 3.7.1 OpenFAST S-function - Global model

Due to time limitations, a de-coupled analysis with OpenFAST and Simpack was made using the example model called *OpenModel* provided with the OpenFAST files and is shown in Figure 3.8 [14]. None of the inputs as described in Table 2.8 was used in this model. Nevertheless, the models run together at the same time.

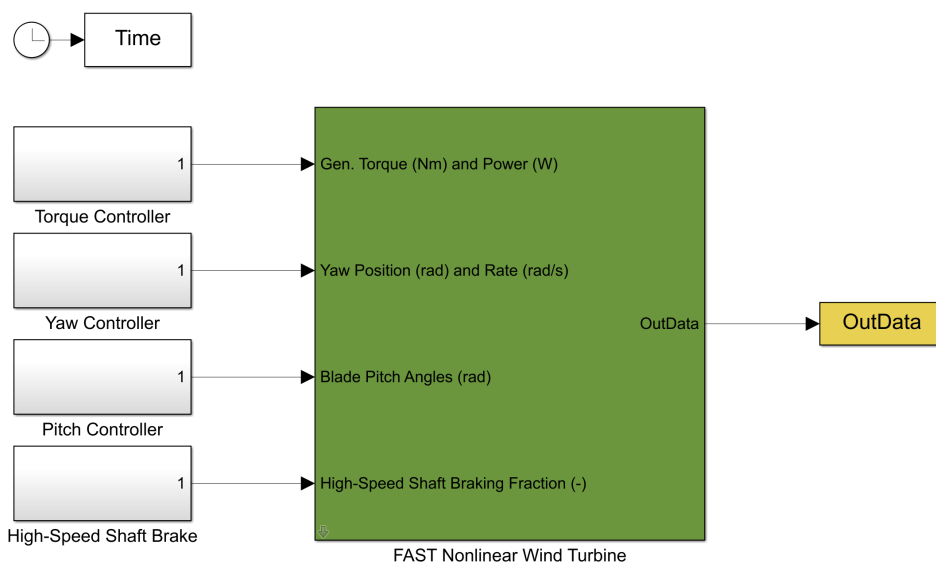


Figure 3.8: Screenshot of *OpenLoop* example model from OpenFAST [14] [52]

The model in Simulink<sup>®</sup> will be run the same way as the example model, meaning they will be run from MATLAB<sup>®</sup>.

If a co-simulation could have been made, the example model following OpenFAST called *Test01\_SIG* shown in Figure 3.9 would be used as an in a start [52]. The simple induction generator is shown in Figure 3.10 and gives a way to introduce the generator torque and the electrical power back to OpenFAST in an effort to make a co-simulation.

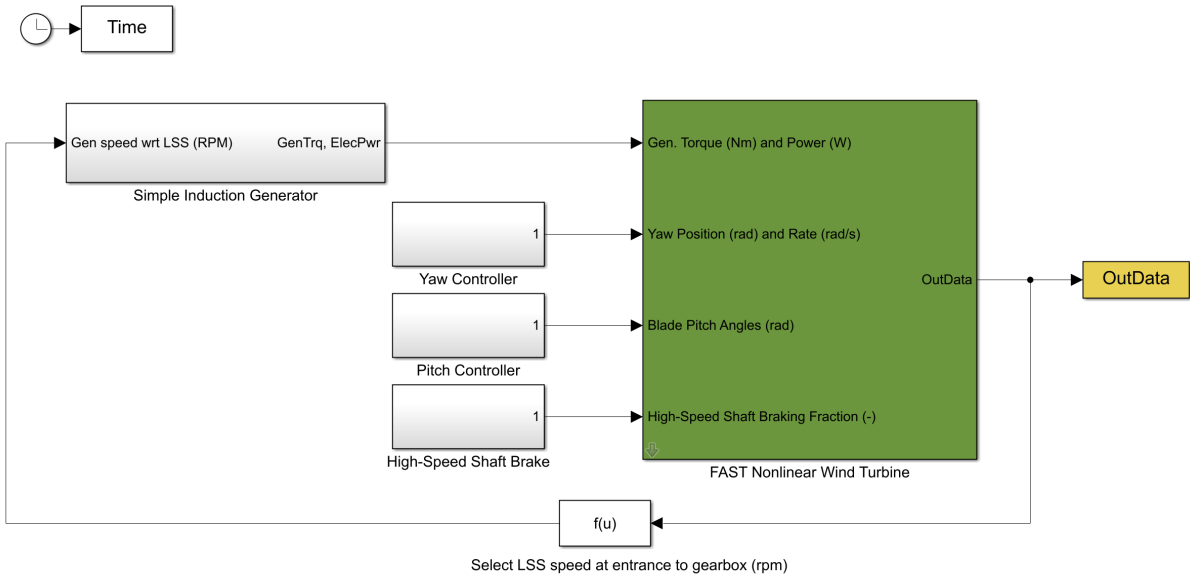


Figure 3.9: Screenshot of *Test01\_SIG* example model from OpenFAST [37] [52]

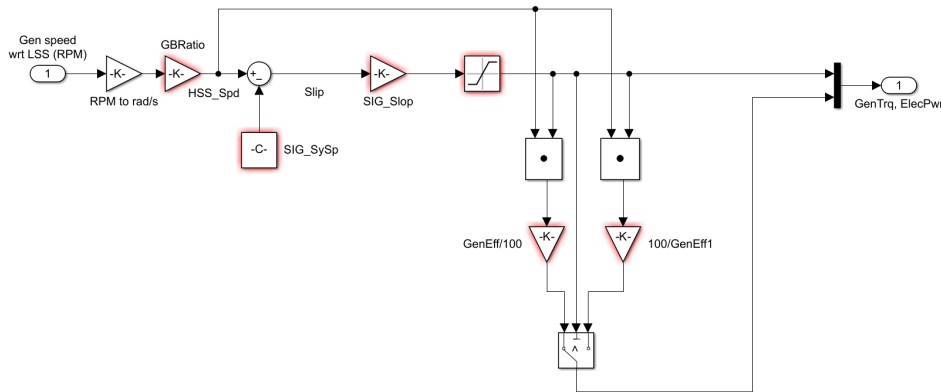


Figure 3.10: Screenshot of Simple Induction Generator from *Test01\_SIG* example model from OpenFAST [37] [52]

In Figure 3.10 the generator speed is taken in and used to find the generator torque, and these are then combined and used to find the electrical power. A switch ensures that the generator efficiency  $\eta_{Gen}$  is used correctly, where Equation (82) is for positive torque and Equation (83) is for negative torque [52].

---


$$P_e = T_{Gen} \cdot \omega \cdot \eta_{Gen} \quad (82)$$

$$P_e = \frac{T_{Gen} \cdot \omega}{\eta_{Gen}} \quad (83)$$

By turning off the two-mass model in OpenFAST and the gear ratio, the generator torque and electrical power may be used as an input to the model in Simulink<sup>®</sup> as shown in Section 2.9.2 [39].

### 3.7.2 Simpack S-function - Drivetrain model

The inputs and outputs for the S-function from Simpack must be defined before the model was exported, as explained in Section 2.13. The functionality for defining *SubVars* will not be used here.

The input was defined by creating a u-Input and, as per tutorial *SIMAT: Data Exchange via the S-Function Export* in Simpack, the Scale factor was set to 1 [12]. Under u-Vector assignment in the same window, the u-Vector was created. The last step was to make a force element, chosen as 93: Force/Torque by u(t), and then add the u-vector element to the DOF it operates in. The force element must be added between a global marker and the local marker on the body. The outputs were defined using y-Output, and the type of outputs were selected based on the desired values. All inputs and outputs defined for the reduced order model are listed in Table 3.6. Note that the generator speed output was only added for the purpose of checking that the PI-controller works by comparing it with the input.

Table 3.6: Inputs and outputs defined for Simpack Model S-function

Parameter	Input/Output	Used in Simpack
Torque	Input	Force Element 93
Thrust	Input	Force Element 93
Generator speed	Input	Control Element 163
INP-A axial force	Output	Output type 12
INP-B axial force	Output	Output type 12
LSS rotational velocity	Output	Output type 14
Generator rotational velocity	Output	Output type 14

Next, the model was exported using a function given in SIMPACK and this will export a .mdl file that may be opened in Simulink<sup>®</sup> [12]. Note that it is possible to add a script to the model that will be ran as soon as the S-function is called, but this was not used nor will it be further discussed here [12].

The model must be configured before it runs. To configure the block, the S-function block parameters was opened as shown in Figure 3.11. When clicking the function of *Write SBR File* a .sbr file with the results for post-processing in Simpack is created when the model is run, where SBR stands for Simpack Binary Result.

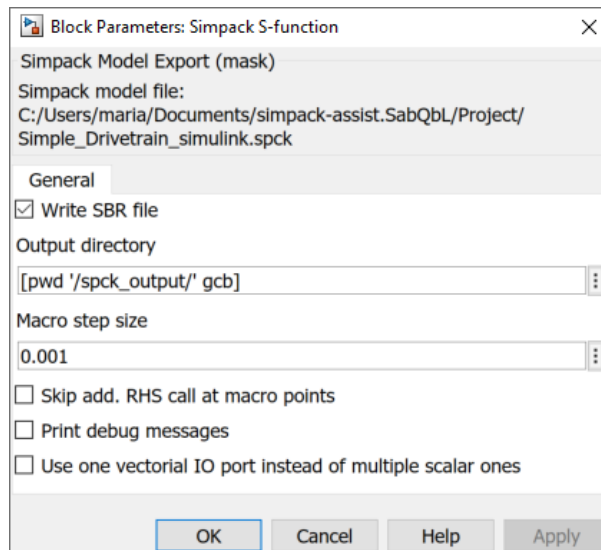


Figure 3.11: Block Parameters for Simpack S-function [12]

Note that if SubVars were defined, there would also be a tab for these in the *Block Parameters* [12].

### 3.8 TurbSim

TurbSim with the Kaimal model as presented in Section 2.2 was used to make the wind field used in OpenFAST. The input file was created based on TurbSim input files provided together with the Nautilus model from Gitlab [16], although some of the values were modified to get the desired conditions [21] [54] [74]. However, the inputs regarding the grid point matrix dimension and the grid change was left unchanged. Additionally, since the input files were for an older version of Turbsim, the input file was updated to fit the input file provided in OpenFAST online documentation [36]. Here, also input files that were provided in *TMR4505 - Marine Structures, Specialization Course, module TMR03 - Integrated Dynamic analysis of Wind Turbines* was conferred [69].

One of the inputs that was given was the surface roughness length of 0.03 m, which is a standard value in TurbSim as well [27]. According to the approximate data given in [40], 0.03 m seems more like the snow surface rather than the open sea. Hence this was changed to 0.005 m according to blown sea. The power law presented in Equation (54) with  $\alpha$  of 0.14 was used in Turbsim [27].

### 3.9 Full model in Simulink<sup>®</sup>

When simulating the full model in Simulink<sup>®</sup>, it is important to note that not all versions of Simpack and Simulink<sup>®</sup> works together [63]. For the simulation, MATLAB<sup>®</sup> version 2019b is used with Simpack version 2021x.

The recommended Solver Configuration in Simulink when running the model is ode23tb in

order to simulate the integrated drivetrain models with OpenFAST and Simscape[39]. This is because of the efficiency of the computation, which is the aim of this thesis as well. As there are no information regarding simulation with Simpack and OpenFAST, it was considered applicable to the case described here as well and ode23tb was used. This also makes it possible to have a different time step for the Simpack model as compared to the FAST model.

The time step used for OpenFAST is 0.025 s according to the original model, and the first 1800 seconds are transient and should be removed. The time step for the drivetrain model should have been calculated according to Equation (64). However, since there is no gear meshing in the final drivetrain model, the time step was calculated by using the highest rotational velocity of the drivetrain multiplied by 2, following the sampling theorem by Nyquist [6]. The resulting time step is 0.001 s for the drivetrain.

The full model with both OpenFAST and Simpack in Simulink<sup>®</sup> is shown in Figure 3.12. A bigger figure is included in Appendix C The input on the left must be given to the OpenFAST module when running the model, but are not used in the simulation. The output from OpenFAST are then picked using the  $f(u)$  functions and multiplied in a gain to convert all values to SI-values [39]. One of the Functions  $f(u)$  is given in Figure 3.13. Additionally, all outputs are sent to the workspace in MATLAB<sup>®</sup> in the OutData block.

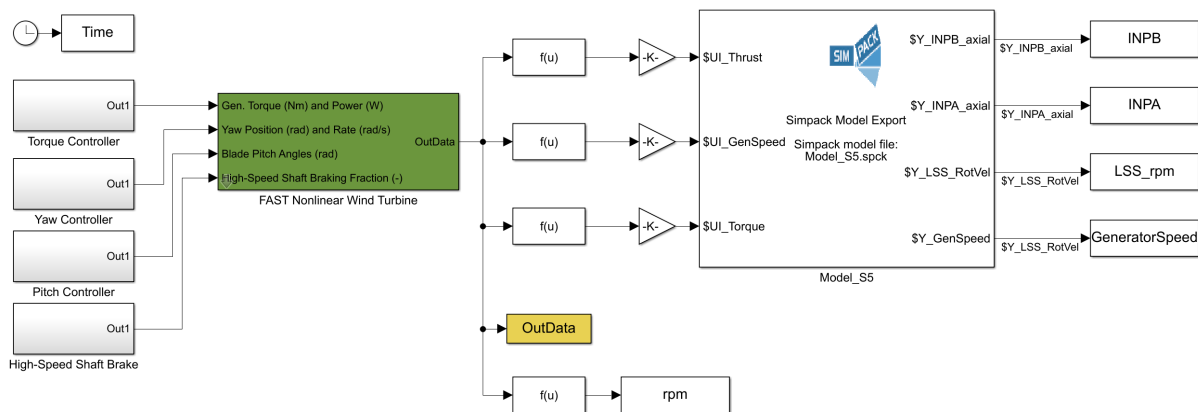


Figure 3.12: Full model in Simulink<sup>®</sup>

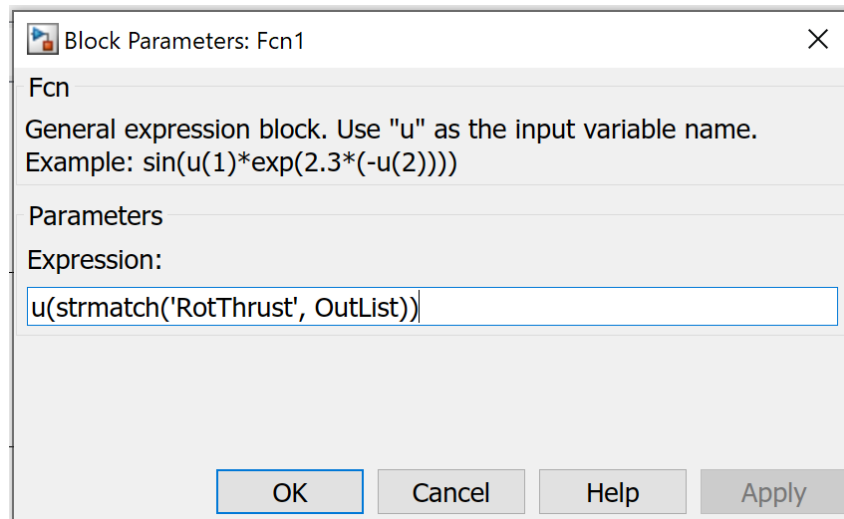


Figure 3.13: Function  $f(u)$  to pick output, adopted from [39]

The Simpack model takes in the thrust and torque to apply to the LSS shaft, and the generator speed is required for the PI-controller for the drivetrain model.

### 3.10 Validation

The models are validated so that the confidence in the models and the results of the simulations are strengthened. It is also a good way to ensure that errors are discovered and removed. The following sections will explain how this has been done.

#### 3.10.1 OpenFAST

To validate the model in OpenFAST and check that the DTU controller provided by Irene Rivera Arriba used for the Nautilus 10 MW floating wind turbine works as intended, the model was run with no waves and steady wind. The steady model uses Equation (54) with a shear exponent of 0.14 as already implemented when downloading the model. According to the Turbsim manual that references 61400-3, 0.14 is the recommended value used for offshore conditions with the Kaimal spectrum. The wind speeds used for the validation are shown in Table 3.7.

Table 3.7: Validation cases for OpenFAST

Case number	Wind Speed [m/s]
1	4
2	8
3	11.4 (rated)
4	14
5	20
6	25

---

The models have a transient of 1800 seconds, hence this was removed and the models were in total run 3000 seconds to validate [54]. The time step is 0.025 s and the generator efficiency is 100 %.

To validate, the thrust and power curve will be plotted as a function of the wind speeds. Additionally, the rotational speed and torque on both the rotor side and the generator side of the drivetrain is plotted. To check that the DTU controller is working to regulate the blade pitch, the blade pitch is also checked for each of the wind speeds listed in Table 3.7. For all parameters, the average value from 1800 s to 3000 is used.

### 3.10.2 Drivetrain

The drivetrain model is validated with the natural frequency of the system, which is a capability within Simpack. Before this analysis is done however, the model must be brought to a static equilibrium that may exclude any errors made in the modelling process. The equilibrium analysis is also done in Simpack with all external forces and control elements disabled. The natural frequency for the 10 MW wind turbine is 4.003 Hz and the model stiffnesses are tuned to achieve this value. The validation is done in Simpack using the function for calculating all the natural frequencies.

## 3.11 Simulation cases

For modelling of the waves in OpenFAST, the JONSWAP/Pierson-Moskowitz spectrum of irregular sea is used.

### 3.11.1 Fatigue from sea state

The first simulation was run to find the influence of the sea state of the main bearing damage. The simulation cases for this is shown in Table 3.8 and was inspired from [54].

Table 3.8: Simulation cases for sea state

Case	Wind speed [m/s]	Turbulence intensity group	Hs [m]	Tp [s]	Classification according to [54]
1	11.4	B	0	0	Operational
2	11.4	B	2.20	8.0	Operational
3	11.4	B	6.20	12.5	Operational
4	11.4	B	10.90	16.0	Extreme

### 3.11.2 Fatigue based on wind speed

From the above simulation cases, the sea state with an Hs of 2.20 m and Tp of 8.0 s was chosen for the further simulation cases used for calculation of the main bearing fatigue. The cases are listed in Table 3.9.



---

Table 3.9: Simulation cases

Case	Wind speed	Turbulence intensity group	Hs	Tp
1	4.0	B	2.20	8.0
2	8.0	B	2.20	8.0
3	10	B	2.20	8.0
4	11.4	B	2.20	8.0
5	12	B	2.20	8.0
6	16	B	2.20	8.0

Each simulation was run for 2400 s and the first 1800 s removed due to transient in OpenFAST [54]. That leaves 10 minutes of simulation time for estimation of the damage of the bearings. All results will be given as a ratio based on a base case defined as:

$$\begin{aligned} \text{Wind speed} &= 11.4 \text{ m/s} \\ \text{Hs} &= 2.0 \text{ m} \\ \text{Tp} &= 8.0 \text{ s} \end{aligned}$$

### 3.11.3 Simulation time

The aim of the full model in Simulink<sup>®</sup> is to have a fast simulation model of the wind energy simulation tool and the reduced order model. The simulation time is therefore of importance and a time analysis was performed. The results was normalised to the the full model to see if Simulink<sup>®</sup> as a platform is a good fit for the integrated simulation. The full model is compared both to running OpenFAST alone and then OpenFAST and the reduced order model consecutively. Because only the simulation time is of interest, the transient time is disregarded and the models are run for 300 seconds.

Ideally, the time ratio of simulation per CPU should have been used for all cases, but this is not available for the simulations in Simpack. Hence, this parameter was only used for comparing the global model in OpenFAST to the full model in Simulink<sup>®</sup>. For comparing all three cases, the real time normalised to the base case was used. Nevertheless, the simulations were all be run on the same computer without any other programs running simultaneously. The details of the computer is given in Table 3.10.

Table 3.10: Computer details for simulation time test

Parameter	Value
Computer type	Surface Pro 4
RAM	8.00 GB
Processor	Intel(R) Core(TM) i7-6650U

When running the model in OpenFAST and Simpack separately, the output from OpenFAST was added to Simpack through .afs files. The time used for this is not included.

---

## 4 Result and Discussion

In the following section results and discussions will be included.

### 4.1 Global model

The chosen simulation programs for the global model was FAST.farm and OpenFAST, for several reasons. First, they are available online and the models may be downloaded directly. Second, OpenFAST and FAST.farm are similar and the transition between them was considered to be easier. Nevertheless, HAWC2 and SIMA would have been good alternatives for the wind turbine simulations.

Of the wind farm simulation tools, FAST.farm was chosen because it was deemed the best program to use. FLORIS have low computational cost, but does not incorporate the dynamics of a wind turbine, which are quite important for the drivetrain loads. Additionally, FLORIS is a low fidelity wind farm simulation tool, meaning that a two mass drivetrain model should be sufficient for this model. SOWFA on the other hand, is a high fidelity tool and including a reduced order model with this was assumed to be redundant. If the model takes a long time to run, it would be of lesser importance that the drivetrain model is slow. DWM is coupled with FAST similarly to FAST.farm. In addition, FAST.farm uses the same super controller as SOWFA as well as the similar principles as the DWM model.

As explained in Section 3.2, it was attempted to use FAST.farm for the integrated simulation with the reduced order drivetrain model. Then the interaction between the different wind turbines, and what the effect these would have on the drivetrain model, would have been included. However, FAST.farm does not support integrated simulations using Simulink<sup>®</sup>, and in hindsight it would have been extensive work creating a script for the integrated simulation. In the end, only OpenFAST was used for the modelling of the global model. This means that none of the turbine interactions will be included. However, turbulence was added in terms of using TurbSim simulations. It also means that the investigation of the difference of operating in a wake or in free turbulent wind was not available.

As presented in Section 3.2 and 3.3, there were issues related to the 10MW DTU controller, the version of the global model and the version of the simulation tools. It was attempted to download a new version of the controller, and it is possible that it was working, but not tuned. However, since a working version of the controller was obtained, it was not further investigated.

### 4.2 Drivetrain

The two mass model presented in Section 2.9.1 is a simple way to find the first torsional frequency of the drivetrain. This model with damping is what is included in OpenFAST and FAST.farm, which does not give any information about the load on the components in the drivetrain. Since the drivetrain is important for the conversion of the wind energy to electrical energy, much of the information of the system is lost, especially when it comes to fatigue of

---

drivetrain components. Nevertheless, it is an easy and flexible way to implement the drivetrain in OpenFAST and FAST.farm, making it easy to accommodate the size, efficiency and type of drivetrain the user desires.

The high fidelity drivetrain model of the 10 MW drivetrain in Section 2.9.3 can also be used for estimation of the fatigue. However, with high fidelity comes computational cost. This may not be a problem in the design phase, but for running fast and simple calculations for estimation of loads and fatigue, it may be too extensive. Nevertheless, it would likely be a good model to use for an extra validation of a reduced order model to ensure that important dynamics of the drivetrain is captured.

A mathematical drivetrain model, as briefly shown in Section 2.9.4, would have been a good alternative to making the model in Simpack. Numerical methods are then used to solve the equations of motions and may be quite fast. However, this is similar to what is already done in Simpack. Additionally, making larger mid-fidelity models can easily become demanding with many bodies. Hence this was disregarded.

According to Amir R. Nejad [46], the fidelity requirements from NREL in Section 2.9.5 is the requirements for a high fidelity simulation of the drivetrain. These are presented to show the minimum recommendation to achieve an accurate simulation of the gearbox. However, there is a trade-off between the accuracy and the speed of the simulation. As an example, the geared model that was designed and presented in Section 3.5.1 included tooth slices of 5, while NREL recommends 35. Even though this model was not used in the end, it was tested and even with 5 slices, the simulation demanded significant time. Nevertheless, these recommendations are noted and may be a good guide for modelling of a drivetrain.

As mentioned, the drivetrain model is made in Simpack. The reason for choosing this instead of Simscape was two fold. On one hand, Simscape Driveline did not include the possibility of both translations and rotations, which made it void for using in this thesis. The inclusion of the axial forces have been a goal from the start of this work, which would not have been possible. On the other hand, Simscape Multibody may have been possible to use, but the lack of knowledge of the software and the difficulty of finding documentation online made it easier to use Simpack instead. It is expected that Simscape multibody and Simpack use the same theory, namely the MBS simulations. However, Simpack was already known and included the possibility of running in Simulink<sup>®</sup> using S-function, thus this was the software of choice.

Although Simpack was ultimately chosen, a Simscape Driveline model of the two mass model was made as presented in Section 3.4. The model is quite simple and requires input of the torque and generator speed. However, the model was useful for tuning the PI-controller in the Simpack model, especially since knowledge of control theory is somewhat limited. It also gave a good understanding of how changing the different values of the model would affect the output as the model gives real time values through the Scope. Thus, even though it was not directly used for any integrated simulations it was still valuable.

Section 3.5 includes the two drivetrain models that was developed in Simpack. The first model with gears included the gear stages and the internal dynamics in torsional direction, in addition to axial forces on the LSS. During the validation there was some errors with this

---

model and the gear stages, which will be presented further in Section 3.10.2. The simpler model that was made did not include the gear dynamics. However, the damage on the main bearings should not be greatly affected by the removal of the gears.

All the bodies made in the two drivetrain models in Simpack was rigid bodies, and this will likely influence the response and forces of the simulations. Adding flexible models according to the fidelity requirements in Section 2.9.5 may improve the accuracy of the responses.

There exist several models for the drivetrain of a wind turbine, although it seems that most of these put emphasis on the gearbox, for example as done by Qin, D. et al. [58]. The gearbox is an important part of the drivetrain, especially since changing this takes a long time as mentioned in the introduction. Hence a model with both gear dynamics and loads on the main bearings is desired. There was an ambition to include the gear loads on the gears, to see what effect simplification of the gears would have on the gear fatigue, but could not be prioritised with respect to time.

### 4.3 Fatigue

The fatigue theory of shaft, bearing and tooth bending fatigue for gears have been presented in Section 2.11. Since the start, there was an ambition of including at least the tooth bending fatigue for the gears in the reduced order model. Ideally, the surface pitting should also have been included in the gear fatigue. However, the main focus has been on the main bearings and the axial forces. Even though the gear fatigue had to be left out, it is still included in the theory as it is an important part of the drivetrain fatigue.

The axial forces was early included in this Master's Thesis. Thrust force from the lift and drag creates an axial force on the shaft, in addition to the pitching motion of the floating wind turbine structure. It should be noted that the radial forces was something that was desired to include, but not prioritised.

Two scripts was made for estimation of the fatigue on the bearings, which are presented in Section 3.6. The first script describes how the calculation would have been done if both radial and axial forces were taken into account. Even though this was made to run in real time during simulation, it would have been the same theory used for a full fatigue evaluation. However, since the radial forces and DOF were not included in the analysis, the script that was used for the simulation results only included the axial forces.

For the fatigue estimation of the main bearings, 64 bins was used even though it was recommended with at least 100 bins according Nejad, A.R. et al. [50]. The reason for not increasing it to 100, is that the model used is a reduced order model and the fatigue outcome is an estimation. Secondly, the recommendation of 100 was related to gears, not bearings. Although, it would have been easy to change this the way the fatigue script were made.

---

## 4.4 Co-simulation vs de-coupled simulation

From the documentation provided for OpenFAST and FAST.farm it was not apparent how to implement the loads and vibrations from the drivetrain model to the global model. It was thought that these implemented a simplified two mass model of the drivetrain to check for natural frequency of the drivetrain in the global model. However, the documentation gave no indication. It looks like the simplified drivetrain in the FAST programs is the drivetrain presented in Section 2.9.1, and is mainly used to solve the equation of motions and for calculation of electrical power out, generator speed and generator torque.

It would have been interesting to implement the reaction forces from the LSS in the drivetrain model to the hub in the global model in a co-simulation. However, the knowledge of OpenFAST and FAST.farm is insufficient at this point. The task of direct co-simulation is considered difficult without a better knowledge of Fortran, which is deemed too big of a task for now. It was decided to make a de-coupled analysis and see if it would be possible to make an integrated simulation with all the models together, where the drivetrain model would get input from the FAST model. The integrated simulation of OpenFAST and Simpack was run in Simulink<sup>®</sup> in the end, although it was done as a de-coupled analysis.

The FMI/FMU capability could be included, but it does not look like it is currently supported by the global wind energy models. If this would have been possible, it appear to be a good tool that allows co-simulation of different models. However, it implies that this capability must be added to the global modelling tools.

It may be possible to make a co-simulation of the model developed in this thesis with FAST.farm directly by making a DLL and adding this capability in FAST.farm as briefly presented in Section 2.13. That would most likely greatly improve the speed of the de-coupled analysis or co-simulation. It is expected that this would be needed to be coded directly into the software for the global model.

## 4.5 Validation

To ensure that the models work as intended, and to be able to trust the results, the models are validated according to the steps described in Section 3.10.

### 4.5.1 Global Model in OpenFAST

For the validation of the global model in OpenFAST, the steps mentioned in Section 3.10.1 is followed. The thrust and power curve are presented in Figure 4.1 and the curve for blade pitch is shown in Figure 4.2. The curves for rotational speed and torque for the rotor side and generator side can be seen in Figure 4.3 and 4.4 respectively. It should be noted that all plots are made only from a few cases, as given in Table 3.7, with linear interpolation between each of these values. This means that there will be some inaccuracies in the plots and only the points actually simulated will have correct values.

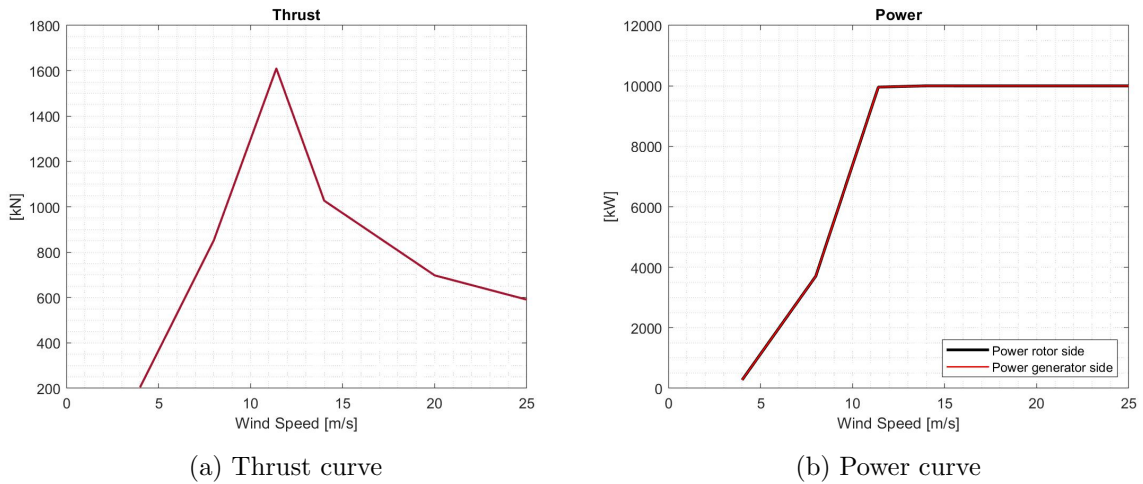


Figure 4.1: Angular velocity and Torque at Rotor side

The thrust curve follows the shape as expected with the maximum thrust at the rated wind speed since the maximum power is taken from the wind [69]. Additionally, it is expected that the thrust should be smallest at the lowest wind speed and second lowest at the highest wind speed.

The power curve shows one curve from the power at rotor side and one from the generator side. These are found from multiplying the torque and the rotational speed at each side of the drivetrain. The curve follows the expected trend, starting at the lowest value at the cut-in speed, increasing up to the rated power at the rated wind speed and then constant until the cut out wind speed [69]. Both power curves are on top of each other, which is as expected since the generator efficiency input is 100 %.

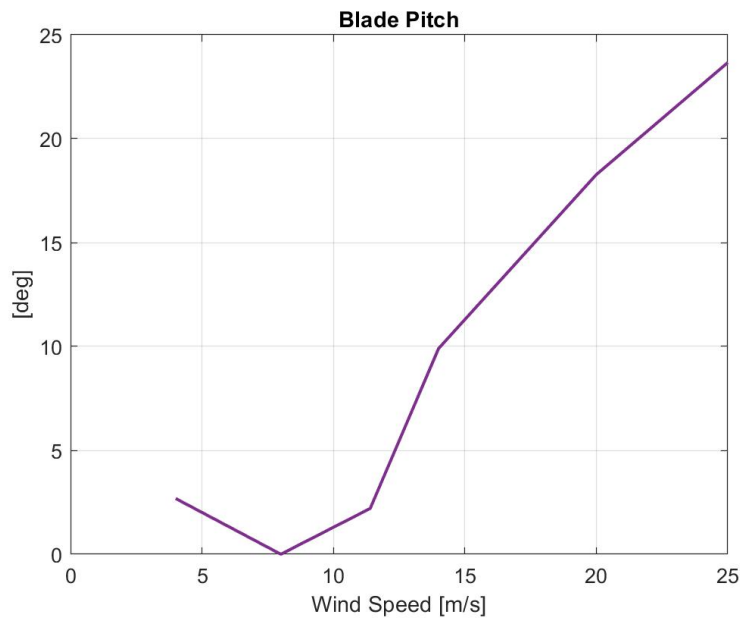


Figure 4.2: Average blade pitch degree per wind speed

Figure 4.2 shows the average blade pitch per wind speed. The blade pitch for all three blades were checked and they all behaved the same, therefore only one curve is plotted. It follows a curve with a pitch for lower wind speeds, then down to zero before it increases again. The plot shows that the pitch controller works and the blades are pitched according to wind speed.

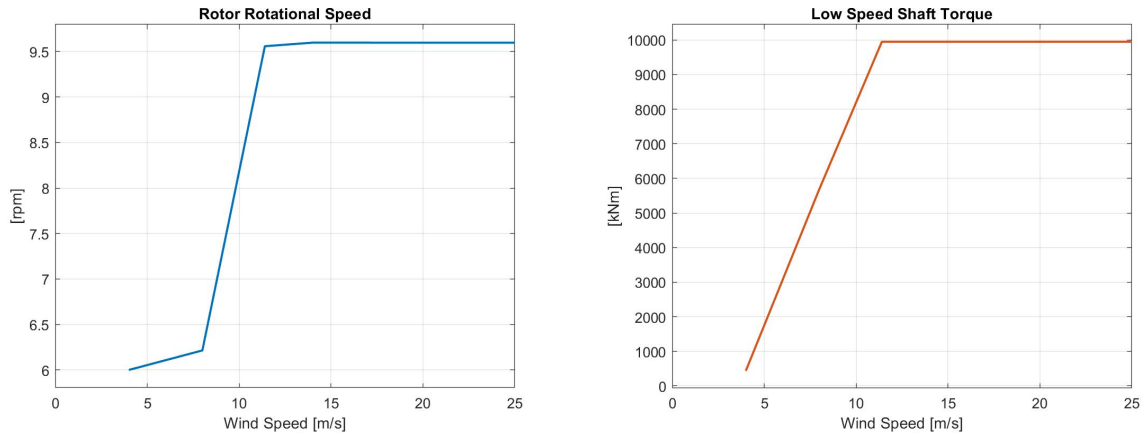


Figure 4.3: Angular velocity and Torque at Rotor side

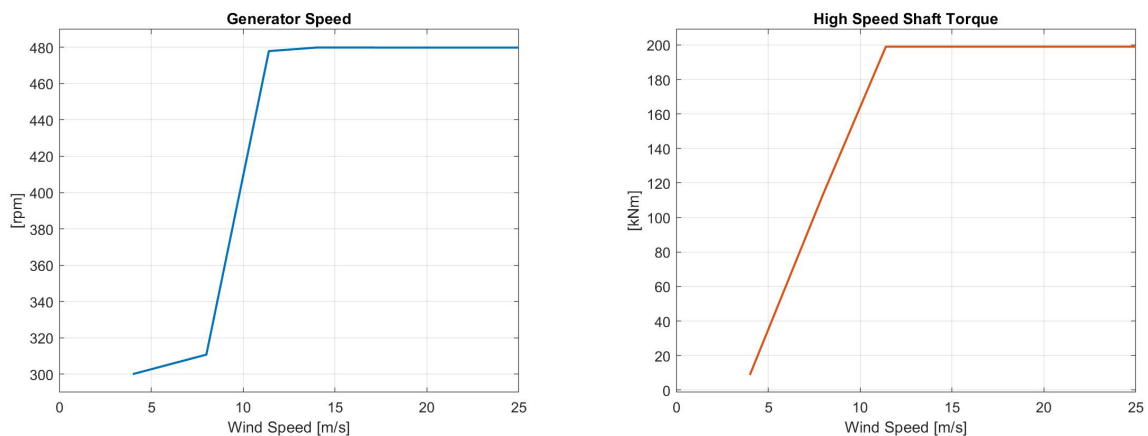


Figure 4.4: Angular velocity and Torque at Generator side

The plots of the rotational speed and torque in Figure 4.3 and 4.4 does not give much more information than the power curve. They are as expected, although the rotational speeds are a bit lower for rated value than for larger wind speeds. This is also present in the power curve, but it is not as visible due to the small difference compared to the large total value. The same applies for the torque.

The lower value of the rotational speeds at rated wind speed is expected to come from oscillations of the platform. As can be seen in Figure 4.5a, the platform pitch has a much larger standard deviation around the rated wind speed than around the other wind speeds, where the standard deviation is barely visible. This will affect the inflow wind on the rotor, and the rotational speed of the drivetrain will oscillate as shown in Figure 4.5b. Unless the time series is cut so that the position and motions are the same at start and end of the time series, the mean value will not be exactly the middle value.

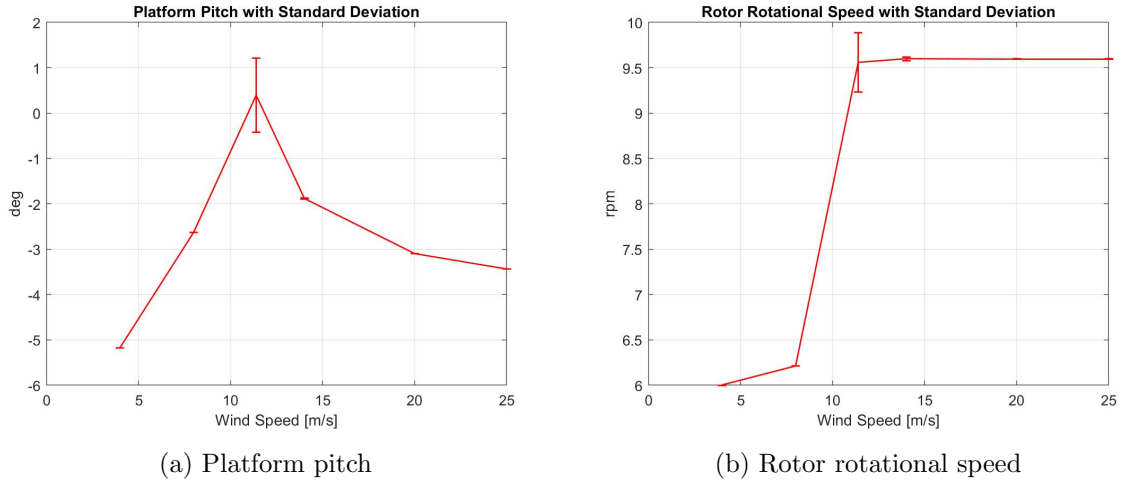


Figure 4.5: Platform pitch motion and Rotor rotational speed with standard deviations

The the big oscillations of the platform is assumed to come from the negative damping problem as presented in Section 2.5.2. Because the thrust force is the largest for the rated wind speed, it is expected that the oscillations will be the largest here as well.

Based on the above, the OpenFAST model is deemed to be working.

#### 4.5.2 Drivetrain model with gears

The validation for the model developed in Section 3.5.1 was done according to Section 3.10.2. The lowest frequency measured was:

$$f_n = 25.1787$$

This is significantly larger than what the value of the drivetrain, and changing the values of the inertias and stiffnesses did not affect the results. Simpack have the functionality of animating the modes, and the figures of this animation is shown in Figure 4.6. It shows that the planets of gear stage 1 move radially in addition to rotational, which is a DOF they should not have.

Another observation not visible in these figures is that only the LSS and gear stage 1 is moving, while the other bodies are still. Even fixing the movement of the generator does not affect the natural frequency, which hints that there are some errors in gear stage 1.

The investigation into this issue was done with help from Shuaishuai Wang, which expected that this error may be caused by the DOF for the planets only being rotational, leading to infinite stiffness in the other directions [72]. This would also explain why the other stiffnesses and inertias would not affect the natural frequency. He recommended that instead of this, bearings could be added to the planet gears with lower stiffness. However, in respect of time, it was decided to not continue with this model for the simulations, and a simpler model of the drivetrain was made to get results for the bearing damage.



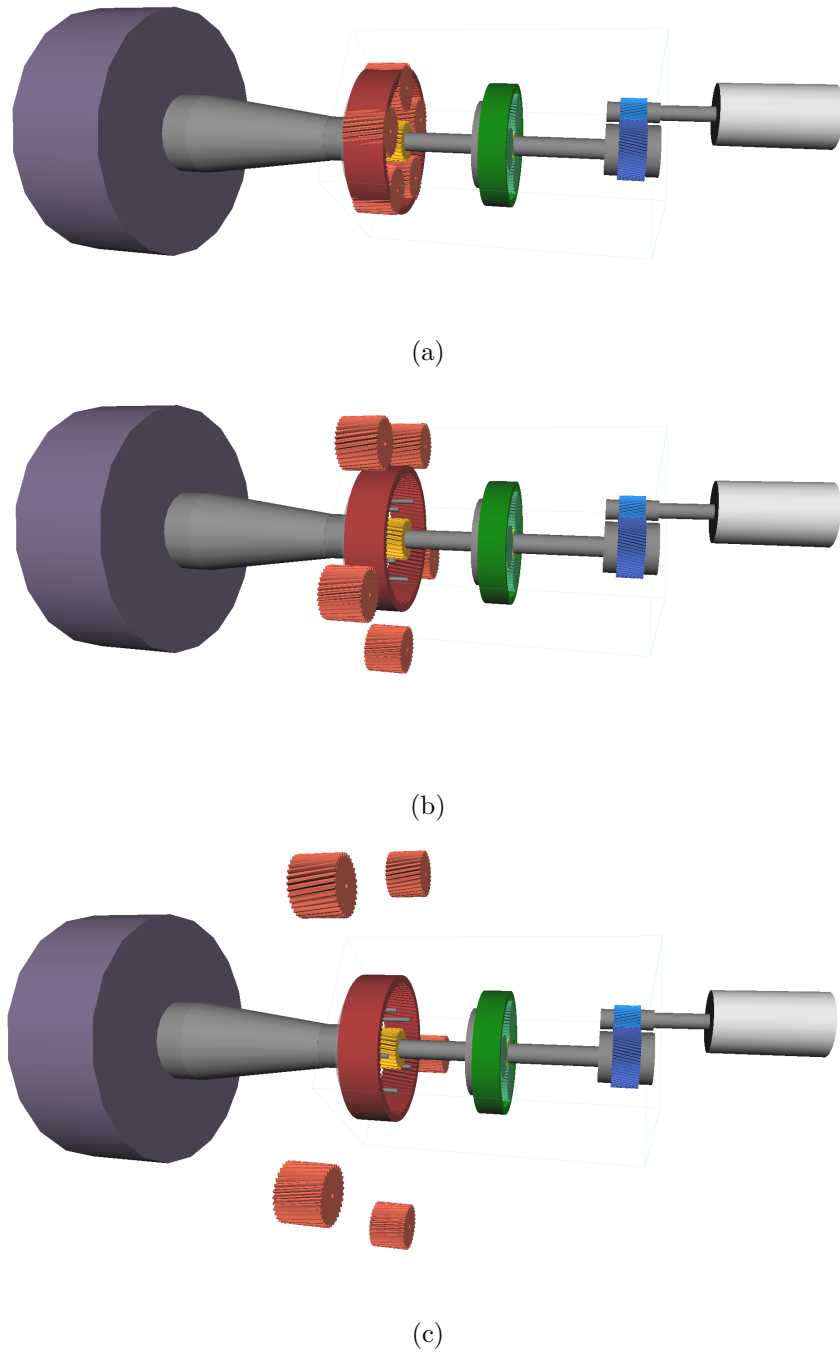


Figure 4.6: Animation of natural frequency mode of drivetrain

### 4.5.3 Drivetrain model with one gear

The drivetrain model presented in Section 3.5.2 that uses only the constraint for the gear was also validated according to procedure presented in Section 3.10.2.

The natural frequency of the drivetrain is:

$$f_n = 4.003$$

---

with stiffness of:

$$\begin{aligned}k_{gen} &= 3\,000\,000 \text{ Nm/rad} \\k_{LSS1} &= 4\,854\,600\,000 \text{ Nm/rad} \\k_{LSS2} &= 4\,854\,600\,000 \text{ Nm/rad}\end{aligned}$$

It might be expected that the stiffness of the system may be calculated directly from the equivalent stiffness using the procedure given in Section 2.9.1, and the equivalent stiffness provided for the 10 MW drivetrain [73]. However, the inertia of the generator is not given in that article and is estimated, leading to the stiffness being different.

#### 4.6 Tuning of PI parameters

The tuner in Simulink<sup>®</sup> for the Simscape Driveline model gave the following values for the PI controller for the two mass torsional model using rotor side stiffness of  $3\,356\,700\,000 \text{ Nm/rad}$  and generator side stiffness of  $3\,000\,000 \text{ Nm/rad}$ :

$$\begin{aligned}k_p &= 430\,298 \\k_i &= 686\,065\end{aligned}$$

For the finally tuned model, the stiffness of the main shaft was set to  $9\,696\,120\,000 \text{ Nm/rad}$  ( $4\,848\,060\,000 \text{ Nm/rad}$  on either side) and the stiffness of the generator side was left unchanged. That gave the following gains for the PI-controller:

$$\begin{aligned}k_p &= 644\,280.3 \\k_i &= 1\,561\,851.0\end{aligned}$$

Better tuning of the PI-controller could probably be achieved by further tuning the gains. However, the response was deemed within an acceptable range.

#### 4.7 Fatigue based on sea state

Figure 4.7 and 4.8 shows the damage for the main bearings INP-A and INP-B, where all values are given as a the value divided by the base case, which is simulation case number 2. The details of the cases are presented in Table 3.8: case 1 have no sea, case 3 have higher sea with larger  $T_p$  and case 4 is considered an extreme case

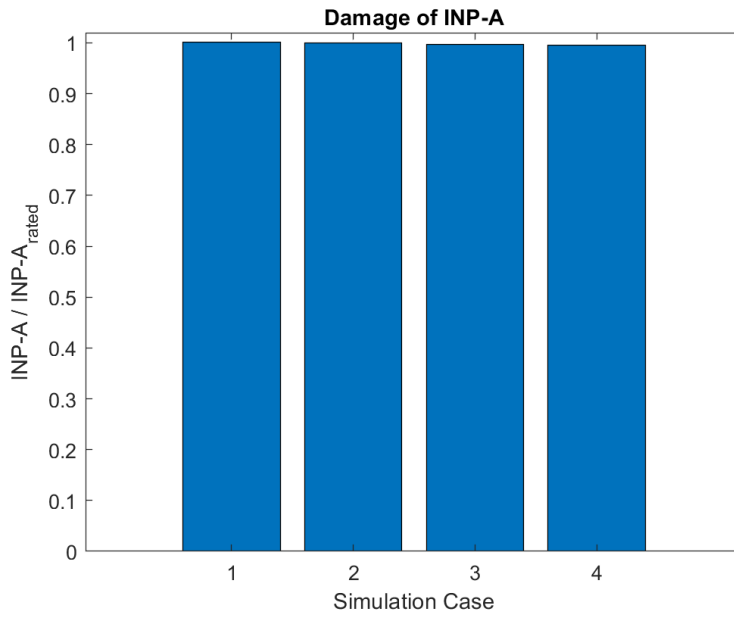


Figure 4.7: Damage ratio of INP-A for different sea states normalised to simulation case 2, as described in Table 3.8

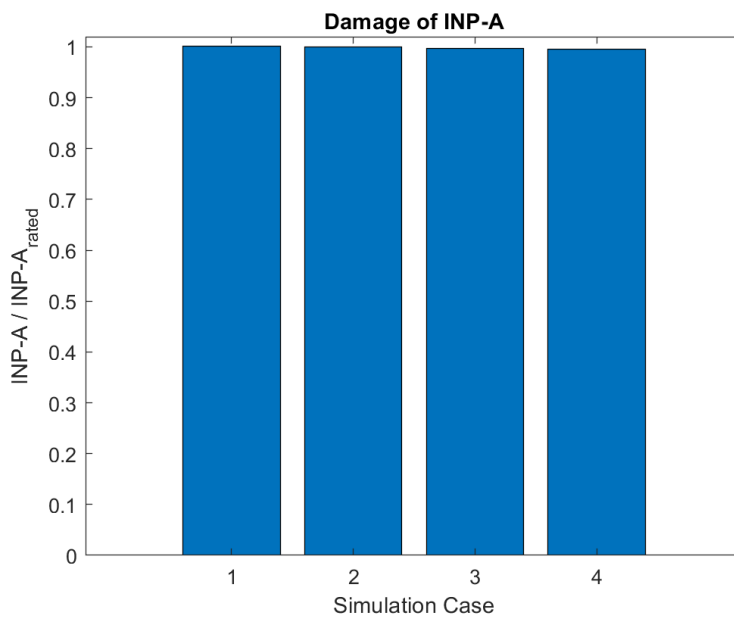


Figure 4.8: Damage of INP-B for different sea states normalised to simulation case 2, as described in Table 3.8

From these values it is apparent that the sea state does not affect the damage in the bearings significantly. Although the damage looks the same for all cases, it is a highest for simulation case 1 and lowest for simulation case 4. This indicates that waves contribute to reducing the damage due to thrust in the main bearings, although it is very limited.

By reviewing the values given in Figure 4.5a, it makes sense that the waves does not influence the damage much, as it seems like the platform pitch is large based on the dynamics of the

wind turbine itself. Even the extreme case gives smaller values than the base case, although extreme cases will not be reviewed as part of this thesis.

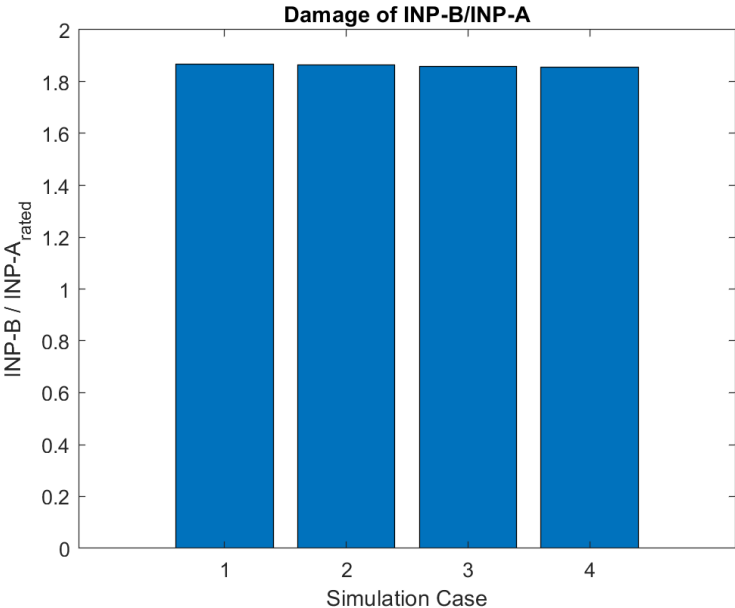


Figure 4.9: Damage of INP-B normalised to simulation case 2 of INP-A for different sea states, as described in Table 3.8

Figure 4.9 shows the ratio of the INP-B damage divided by the damage of INP-A for base case. It was initially a bit unexpected that the damage for this bearing is almost twice that of INP-A, especially since the stiffness of INP-A is larger in the axial direction as compared to INP-B. Figure 4.10 also shows that the main bearing INP-A absorbs more forces than INP-B.

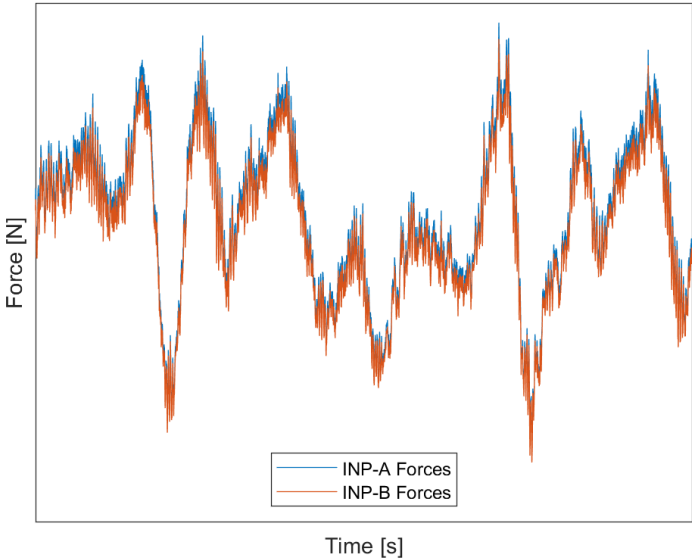


Figure 4.10: Forces in INP-A and INP-B for base case

However, for INP-B, the basic load rating used in Equation (77) is lower, being 4600 N as compared to 5600 N for INP-A. This factor is also raised to the power of  $a$ , which is  $10/3$  for roller bearings. The resulting factor that each of the dynamic equivalent loading is multiplied with is:

$$\begin{aligned} \text{INP-A: } & \left( \frac{1}{4600} \right)^{10/3} = 6.18e - 13 \\ \text{INP-B: } & \left( \frac{1}{5600} \right)^{10/3} = 3.21e - 13 \end{aligned}$$

Hence, the big difference between INP-A and INP-B is explained by these factors. Nevertheless, it indicates that the axial forces are something that may lead to higher damage in INP-B than in INP-A for these parameters.

## 4.8 Fatigue

Figure 4.11 and 4.12 shows the damage from the axial forces for the bearings using the simulation cases presented in Table 3.9.

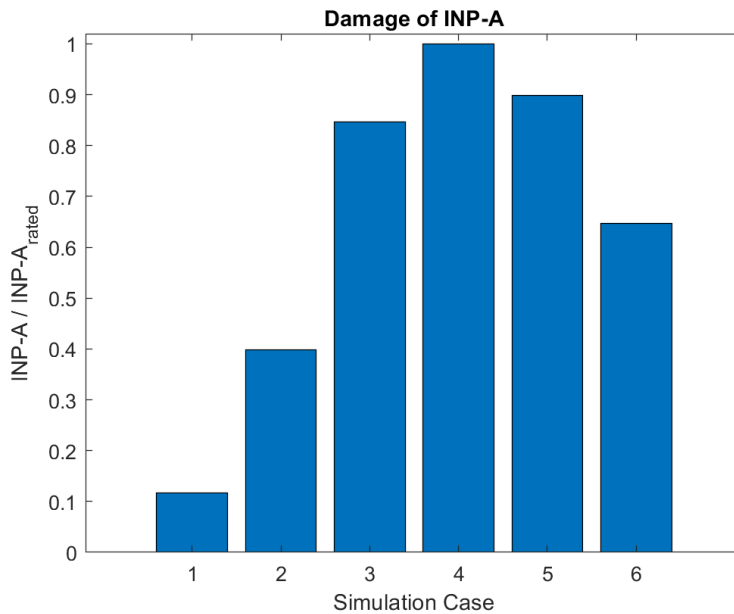


Figure 4.11: Damage of INP-A Per Simulation Case, normalised to simulation case 2, as described in Table 3.9

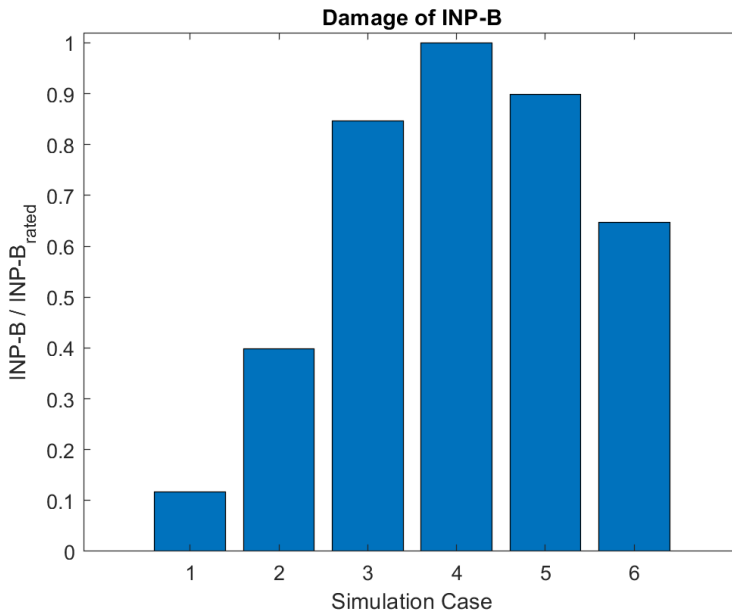


Figure 4.12: Damage of INP-B Per Simulation Case, normalised to simulation case 2, as described in Table 3.9

Since the thrust is largest for the rated wind speed, it is logical that largest damage is at this wind speed. It follows the thrust curve in Figure 4.1a as expected. Case 2 gives lower damage than case 6, even though the wind speed for case 2 is closer to the rated wind speed of 11.4 m/s. The damage for case 5 is slightly higher than for case 3, while the latter is further away from the rated wind speed. However, above the rated wind speed, the power extraction is also higher than below, hence the higher damage for case 5 and 6 does not mean that the damage per MW power produced is lower for case 1 to 3.

Figure 4.13 shows the thrust with standard deviations, normalised to simulation case 4. Comparing this figure to Figure 4.11 and 4.12 shows the relationship of thrust to the damage in INP-A and INP-B, which is as expected. Secondly, the standard deviations are much larger for the simulation cases above the base case.

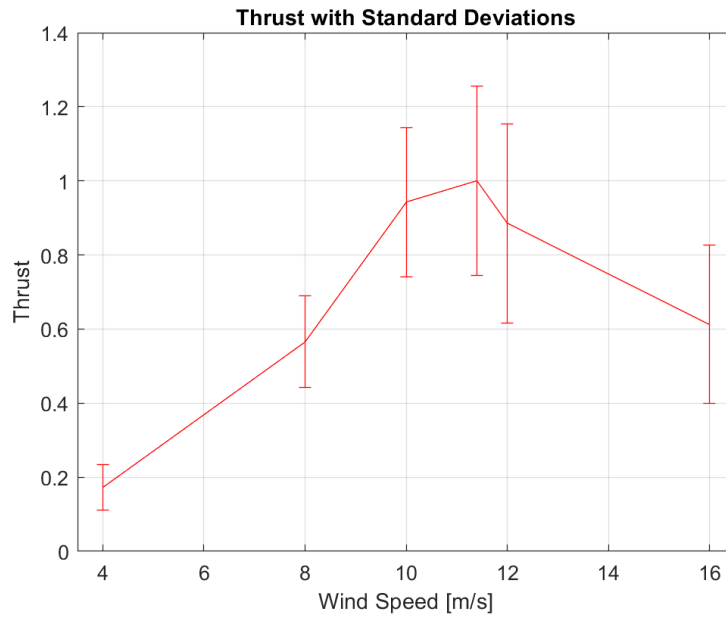


Figure 4.13: Thrust with standard deviations, normalised to simulation case 4

Figure 4.14 shows the damage of INP-B normalised to the base case for INP-A. As for Figure 4.9, the damage for INP-B is almost twice the damage of INP-A due to the parameters of the bearings.

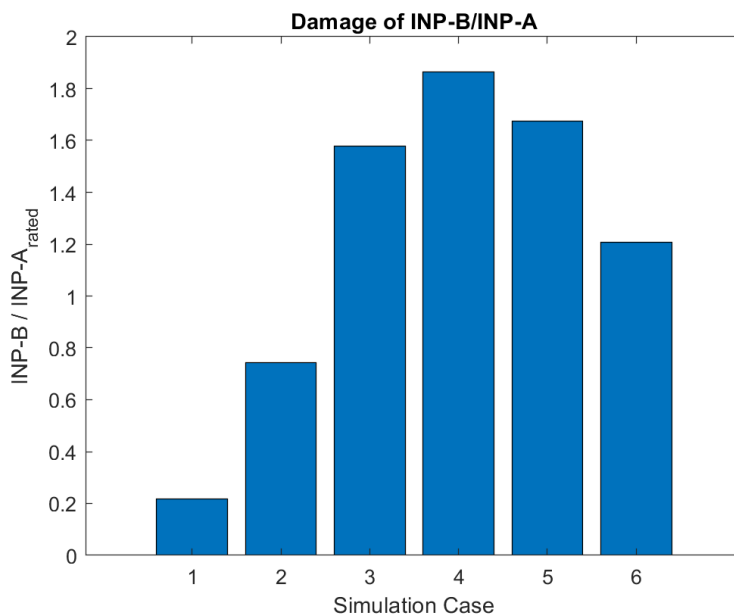


Figure 4.14: Forces in INP-B normalised for INP-A for base case

It was thought to include 20 m/s and 25 m/s in the simulation cases, however, due to the error message in OpenFAST for these values. The error message can be seen in Figure 4.15. It was however included in the validation of the model as those were merely to check the model rather than achieve results.

---

```
FAST_Solution:FAST_AdvanceStates:ED_ABM4:ED_CalcContStateDeriv:SetCoordSy:Small angle assumption violated in SUBROUTINE SmlRotTrans() due to a large blade deflection (ElastoDyn SetCoordSy). The solution may be inaccurate. Simulation continuing, but future warnings from SmlRotTrans() will be suppressed.
```

Figure 4.15: Error message in OpenFAST for wind speed above 20 m/s

## 4.9 Simulation time

The simulation times normalised to the integrated full model in Simulink<sup>®</sup> is shown in Table 4.1.

Table 4.1: Normalised simulation times for the models, normalised to base case

Simulation case	Normalised Real time	Normalised Sim/CPU ratio
Integrated model	1.000	1.00
OpenFAST	0.738	1.23
OpenFAST + Simpack	0.739	-

The results show that running the full model in Simulink<sup>®</sup> is time consuming compared to running the models separately, which only takes about 74 % of the time. This is without including the time for arranging the input files in Simpack from the output files from OpenFAST. However, this could have been done by making a separate script, that would probably not demand a lot of computational power.

Looking at the differences of running OpenFAST with and without Simpack indicates that the reduced order Simpack model is fast. Hence, the reduced order model have low computational according to the objective.

The integrated model is run using a MATLAB<sup>®</sup> script to start the model in Simulink<sup>®</sup>. This will add to the time, and probably make the execution slower. Hence, the best approach may be to run the script directly from Simulink<sup>®</sup>.

However, the results here indicate that it may be better to use a different method than Simulink<sup>®</sup> for integrated simulation of the global model and the drivetrain model when computational cost is important.

## 4.10 Simulation of full model

Table 4.2 shows the maximum values of the forces in the bearings as compared to the thrust force for the rated wind speed.

Max force	Value
Thrust	2.3744e+06
INP-A axial force	1.2056e+06
INP-B axial force	1.1664e+06

Table 4.2: Thrust force and forces on bearings for Base Case



---

These values are mostly shown to build confidence in the model and to possibly exclude any errors in the model. It shows that the forces in the two bearings are not more than the thrust force combined.

---

## 5 Challenges and further work

The work performed have involved numerous challenges and more time is needed to implement all the capabilities that were desired.

### 5.1 Challenges

One of the main challenges faced in this Master's Thesis have been to get the models of the floating wind turbines to work with a recent version of OpenFAST and FAST.farm, as it was developed for a 32-bit version of FAST. These programs are written in Fortran and ran using Windows Command prompt, which both were unfamiliar prior to this Master's Thesis. The error messages from running the models and the online documentation did not always give a clear instruction on how to correct the errors, or why it was not working. Although it is believed that this is a common issue in programming work, it has been frustrating at times, especially with the deadline closing in. The amount of time put into this issue with a trial and error, moving things around, deleting things and checking if it still works have restricted the time to do modelling, investigation into developing the drivetrain model and running simulations.

Surprisingly, finding information about how the wind turbine drivetrain was implemented in OpenFAST and FAST.farm was difficult. The investigation into this issue included both reading Fortran code, looking through the equations of motion in the program and reading the online documentation and different papers and reports. Although much information was collected, and some of the governing equations were given, it was still challenging to understand exactly how it would be possible to implement a new drivetrain into the code.

The implementation of gears in the reduced order model was not straight forward, and in the end it was abandoned due to time. Finding out why the drivetrain natural frequency was so high and why the model did not behave as expected in the animations was challenging.

### 5.2 Further work

The reduced order model had less capabilities than desired in the end. The main further work is to continue developing the reduced order model. This may be done by getting the model presented in Section 3.5.1 to work, including the radial forces on the main shaft and include fatigue of the gears. Then the fatigue of the main bearings due to both axial and radial load in addition to the gear fatigue could be included.

There are several ways the drivetrain model could be expanded when the above mentioned steps are achieved. It would be interesting to include the disturbance from the grid in drivetrain to investigate how that affects the HSS bearings. Also, some flexible bodies could be included, especially the main shaft. A sensitivity analysis on the number of points in the flexible shaft could then be run.

Further work should also focus around the possibility of including a reduced order model

---

directly in the FAST.farm environment. With a more extensive understanding of Fortran and a mathematical model for the drivetrain, or alternatively of making a .dll file to implement directly with the model, would possibly be a better solution for making a fast model.

It would also have been interesting to check how much the fidelity of the drivetrain components would have affected both the results and the simulation time. Especially to investigate if a simpler force element for the gears in the reduced order model presented in Section 3.5 would be sufficient. A sensitivity analysis could be run to see the trade off between one and the other.

---

## 6 Conclusion

In this thesis the aim has been on making a reduced order model of a drivetrain that accounts for the axial forces on the main shaft in addition to the torsional DOF. The Master's Thesis have reviewed the topic of integrating a reduced order drivetrain model with wind turbine and wind farm simulation tools.

First, the background theory for simulation of global and drivetrain model have been presented, including external environmental loads and modelling of these, theory on wind farm level, wind turbine level and drivetrain level, in addition to fatigue theory. Additionally, de-coupled analysis and the possibility of co-simulation using different solutions have been presented.

The next section described the methodology and the actions performed in the thesis, from working with FAST.farm and OpenFAST to the development of models of the drivetrain both in Simscape and in Simpack, including fatigue estimation. The possibility of integrated simulation in Simulink<sup>®</sup> using S-function was presented. Then the TurbSim input for the turbulence model was shown before the full model of the global model with the developed reduced order drivetrain in Simulink<sup>®</sup> was presented, including how this is run. A subsection on how the models were validated followed and the methodology section was concluded with presentation of the simulation cases.

After the methodology, the result and discussion were covered and started with the discussion of the theory and methodology for the global model, the drivetrain, fatigue and co-simulation versus de-coupled simulation. Further, the validation of the different models were presented with comments regarding the results and what did not work as intended. A subsection regarding the tuning of the PI controller for controlling the generator speed using the Simscape model with the results of this was included. The last three subsections included results and discussions of the fatigue and the full model simulation using Simulink<sup>®</sup>.

At the end of the thesis, a section covering the challenges faced and recommendation for further work was included, presenting the difficulties and the possibility of further improvement of the work done.

The background theory showed that FAST.farm and OpenFAST with Nautilus floating 10 MW wind turbine were the preferred tools and model to use for the global model. Similarly, it was showed that Simpack would be a suitable tool for the drivetrain model. The validation of OpenFAST using the Nautilus model showed that the wind turbine behaved as expected and it was deemed to be working. The validation of the reduced order model developed in Simpack was a bit more tricky because of the issues with the gears of gear stage 1, a simplified version was made. This was validated using the natural frequency.

The reduced order model achieved in this Master's Thesis is less detailed than desired and including the radial forces and gears for fatigue calculation is recommended further work. Nevertheless, a functional reduced order model that may be used for estimation of the fatigue damage of the main bearings is developed. The model also includes the axial DOF for the main shaft, which is currently not available for the wind energy tools discussed in this thesis.

---

The main outcome from the fatigue results is that INP-B is more sensitive to the axial loads than INP-A with the parameters used here, and that the damage follows the thrust curve. It has also been shown that the sea state does not affect the damage results significantly, and that waves contribute to less damage in the main components. Lastly, the amplitude of damage of the main components follows the thrust curve for the model developed.

The simulation time for the full model in Simulink<sup>®</sup> was significantly slower than running the models separately, indicating that this is not the best solution for integrated simulation of a global model and the drivetrain model.

## 6.1 Contribution

The advantages of a reduced order drivetrain is the possibility of using the model in areas that require fast simulation models. Examples of this is the digital twin that helps with decision making based on real-time data or for the use in wind farm control for with the objective of reducing the fatigue on the drive train components. This may open possibilities to estimate the consequences for the drivetrain by different modes of operation of the wind farm.

---

## Bibliography

- [1] Erin Bachynski. ‘Basic aerodynamics for wind turbines’. Lecture note. NTNU Lectures in the Fall of 2021.
- [2] Erin E. Bachynski et al. ‘Marine Dynamics - TMR 4182 Marine Dynamics’. Lecture note. Department of Marine Technology, Faculty of Engineering Science and Technology - NTNU. Jan. 2019.
- [3] *BasicDTUController*. Accessed 20.03.2022. URL: <https://gitlab.windenergy.dtu.dk/OpenLAC/BasicDTUController/-/tree/master/>.
- [4] *Bearing basics*. Accessed 09.06.2022. URL: <https://www.skf.com/group/products/rolling-bearings/principles-of-rolling-bearing-selection/general-bearing-knowledge/bearing-basics>.
- [5] Diederik van Binsbergen. ‘Effects of Induction and Wake Steering Control on Drivetrain Fatigue and Wind Farm Power Production’. MA thesis. Norway and The Netherlands: NTNU and TU Delft, 2020.
- [6] Halvor Bothner-By. *Signalteori*. In: Accessed 26.06.2022. Store Norske Leksikon, Nov. 2020. URL: <https://snl.no/signalteori>.
- [7] *Build a Drivetrain Model*. Accessed 29.04.2022. URL: <https://se.mathworks.com/help/phymod/sdl/ug/building-a-driveline-model.html>.
- [8] Tony Burton et al. *Wind Energy Handbook*. Second edition. John Wiley & Sons Ltd., 2011. ISBN: 978-1-119-99272-1.
- [9] Amanullah Choudhry et al. ‘Effects of Wake Interaction on Downstream Wind Turbines’. In: *Wind Engineering* (Oct. 2014). DOI: 10.1260/0309-524X.38.5.535.
- [10] International Electrotechnical Commission. *Wind energy generation systems - Part 1: Design requirements*. Edition 4.0. NEK IEC 61400-1:2019. Switzerland: Norsk Elektroteknisk Komite, 2019. ISBN: ISBN 978-2-8322-6253-5.
- [11] MODELISAR Consortium and The Modelica Association Project FMI. *Functional Mock-up Interface Specification*. Accessed 08.06.2022. 2022. URL: <https://fmi-standard.org/docs/3.0/>.
- [12] Dassault Systèmes Simulia Corp. *SIMULIA User Assistance 2021x - Simpack User Assistance*. Documentation implemented in Simpack 2021x. 2020.
- [13] Rick Damiani, Jason Jonkman and Greg Hayman. *SubDyn User’s Guide and Theory Manual*. Technical Report NREL/TP-5000-63062. Sept. 2015.
- [14] National Renewable Energy Laboratory - dev. *OpenFAST Documentation*. Version v.3.0.0. Accessed 06.12.2021. Nov. 2020. URL: <https://openfast.readthedocs.io/en/dev/index.html#>.
- [15] DNV. *Floating Offshore Wind*. Accessed 16.12.2021. URL: <https://www.dnv.com/focus-areas/floating-offshore-wind/index.html>.
- [16] *DTU 10MW Reference Wind Turbine*. Accessed 28.01.2022. URL: <https://rwt.windenergy.dtu.dk/dtu10mw/dtu-10mw-rwt/-/tree/master/>.

- 
- [17] Saeed Ebrahimi and Peter Eberhard. ‘Aspects of Contact Problems in Computational Multibody Dynamics’. In: *Multibody Dynamics*. Springer, 2007, pp. 23–47. ISBN: 978-1-4020-5684-0. DOI: [https://doi.org/10.1007/978-1-4020-5684-0\\_2](https://doi.org/10.1007/978-1-4020-5684-0_2).
- [18] S. Faulstich, B. Hahn and P. J. Tavner. ‘Wind turbine downtime and its importance for offshore deployment’. In: *Wind Energy* 14 (3 2010), pp. 327–337. DOI: 10.1002/we.421.
- [19] *FMI - Functional Mock-Up Interface*. Accessed 08.06.2022. URL: <https://fmi-standard.org/about/>.
- [20] Juan Gallego-Calderon and Anand Natarajan. ‘Assesment of wind turbine drive-train fatigue loads under torsional excitation’. In: (2015). DOI: 10.1016/j.engstruct.2015.09.008.
- [21] J. Galvan et al. *Definition and analysis of NAUTILUS-DTU10 MW floating offshore wind turbine at Gulf of Maine, experiments at Sintef Ocean and Polimi*. Tecnalia RI, Derio, Basque Country, Spain, 2018.
- [22] I.P. Girsang et al. *Gearbox and Drivetrain Models to Study Dynamic Effects of Modern Wind Turbines*. Conference paper NREL/CP-5500-58960. Presented at the IEEE Energy Conversion Congress and Exposition. Denver, Colorado: National Renewable Energy Laboratory (NREL), Sept. 2013.
- [23] Y. Guo et al. *Recommendations on Model Fidelity for Wind Turbine Gearbox Simulations*. Conference paper NREL/CP-5500-58960. To be presented at the Conference for Wind Power Drives (CWD). Aachen, Germany: National Renewable Energy Laboratory (NREL), Mar. 2015.
- [24] Martin O. L. Hansen. *Aerodynamics of Wind Turbines*. Second edition. Earthscan, 2008. ISBN: 978-1-84407-438-9.
- [25] Gunnar Härkegård. *Dimensjonering av maskindeler*. 3rd edition. Fagbokforlaget Vigmostad & Bjørke AS, 2004. ISBN: 978-82-519-1970-8.
- [26] IBM. *What is a digital twin?* Accessed 01.07.2022. URL: <https://www.ibm.com/topics/what-is-a-digital-twin>.
- [27] B. J. Jonkman. *Turbsim User’s Guide v2.00.00 - DRAFT VERSION*. Tech. rep. Accessed 06.06.2022. June 2016. URL: [https://www.nrel.gov/wind/nwtc/assets/downloads/TurbSim/TurbSim\\_v2.00.pdf](https://www.nrel.gov/wind/nwtc/assets/downloads/TurbSim/TurbSim_v2.00.pdf).
- [28] J. Jonkman et al. *Validation of FAST.Farm Against Large-Eddy Simulations*. Journal of Physics: Conference Series 1037 062005. 2018. DOI: 10.1088/1742-6596/1037/6/062005.
- [29] Jason Jonkman and Kelsey Shaler. *FAST.Farm User’s Guide and Theory Manual*. National Renewable Energy Laboratory - Technical Report NREL/TP-5000-78485. Apr. 2021. URL: <https://www.nrel.gov/docs/fy21osti/78485.pdf>.
- [30] Jason Jonkman et al. *Development of FAST.Farm: A New Multiphysics Engineering Tool for Wind Farm Design and Analysis*. Conference Paper. To be presented at AIAA SciTech 2017. Grapevine, Texas, Jan. 2017.
- [31] Jason Jonkmann. *Customizing Jacket model in FAST.v8*. Accessed 04.06.2022. URL: <https://forums.nrel.gov/t/customizing-jacket-model-in-fast-v8/1121/>.
- [32] Mette Bischoff Kristiansen. *Welcome to HAWC2*. Accessed 11.06.2021. URL: <https://www.hawc2.dk/HAWC2-info>.
-

- 
- [33] National Renewable Energy Laboratory. *AeroDyn*. Accessed 25.11.2021. URL: <https://www.nrel.gov/wind/nwtc/aerodyn.html>.
- [34] National Renewable Energy Laboratory. *HydroDyn*. Accessed 26.11.2021. URL: <https://www.nrel.gov/wind/nwtc/hydrodyn.html>.
- [35] National Renewable Energy Laboratory. *OpenFAST Documentation*. Version v.2.4.0. Accessed 19.11.2021. Nov. 2020. URL: <https://raf-openfast.readthedocs.io/en/docs-fast8readme/index.html>.
- [36] National Renewable Energy Laboratory. *OpenFAST Documentation*. Version v3.1.0. Accessed 10.06.2022. Mar. 2022. URL: <https://raf-openfast.readthedocs.io/en/docs-turbsim/index.html>.
- [37] National Renewable Energy Laboratory. *OpenFAST Documentation - main*. Version v3.0.0. Accessed 19.11.2021. Nov. 2021. URL: <https://openfast.readthedocs.io/en/main/index.html>.
- [38] Eben Lenfest et al. *Tuning of Nacelle Feedback Gains for Floating Wind Turbine Controllers using a Two-DOF Model*. Conference paper NREL/CP-5000-76558. Presented at the ASME 2020 39th International Conference on Ocean, Offshore and Arctic Engineering, National Renewable Energy Laboratory (NREL), Aug. 2020.
- [39] M.Singh et al. *Simulation for Wind Turbine Generators - With FAST and MATLAB-Simulink Modules*. Technical Report NREL/TP-5D00-59195. National Renewable Energy Laboratory (NREL), Apr. 2014.
- [40] James Manwell, Jon McGowan and Anthony Rogers. *Wind Energy Explained. Theory, Design and Application*. Second edition. John Wiley & Sons Ltd., 2010. ISBN: 978-1-119-99436-7.
- [41] MathWorks. *Simscape*. Accessed 25.04.2022. URL: <https://se.mathworks.com/products/simscape.html#mulsch>.
- [42] MathWorks. *Simscape Driveline*. Accessed 20.05.2022. URL: <https://se.mathworks.com/products/simscape-driveline.html>.
- [43] MathWorks. *Simscape Multibody*. Accessed 20.05.2022. URL: <https://se.mathworks.com/products/simscape-multibody.html>.
- [44] MathWorks. *What Is an S-function*. Accessed 02.05.2023. URL: <https://se.mathworks.com/help/simulink/sfg/what-is-an-s-function.html>.
- [45] Mathworks. *SIMPACK*. Accessed 13.12.2021. URL: [https://se.mathworks.com/products/connections/product\\_detail/simpack.html](https://se.mathworks.com/products/connections/product_detail/simpack.html).
- [46] Amir R. Nejad. *Conversations and guidance*. Discussion. 2022.
- [47] Amir R. Nejad. *Drivetrain in wind turbines - Multi-body dynamics and dynamic analysis of drivetrains*. LECTURED Fall of 2019. Oct. 2018.
- [48] Amir R. Nejad et al. 'Development of a 5 MW Reference Gearbox for Offshore Wind Turbines'. In: *Wind Energy* (July 2015), pp. 1089–1106. DOI: 10.1002/we.1884.
- [49] Amir Rasekhi Nejad. 'Modelling and analysis of drivetrains in offshore wind turbines'. In: *Offshore Wind Energy Technology*. Wiley, 2018, pp. 37–94. ISBN: 978-1-119-09776-1.
-



- 
- [50] Amir Rasekhi Nejad, Zhen Gao and Torgeir Moan. ‘On long-term fatigue damage and reliability analysis of gears under wind loads in offshore wind turbine drivetrains’. In: *International Journal of Fatigue - Volume 61* (Apr. 2014), pp. 116–128. DOI: <https://doi.org/10.1016/j.ijfatigue.2013.11.023>.
- [51] NREL. *FLORIS: FLOW Redirection and Induction in Steady State*. Accessed 08.12.2021. 2021. URL: <https://www.nrel.gov/wind/floris.html>.
- [52] *OpenFAST*. Accessed 15.01.2022. URL: <https://github.com/OpenFAST>.
- [53] Ørsted. *Europe powered by Green Energy*. URL: <https://orsted.com/-/media/www/docs/corp/com/about-us/north-seas/rsted-paper-01---europe-powered-by-green-energy-uk.ashx>.
- [54] A. Pegalajar-Jurado et al. *D4.5 - State-of-the-art models for the two LIFES50+ 10MW floater concepts*. Apr. 2018.
- [55] Antonio Pegalajar-Jurado et al. *State-of-the-art model for the LIFES50+ OO-Star Wind Floater Semi 10MW floating wind turbine*. 2018.
- [56] Bjørnar Pettersen. *Marin Teknisk 3 - Hydrodynamikk*. Pensumhefte. Akademika, 2018.
- [57] Andy Platt, Bonnie Jonkman and Jason Jonkman. *InflowWind User’s Guide*. July 2016.
- [58] Datong Qin, Jianhong Wang and Teik C. Lim. ‘Flexible Multibody Dynamic Modeling of a Horizontal Wind Turbine Drivetrain System’. In: (2009). DOI: 10.1115/1.3211094.
- [59] W. Dheelibun Remigius and Anand Natarajan. ‘A review of wind turbine drivetrain loads and load effects for fixed and floating wind turbines’. In: (July 2021). Department of Wind Energy, DTU. DOI: 10.1002/wene.417.
- [60] Reinhold von Schwerin. *MultiBody System SIMulation - Numerical Methods, Algorithms and Software*. Springer-Verlag Berlin Heidelberg GmbH, 1999. ISBN: 978-3-540-65662-3.
- [61] Ahmed A. Shabana. *Multibody Systems*. Fourth Edition. Cambridge University Press, 2013.
- [62] Wei Shi et al. ‘Dynamic Modeling and Analysis of a Wind Turbine Drivetrain Using the Torsional Dynamic Model’. In: *International Journal of Precision Engineering and Manufacturing, Vol 14*. (2013), pp. 153–159. DOI: 10.1007/s12541-013-0021-2.
- [63] *Simpack - Software Compatibility*. Accessed 05.05.2022. URL: <https://www.3ds.com/support/hardware-and-software/simulia-system-information/simpack/simpack-software-compatibility/>.
- [64] Sintef. *Offshore Wind*. Accessed 14.12.2021. URL: <https://www.sintef.no/en/software/sima2/offshore-wind/>.
- [65] Sintef. *Sima*. Accessed 14.12.2021. URL: <https://www.sintef.no/programvare/sima/>.
- [66] International Organization for Standardization. *ISO 1122-1: Vocabulary of gear terms - Part 1: Definitions related to geometry*. Second edition. Reference number: ISO 6336-1:1998(E/F). Switzerland: International Organization for Standardization, 1998.
- [67] International Organization for Standardization. *ISO 6336-3: Calculation of load capacity of spur and helical gears - Part 3: Calculation of tooth bending strength*. Third edition. Reference number: ISO 6336-3:2019(E). Switzerland: International Organization for Standardization, Nov. 2019.
-

- 
- [68] Dassault Systèmes. *SIMPACK - Multibody System Simulation Software*. Accessed 07.12.2021. URL: <https://www.3ds.com/products-services/simulia/products/simpack/>.
- [69] *TMR4505 - Marine Structures, Specialization Course, module TMR03 - Integrated Dynamic analysis of Wind Turbines*. 2021.
- [70] United Nations, Division for Sustainable Development Goals (DSDG). *The 17 Goals*. Accessed 16.12.2021. URL: <https://sdgs.un.org/goals>.
- [71] Q. Wang et al. *BeamDyn User's Guide and Theory Manual*. Available at [www.nrel.gov/publications](http://www.nrel.gov/publications). Mar. 2016.
- [72] Shuaishuai Wang. *Discussion regarding drivetrain model*. Discussion. June 2022.
- [73] Shuaishuai Wang, Amir R. Nejad and Torgeir Moan. 'On design, modelling, and analysis of a 10-MWmedium-speed drivetrain for offshore wind turbines'. In: *Wind Energy* (Jan. 2020), pp. 1099–1117. DOI: <https://doi.org/10.1002/we.2476>.
- [74] Wei Yu, Kolja Müller and Frank Lemmer. *D4.2 - Public Definition of the Two LIFES50+ 10MW Floater Concepts*. Apr. 2018.
- [75] Yang Zhiyin. 'Large-eddy simulation: Past, present and the future'. In: *Chinese Journal Aeronautics, Volume 28* (2015), pp. 11–24. DOI: <https://doi.org/10.1016/j.cja.2014.12.0072>.

---

# Appendix

## A Simpack Driveline model

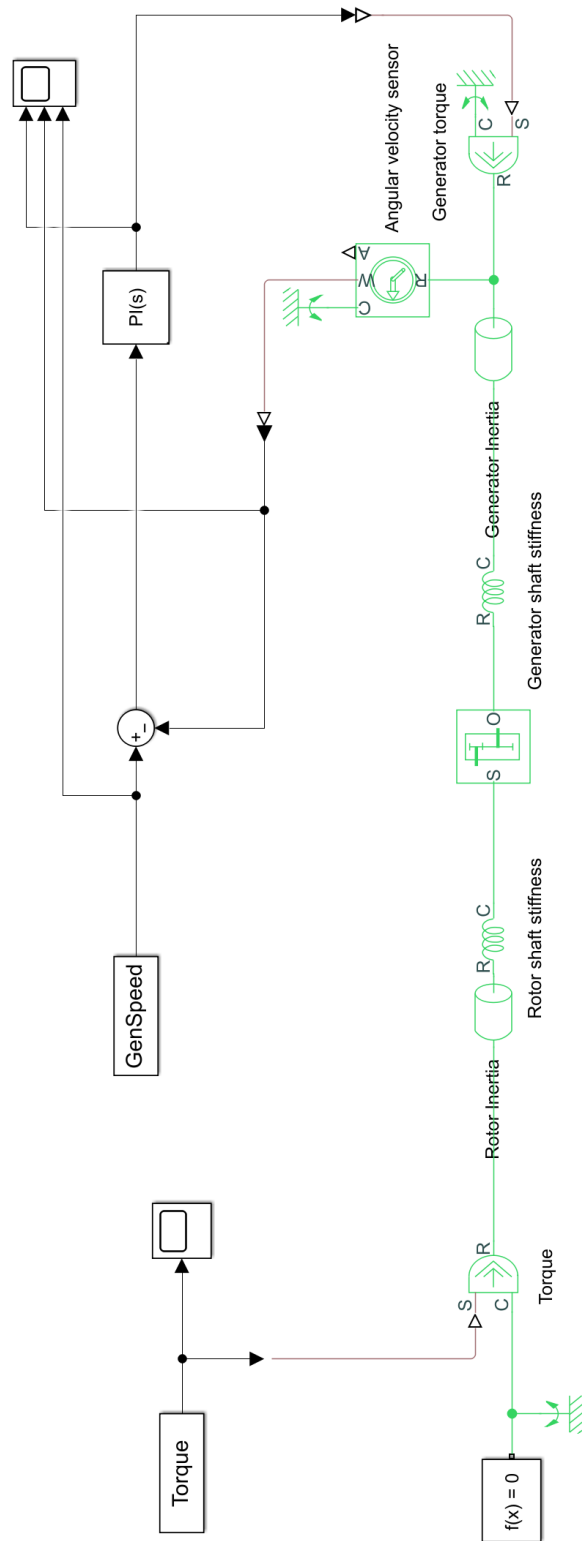


Figure A.1: Simscape Driveline two mass model

B 2D figure of model

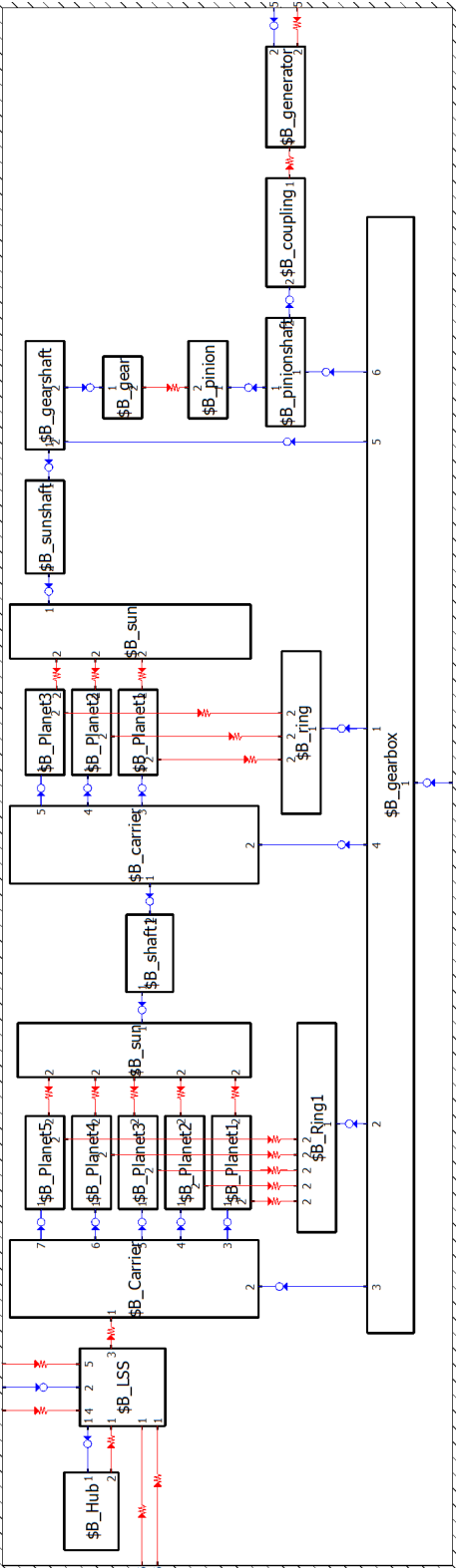


Figure B.1: 2D figure of drivetrain model in Simpack

# C Full model in Simulink®

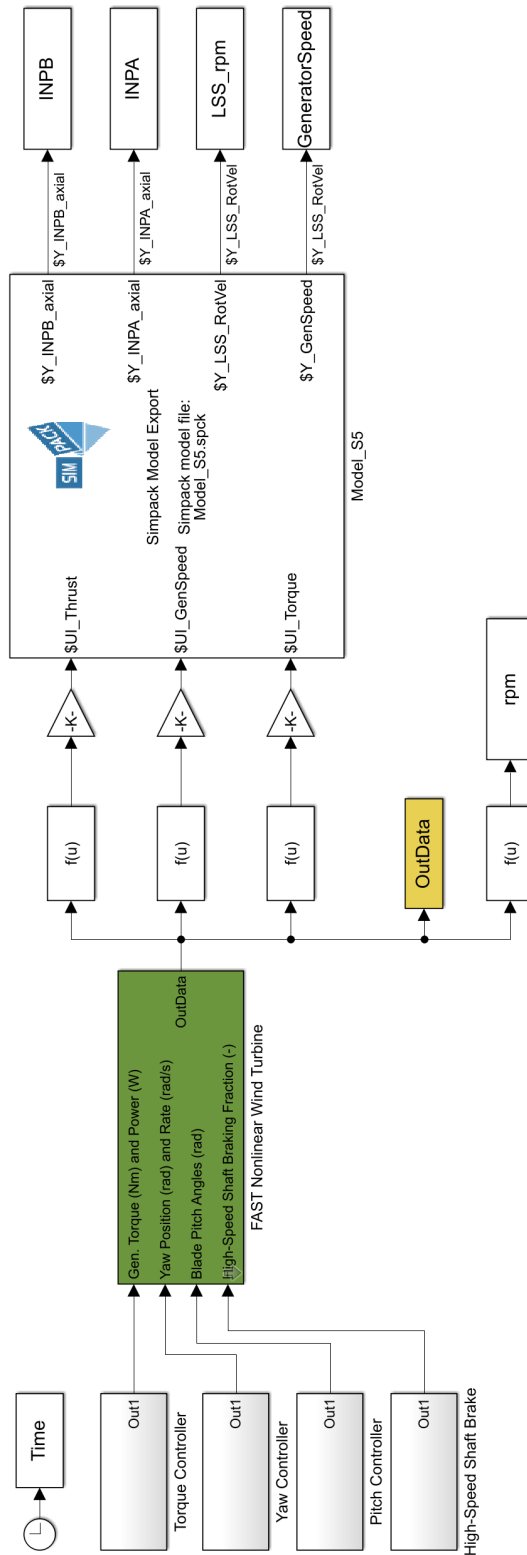


Figure C.1: Full model in Simulink®

